Marco António Mesquita Moreira

Bachelor degree in Science of Micro and Nanotechnologies Engineering

Composition ratio effect in IGZO using solution combustion synthesis for TFT applications

Dissertation submitted in partial fulfillment
of the requirements for the degree of

Master of Science in
Micro and Nanotechnologies Engineering

Supervisor:	Dr. Rita Maria Mourão Salazar Branquinho, Assistant Professor, Faculty of Sciences and Technology New University of Lisbon
Co-supervisor:	Dr. Pedro Miguel Cândido Barquinha, Assistant Professor, Faculty of Sciences and Technology New University of Lisbon

Examination Committee

Chairperson:	Dr. Rodrigo Ferrão de Paiva Martins, Full Professor, FCT-UNL
Raporteurs:	Dr. Henrique Leonel Gomes, Assistant Professor, FCT-UAlg

FACULDADE DE
CIÊNCIAS E TECNOLOGIA
UNIVERSIDADE NOVA DE LISBOA

September, 2017

Composition ratio effect in IGZO using solution combustion synthesis for TFT applications

Copyright © Marco António Mesquita Moreira, Faculty of Sciences and Technology, NOVA University of Lisbon.
The Faculty of Sciences and Technology and the NOVA University of Lisbon have the right, perpetual and without geographical boundaries, to file and publish this dissertation through printed copies reproduced on paper or on digital form, or by any other means known or that may be invented, and to disseminate through scientific repositories and admit its copying and distribution for non-commercial, educational or research purposes, as long as credit is given to the author and editor.

This document was created using the (pdf)LaTeX processor, based in the "unlthesis" template[1], developed at the Dep. Informática of FCT-NOVA [2].
[1] https://github.com/joaomlourenco/unlthesis [2] http://www.di.fct.unl.pt

"Fall in love with some activity, and do it! Nobody ever figures out what life is all about, and it doesn't matter. Explore the world. Nearly everything is really interesting if you go into it deeply enough. Work as hard and as much as you want to on the things you like to do the best. Don't think about what you want to be, but what you want to do. Keep up some kind of a minimum with other things so that society doesn't stop you from doing anything at all."

— Richard Feynman

Acknowledgements

A realização desta dissertação simboliza o fim de uma das etapas mais importantes e marcantes da minha vida: a obtenção do grau académico de mestre. E é com um enorme orgulho e satisfação que vejo esta etapa concluída, que não seria possível sem a contribuição de várias pessoas com quem convivi ao longo destes últimos anos.

Em primeiro lugar gostaria de agradecer à minha instituição, a Faculdade de Ciências e Tecnologia da Universidade Nova de Lisboa, e ao Departamento das Ciências dos Materiais, por todas as experiências e momentos ao longo destes anos da vida académica.

Em segundo lugar gostaria de agradecer ao professor Rodrigo Martins e à professora Elvira Fortunado pela criação do curso de Engenharia de Micro e Nanotecnologias, assim como o seu esforço, dedicação e competência em disponibilizar o CENIMAT|I3N e CEMOP como locais de investigação com excelentes condições de trabalho de investigação científica, e permitindo assim a realização desta dissertação.

Um especial agradecimento à minha orientadora Rita Branquinho por me ter integrado neste trabalho e acompanhado ao longo do todo o semestre o trabalho desta tese, assim como a sua preciosa ajuda e na partilha de ideias e opiniões, e pelas reuniões semanais ao longo da tese. Gostaria também de agradecer meu co-orientador Pedro Barquinha pelas ideias e sugestões dadas para o trabalho. O apoio de ambos foi essencial para a realização desta tese, e por isso um especial obrigado!

Um especial agradecimento ao Emanuel Carlos, pelo seu papel de "terceiro orientador"; o seu esforço e apoio ao meu trabalho laboratorial e no decorrer da tese foram fulcrais, assim como a sua paciência em ouvir as minhas dúvidas e ajudar-me mesmo quando a sua disponibilidade era reduzida.

A toda a equipa do CENIMAT que me auxiliou na obtenção de dados, esclarecimento de dúvidas, disponibilização de material para o laboratório, das quais destaco o Prof. Luís Pereira, Daniela Gomes, Joana Pinto, Ana Pimentel, Alexandra Gonçalves, Sónia Pereira, Tomás Calmeiro, Sofia Ferreira, Beatriz Coelho e Daniela Salgueiro.

A todo o pessoal do CENIMAT e CEMOP com quem tive o prazer de partilhar tardes de futebol como forma de desanuviar no final de um dia de trabalho, e ao pessoal do Open Space pelos bons momentos de diversão e e convívio, e apoio prestado ao meu trabalho.

Ao Pedro Trigo, um parágrafo aqui não chega para descrever a nossa amizade, que combinada com o nosso trabalho em conjunto ao longo desta tese foram essenciais. Um obrigado também pelas nossas gargalhadas, companhia, boleias e almoços.

Ao Alexandre Fonseca acima de tudo pela nossa relação de amizade ao longo destes anos, que foi essencial para ultrapassar os momentos menos bons, assim como a importância das noitadas de estudo e o convívio.

Aos meus amigos e colegas de Micro e Nano que me acompanharam ao longo deste precurso académico, com quem partilhei grandes momentos de diversão, trabalhos de grupo, madrugadas a estudar, entre outras experiências enriquecedoras. Obrigado José Rosa, Tomás, Ângelo, Ismael, Gonçalo, Monteiro, Zé Rui, Ribas, Saraiva, Correia, Chamiço, Farinha, Tiago, Vasco, Shiv, Pinela, João Afonso, Viorel, Luís, Coroa, Beaumont, Daniela, Cátia, Inês, Luís,

David, Xana, Emma, Marta, Jolu, Crespo, e todos aqueles que não referenciei mas também contribuíram para a minha experiência académica.

Aos meus amigos da minha terra, em especial ao André, Alves, Bruno, João Vaz, Milton, Janeta, Barroca, Croca, Estevam, Mamins, David, Plácido, Toste e todos aqueles com quem convivi bons momentos ao longo destes anos.

Por fim gostaria de agradecer à minha família, nomeadamente ao meu irmão Nelson e e em especial aos meus pais, Maria e António, pela sua motivação e pelo esforço e sacrífício a que se submeteram ao longo destes últimos anos de forma a proporcionarem-me esta educação académica, pelo apoio ao longo da minha vida e por me tornarem a pessoa que hoje sou. Por estes motivos, este trabalho é dedicado a vocês.

Abstract

Amorphous indium-gallium-zinc oxide (a-IGZO) is the most used semiconductor in metal oxide-based thin-film transistors (TFTs) for flat-panel displays (FPDs) applications due to its superior electrical characteristics. However, its properties are not yet optimised and are far away from the intended when produced by solution, and their development is crucial to implement in plastic flexible substrates and decrease the associated costs. This work aimed to evaluate a-IGZO thin films produced by solution by varying the metallic cations molar ratio and the number of deposited layers, to apply as active channel layer in TFTs and study their performance. To make TFTs compatible with flexible substrates, the chemical method solution combustion synthesis (SCS) with urea as fuel was used to reduce the high-temperature annealing during the process. Optimised films were obtained for three-layer a-IGZO with metallic cations molar ratio of In_2O_3:Ga_2O_3:ZnO = 3:1:1. After this, a-IGZO TFTs showing the best results were optimised by patterning the semiconductor. Optimised TFTs show good reproducibility with an average on-off ratio of $(4.19 \pm 6.42) \times 10^7$, mobility of $(1.75 \pm 0.83) \times 10^{-2}$ cm^2 V^{-1} s^{-1}, subthreshold slope of 0.63 ± 0.11 V/dec, turn-on voltage of 0.58 ± 0.79 V and threshold voltage of 3.83 ± 0.87 V.

Keywords: Amorphous indium-gallium-zinc oxide, solution combustion synthesis, multi-layer active channel, solution TFTs, transparent semiconductor oxides.

Resumo

O óxido de índio-gálio-zinco amorfo (a-IGZO) é o semicondutor mais usado nos transístores de filme fino (TFTs) baseados em óxidos metálicos para aplicações de displays de tela plana, devido à suas características eléctricas superiores. No entanto, quando produzido por solução, as propriedados de filmes finos de a-IGZO não estão optimizadas e aquém do desejado, e o seu melhoramento é crucial para implementar em substratos flexíveis e diminuir os custos associados. Este trabalho destinou-se avaliar filmes finos de a-IGZO produzidos por solução, variando a proporção molar de catiões metálicos e o número de camadas depositadas de a-IGZO, para aplicar como camada activa do canal em TFTs e estudar a sua performance. De forma a tornar os TFTs compatíveis com substratos flexíveis, o método químico de síntese de solução por combustão com ureia como fuel foi usado para reduzir a temperatura elevada de recozimento durante o processo. Os filmes optimizados foram obtidos para a-IGZO de 3 camadas, com a proporção molar de In_2O_3:Ga_2O_3:ZnO = 3:1:1. Após isto, TFTs de a-IGZO com os melhores resultados foram optimizados através de padronização do semicondutor. Os TFTs optimizados apresentam uma boa reprodutibilidade com uma razão *on-off* de $(4.19 \pm 6.42) \times 10^7$, mobilidade de $(1.75 \pm 0.83) \times 10^{-2}$ cm^2 V^{-1} s^{-1}, *subthreshold slope* de 0.63 ± 0.11 V/dec, tensão *on* de 0.58 ± 0.79 e tensão limiar de 3.83 ± 0.87 V.

Palavras-chave: Óxido de índio-gálio-zinco amorfo, síntese de solução por combustão, canal activo multicamada, TFTs por solução, óxidos semicondutores transparentes.

Contents

List of Figures xv

List of Tables xvii

Acronyms xix

Symbols xxi

Motivation and Objectives xxiii

1 Introduction 1

1.1 Metal oxide semiconductors 1
1.2 Amorphous indium-gallium-zinc oxide 2
1.3 Solution-based electronics 2
1.4 Solution combustion synthesis 3
1.5 Thin film transistors 3

2 Materials and Methods 7

2.1 Precursor solutions preparation and characterisation 7
2.2 Thin films deposition and characterisation 8
2.3 Electronic devices fabrication and characterisation 8

3 Results and Discussion 11

3.1 Solutions characterisation 11
3.1.1 Thermal characterisation 12
3.2 Thin films characterisation 13
3.2.1 Optical characterisation 14
3.2.2 Structural and morphological characterisation 16
3.3 Electrical characterisation of solution-based IGZO TFTs 19

4 Conclusions and future perspectives 29

Bibliography 31

A Redox reactions 37

B IGZO solutions viscosity 39

C DSC-TG analysis of IGZO solutions 41

D Reflectance of thin films 43

E Calculation of E_{opt} of IGZO thin films 45

F Variation of transconductance with voltage **47**

G Stabilisation and output curves non-patterned TFTs **53**

H Patterned 3-layer TFTs annealed at 180 °C **61**

I Stabilisation and output curves of TFTs annealed at 120 °C **65**

J Comparison of TFTs in this work with literature **67**

List of Figures

1.1 a) Schematic reaction coordinate comparing the energetics for SCS and for conventional sol-gel solution processing; b) comparison of SCS and conventional reactions to form metal oxides. . . . 3
1.2 Structure of a staggered bottom-gate TFT. . . . 4
1.3 Typical transfer and output characteristics of a TFT. . . . 5

3.1 FT-IR spectra of IGZO solutions, with different molar ratios. . . . 11
3.2 DSC-TG analysis of IGZO 3:1:1 precursor solutions with 2-ME as solvent and using urea as fuel or not. . . . 12
3.3 FT-IR spectra of 3-layer IGZO thin films on Si substrates, with different molar ratios, after annealing at 300 °C for 30 min. . . . 13
3.4 Transmittance spectra of IGZO thin films on glass substrates. . . . 15
3.5 GAXRD diffractograms of 3-layer IGZO thin films on Si substrates, with different molar ratios. . . . 16
3.6 Morphological characterisation IGZO a) 1:1:1, b) 2:1:2, c) 2:1:1 and d) 3:1:1 thin films for a concentration of 0.2 M. AFM deflection images of 2×2 μm^2 to an annealing at 300 °C during 30 min, with different number of IGZO layers. . . . 17
3.7 SEM surface of 3-layer IGZO 3:1:1 thin film on Si substrate, with annealing 300 °C for 30 min. . . . 18
3.8 Molecular concentration (%) of each metallic oxide in IGZO thin films with 3 layers on Si substrates, annealed at 300 °C for 30 min. . . . 18
3.9 Stabilisation curves of IGZO 1:1:1, 2:1:2 and 2:1:1 0.2 M TFTs with 1, 2 and 3 active layers, without urea as fuel. . . . 20
3.10 Transfer curve of IGZO 2:1:1 0.2 M TFTs with 1 active layer, without urea as fuel. 21
3.11 Transfer curve of IGZO 1:1:1 0.2 M TFT with 1 active layer, measured initially and 8 weeks later. . . . 21
3.12 Transfer curves of IGZO 2:1:2 0.2 M TFTs with 1 and 2 active layers, measured initially and 8 weeks later. . . . 22
3.13 Transfer curves of IGZO 2:1:1 0.2 M TFTs with 1, 2 and 3 active layers, measured initially and 8 weeks later. . . . 23
3.14 Transfer curves of IGZO 3:1:1 0.2 M TFTs with 1, 2 and 3 active layers, measured initially and 8 weeks later. . . . 24
3.15 a) Transfer curves of patterned IGZO 3:1:1 3-layer IGZO; b) variation of maximum I_{DS} with W values studied. . . . 27

C.1 DSC-TG analysis of IGZO 1:1:1 and 2:1:2 precursor solutions with 2-ME as solvent and using urea as fuel or not. . . . 41
C.2 DSC-TG analysis of IGZO 2:1:1 precursor solutions with 2-ME as solvent and using urea as fuel or not. . . . 42

D.1 Reflectance spectra of IGZO thin films on glass substrates. 43

E.1 Tauc-bandgap plots for the calculation of E_{opt}. 46

F.1 Transconductance curve of IGZO 1:1:1 0.2 M TFT with 1 active layer, measured initially and 8 weeks later. 47
F.2 Transconductance curves of IGZO 2:1:2 0.2 M TFT with 1 and 2 active layers, measured initially and 8 weeks later. 47
F.3 Transconductance curves of IGZO 2:1:1 0.2 M TFT with 1, 2 and 3 active layers, measured initially and 8 weeks later. 48
F.4 Transconductance curves of IGZO 2:1:1 0.2 M TFT with 1, 2 and 3 active layers, measured initially and 8 weeks later. 49
F.5 Transconductance curves of TFTs annealed at 120 °C with patterned IGZO 3:1:1 3 layers, measured initially and 8 weeks later. 50
F.6 Transconductance curves of TFTs annealed at 180 °C with patterned IGZO 3:1:1 3 layers, measured initially and 8 weeks later. 51

G.1 Stabilisation curves of IGZO 1:1:1 0.2 M with 1, 2 and 3 active layers. 53
G.2 Stabilisation curves of IGZO 2:1:2 0.2 M with 1, 2 and 3 active layers. 54
G.3 Stabilisation curves of IGZO 2:1:1 0.2 M with 1, 2 and 3 active layers. 55
G.4 Stabilisation curves of IGZO 3:1:1 0.2 M with 1, 2 and 3 active layers. 56
G.5 Output curve of IGZO 1:1:1 0.2 M with 1 active layer. 57
G.6 Output curves of IGZO 2:1:2 0.2 M with 1 and 2 active layers. 57
G.7 Output curves of IGZO 2:1:1 0.2 M with 1, 2 and 3 active layers. 58
G.8 Output curves of IGZO 3:1:1 0.2 M with 1, 2 and 3 active layers. 59

H.1 Stabilisation curves of TFTs annealed at 180 °C with patterned IGZO 3:1:1 3 layers, measured initially and 8 weeks later 61
H.2 Saturation curves of TFTs annealed at 180 °C with patterned IGZO 3:1:1 3 layers, measured initially and 8 weeks later 62
H.3 Ouput curves of TFTs annealed at 180 °C with patterned IGZO 3:1:1 3 layers, measured initially and 8 weeks later 63

I.1 Stabilisation curves of IGZO 3:1:1 0.2 M with W/L of 80/20, 160/20, 320/20 μm/μm, annealed at 120 °C 65
I.2 Output characteristics of patterned IGZO 3:1:1 3 Layers, annealed at 120 °C . . 66

List of Tables

3.1 Characteristic absorbance peaks and associated vibrational modes of the corresponding chemical bonds for analysed FT-IR spectra of IGZO solutions. 11
3.2 Thickness of measured films (nm) by spectroscopy ellipsometry, for all IGZO molar ratios, with films spin coated onto Si substrates and annealed at 300 °C. . 14
3.3 E_{opt} of measured films (eV) determined by linear fit of Tauc-plots, for all IGZO molar ratios, with films spin coated onto Si substrates and annealed at 300 °C. . 15
3.4 Average and standard deviation of electrical parameters of three measured TFTs with IGZO 1:1:1 1 layer as channel layer, measured initially and 8 weeks later. . 22
3.5 Average and standard deviation of electrical parameters of three measured TFTs with IGZO 2:1:2 as channel layer, measured initially and 8 weeks later. 22
3.6 Average and standard deviation of electrical parameters of three measured TFTs with IGZO 2:1:1 as channel layer, measured initially and 8 weeks later. 23
3.7 Average and standard deviation of electrical parameters of three measured TFTs with IGZO 3:1:1 as channel layer, measured initially and 8 weeks later. 24
3.8 Average and standard deviation of electrical parameters of three measured TFTs annealed at 120 °C with patterned-IGZO 3:1:1 as channel layer, measured initially and 8 weeks later. 27

A.1 Reduction and oxidation reactions. 37
A.2 Combination of metal nitrate reduction and fuel oxidation reactions. 37
A.3 Valence of the reagents. 38
A.4 Number of moles of fuel per mole of oxidiser to ensure stoichiometry of the redox reaction. 38
A.5 Overall reactions with correct stoichiometry. 38

B.1 Viscosities of IGZO solutions with and without urea, and 2-ME. 39

E.1 R^2 of each linear fit for determination of E_{opt}. 46

H.1 Average and standard deviation of electrical parameters of three measured TFTs annealed at 180 °C with patterned-IGZO 3-layer 3:1:1 as channel layer, measured initially and 8 weeks later. 63

J.1 Selected processing details for several reported solution based TFTs deposited by solution processes ("n. a." means that the related data is not mentioned in the literature). 67

Acronyms

2-ME 2-Methoxyethahol.

a-Si Amorphous Silicon.

a-IGZO Amorphous Indium-Gallium-Zinc Oxide.

AFM Atomic Force Microscopy.

ALD Atomic Layer Deposition.

AMOLED Active-Matrix Organic Light-Emitting Diode.

ATR Atenuated Total Reflectance.

CBM Conduction Band Minimum.

CEMOP Center of Excellence in Microelectronics and Optoelectronic Processes.

CENIMAT Centro de Investigação de Materiais.

CVD Chemical Vapor Deposition.

DIW Deionised Water.

DSC Differential Scanning Calorimetry.

EDS Electron Dispersive X-Ray Spectroscopy.

FET Field Effect Transistor.

FPD Flat-Panel Display.

FSR Full Scale Range.

FT-IR Fourier Transform-Infrared Spectroscopy.

GAXRD Grazing Angle X-Ray Diffraction.

I-V Current-Voltage.

IGZO Indium-Gallium-Zinc Oxide.

IPA Isopropyl Alcohol.

IZO Indium Zinc Oxide.

M-O-M Metal-Oxide-Metal.

NIR Near Infrared.

OV Oxidizing Valence.

PLD Pulsed Laser Deposition.

PR Photoresist.

Rms Root mean square.

RV Reducing Valence.

SCS Solution Combustion Synthesis.

SEM Scanning Electron Microscopy.

TAOS Transparent Amorphous Oxide Semiconductor.

TCO Transparent Conducting Oxide.

TFT Thin Film Transistor.

TG Thermogravimetry.

TSO Transparent Semiconducting Oxide.

UV Ultraviolet.

Vis Visible.

ZTO Zinc Tin Oxide.

Symbols

$\mathbf{A}$	Optical absorption
$\mathbf{C_i}$	Gate capacitance per unit area
$\mathbf{d_s}$	Thickness
$\mathbf{E_F}$	Fermi Level
$\mathbf{E_{opt}}$	Optical bandgap
φ	Fuel/oxidizer ratio
$\mathbf{g_m}$	Transconductance
h	Planck constant
$\mathbf{I}$	Current
$\mathbf{I_{DS}}$	Drain-to-source current
$\mathbf{I_G}$	Gate leakage current
$\mathbf{I_{off}}$	Drain current in off-state
$\mathbf{I_{on}}$	Drain current in on-state
$\mathbf{I_{on}/I_{off}}$	On-off current ratio
L	Channel length
ν	Frequency
N	Carrier concentration
$\mathbf{R}$	Reflectance

$\mathbf{R}^2$ Coefficient of determination

SS Subthreshold Slope

$\mathbf{T}$ Transmittance

$\mathbf{V}$ Voltage

$\mathbf{V_{DS}}$ Voltage between the drain and source

$\mathbf{V_{GS}}$ Voltage between the gate and source

$\mathbf{V_{Hyst}}$ Hysteresis voltage

$\mathbf{V_{on}}$ Turn-on voltage

$\mathbf{V_{T}}$ Threshold voltage

μ_{FE} Field-effect mobility

μ_{sat} Saturation mobility

σ Conductivity

$\mathbf{U}$ Urea

$\mathbf{W}$ Channel width

χ^2 Error function

Motivation and Objectives

Printed electronics is an expanding research area due to the potential applications in technology and their impact in society. Therefore, the development of solution-based materials is crucial for electronic applications, namely transparent flexible electronics. Metal oxide-based Thin Film Transistors (TFTs) produced by solution must have good properties such as high electrical performance, reproducibility, low cost and need to be processed at low temperatures to enable their application in plastic flexible substrates.

Since it is required a semiconductor material for the active channel layer of the TFTs, the synthesis of Transparent Amorphous Oxide Semiconductors (TAOSs) is essential to the development of solution-based electronics. Amorphous Indium-Gallium-Zinc Oxide (a-IGZO) is by far the most used semiconductor for oxide-based Flat-Panel Displays (FPDs) industry, due to its high electrical performance. However, when produced by solution, its electrical properties are not yet optimised, which is the main motive to the study of solution-processed a-IGZO thin films in this work.

The main objective of this work is the study, production and optimisation of solution-based a-IGZO thin films with the benefits of Solution Combustion Synthesis (SCS), by using solutions with metallic salts for their application as active channel layer in TFTs. To achieve this, several tasks will be employed:

- Production and characterisation of solutions with different metallic cations molar ratios;
- Production and characterisation of single and multilayer-active channel TFTs.

Chapter 1

Introduction

1.1 Metal oxide semiconductors

Over the recent years, research in electronic circuits fabricated on flexible transparent substrates led to the emergence of transparent flexible electronics, which is expected to meet emerging technological demands of most of microelectronics devices in the next years, in particularly displays [1, 2]. Although FPDs have been developed using Amorphous Silicon (a-Si) TFTs [3, 4], they have low field-effect mobility [1, 2, 5–7], and do not have high transparency and mechanical flexibility, the fundamental pillars of emerging flexible transparent electronics [6, 8]. Organic semiconductors have been intensively studied as a-Si substitute, however they have low mobility and are less stable [1, 6, 9]; moreover, polycrystalline Si has better mobility compared to a-Si, but it has poor area uniformity due to grain boundaries and processing issues [10, 11].

Metal oxides materials have emerged as an alternative to Si technology, due to their performance as (semi)conductive materials, with excellent optical transparency and electrical properties [12–15]. Among devices, transparent TFTs with metal oxide semiconductors as active layer have been extensively reported over the last years, with the development and optimisation of such materials being the key to the emergence of backplane TFTs for the next generation of FPDs [16–18]. Also, TFTs can be fabricated on flexible substrates if metal oxides are used for all components, including the active, dielectric and the electrodes layers [2, 19]. Metal oxides such as ZnO, Zinc Tin Oxide (ZTO) and Indium-Gallium-Zinc Oxide (IGZO) have been reported to various applications, including Active-Matrix Organic Light-Emitting Diode (AMOLED) displays, wearable sensor arrays, flexible displays and flexible solar cells [6, 8, 20–24].

Despite crystalline oxide semiconductors have been reported, they require very high annealing temperatures, incompatible with most flexible substrates [2, 5]. TAOSs have been intensively studied and reported since Hosono *et al.* proposed that oxides composed by post-transition-metal cations with an electron configuration of $(n-1)d^{10}ns^0$ (for $n \geq 5$) create a large overlap of their spherical isotropic ns-orbitals. These are the main elements of the conduction band, forming a conduction pathway with electron mobilities $> 10\ cm^2\,V^{-1}\,s^{-1}$, comparable to those of the corresponding crystalline phases [2, 25–29].

TAOSs are the most used class of materials as TFTs channel layers due to their superior electrical characteristics compared to Si-based and organic devices, and their development is essential for transparent electronic applications; their advantages include: high mobilities, excellent environmental/thermal stability, high optical transparency, low processing temperature, wide processing temperature window, low operation voltage, good uniformity and surface flatness, low leakage current, and ease of fabrication [17, 30, 31].

1.2 Amorphous indium-gallium-zinc oxide

IGZO is by far the most studied and used TAOS in different applications, mainly as semiconducting n-channel layer for FPD applications, due to the high field-effect mobility, small subthreshold slope (SS) and good uniformity. In addition, solution-processing of IGZO can be used to print TFTs, allowing to be used on flexible substrates [14, 32–36].

Structurally, a-IGZO is a multicomponent TAOS composed by three binary systems: In_2O_3, Ga_2O_3 and ZnO. The In^{3+} cations are the main constituent of the conduction band and the only with $n \geq 5$, meaning that their ns orbitals overlap and lead to high mobilities [26]. The incorporation of Zn^{2+} is fundamental to form stable amorphous structures, and while Indium Zinc Oxide (IZO) films have been reported with good properties to apply as Transparent Conducting Oxide (TCO), their application as Transparent Semiconducting Oxide (TSO) is not ideal due to the difficult in decreasing N below 10^{17} cm^{-3} [37]. In IGZO system, Ga^{3+} cation can form strong bonds with oxygen due to its high ionic potential and a small radius, therefore prevents excessive free carrier generation due to oxygen vacancies, although the lack of oxygen vacancies will prevent the prefilling the trapping states, reducing mobility [5, 26]. Furthermore, a quaternary system composed by cations with different sizes promotes the amorphous character and hence electrical uniformity, smooth surfaces and flexibility due to the lack of grain boundaries. [6, 27]. Given this, the electrical properties of a-IGZO can be easily tuned for specific functions by varying cations proportions, therefore an understanding of composition influence on electrical performance is crucial for developing a-IGZO-based TFTs [38].

1.3 Solution-based electronics

There are many deposition methods for metal oxide films; most of them are vacuum-based techniques, such as Atomic Layer Deposition (ALD), Chemical Vapor Deposition (CVD), Pulsed Laser Deposition (PLD) and radio frequency sputtering [2, 39–43]. Although they have been the most used and allow high-quality devices to be produced with reasonable performance and reliability, the high costs, temperature processing, need of vacuum sources and slow processing time are the major problems of these techniques [8, 44–46]. Therefore, solution-processing of metal oxides has become an attractive alternative due to the low-cost, high-throughput, roll-to-roll processing scalability and compositional control. Solution processes have lower equipment costs compared with vacuum-based processes [16, 46–48]. Typical solution deposition methods are spin-coating, spray pyrolysis, dip-coating, inkjet printing, and chemical bath deposition [49–53].

Research on solution-TAOSs has recently earned a lot of attention in large-scale fabrication of large-area electronics, because they are easily processed and have high transparency, opening new horizons for low-cost printable and transparent electronics on flexible substrates [9, 32]. Excellent films with ZnO, ZTO, IZO and IGZO grown by solution processes have been reported for the application of FPDs [13, 24, 30, 53] .

1.4 Solution combustion synthesis

One of the major drawbacks concerning solution-based routes for metal oxides is the need of an annealing step at relatively high temperatures to promote condensation and densification by the degradation of impurities, which adversely affect the device performance [25, 33, 48]. High annealing temperatures restrict the compatibility of TFTs with flexible substrates used in transparent flexible electronics [32, 44, 54, 55].

Given the emergence of flexible electronics, a general approach to low temperature solution processing of metal oxide films called SCS has been developed in the last years [8, 22, 56, 57]. In this method, the introduction of an oxidising agent (in the form of a metal nitrate salt) and a fuel as reducing agent (typically urea) into the precursor solution leads to the enhancement of the oxide precursor potential (Figure 1.1a). When the solution is spin-coated and annealed, a local highly exothermic chemical reaction occurs within the film, which leads to the formation of Metal-Oxide-Metal (M-O-M) lattice and a rapid efficient condensation. The required processing temperature (usually 250-300 °C) acts only as exothermic redox reaction initiator rather than a temperature that must be applied to achieve and to maintain decomposition and phase formation (Figure 1.1b) [58–60].

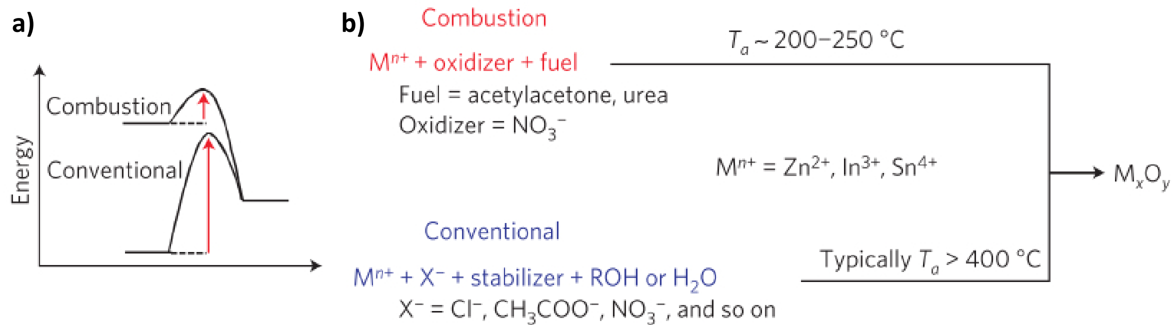

Figure 1.1: a) Schematic reaction coordinate comparing the energetics for SCS and conventional sol-gel solution processing; b) comparison of SCS and conventional reactions to form metal oxides. Adapted from [8].

1.5 Thin film transistors

TFTs are the fundamental building blocks of thin film electronics, because they are mostly used as on-off switches of the pixels in FPDs. They are the key devices for the application of TAOSs in transparent electronics.

A TFT is a Field Effect Transistor (FET) comprising three electrodes (gate, source and drain), a semiconductor placed between the source and drain electrodes, and an insulator (or dielectric) material inserted between the semiconductor and the gate electrode. By applying an electric field between source and drain electrodes, a current (I_{DS}) may flow between these electrodes, being modulated by a voltage applied in the gate electrode, which allows to turn on or off the device, acting as a switch. The semiconductor layer allows the formation of the conduction channel, while the dielectric layer blocks the flow of current between the semiconductor and the gate electrode (Figure 1.2) [37, 61]. TFTs can be classified according

two structures: in a coplanar structure, the electrodes are all on the same side, while in a staggered structure the gate is opposite to the side of drain and source electrodes. For each structure, two configurations are possible: top-gate (or normal) or bottom-gate (or inverted), depending on whether if the gate electrode is on top or bottom of the structure [62].

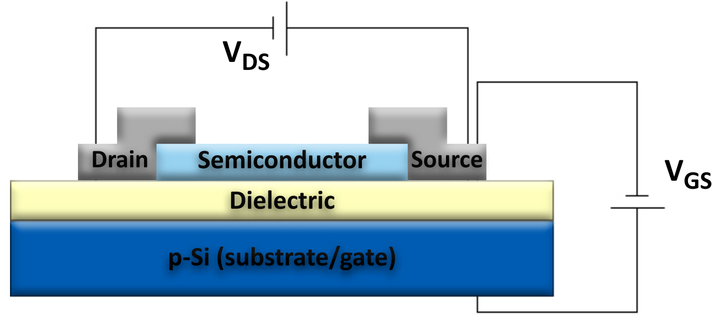

Figure 1.2: Structure of a staggered bottom-gate TFT.

Considering n-type TFTs, they can be classified as enhancement or depletion-mode, whether if the threshold voltage (V_T) is positive or negative. When $V_{GS}>V_T$, for a given applied positive V_{DS} a significant density of electrons is accumulated in semiconductor/dielectric interface, enough to have a current I_{DS} flowing between drain and source, which corresponds to the on-state of the TFT. In contrast, for $V_{GS}<V_T$, the device is off-state, for any given V_{DS} applied. There are two different operation regimes in the on-state, depending of V_{DS} value: linear and saturation regimes. The first one is described by Equation 1.1, when $V_{DS} < V_{GS} - V_T$ [62]:

$$I_{DS} = \frac{W}{L} C_i \mu_{FE} \left[(V_{GS} - V_T) V_{DS} - \frac{1}{2} V_{DS}^2 \right] \quad (1.1)$$

where W and L are the channel width and length, respectively. C_i is the gate capacity per unit area and μ_{FE} is the field-effect mobility. When $V_{DS} \ll V_{GS}-V_T$, by neglecting the quadratic term, a linear relation between I_{DS} and V_{DS} is obtained, maintaining an uniform channel charge density across the channel from source to drain.

The saturation regime is described by Equation 1.2, when $V_{DS} > V_{GS} - V_T$:

$$I_{DS} = \frac{W}{2L} C_i \mu_{sat} (V_{GS} - V_T)^2 \quad (1.2)$$

where μ_{sat} is the saturation mobility. In this regime, the region near the drain is completely depleted (pinch-off effect), leading to a constant and saturated I_{DS} [62].

By analysing the transfer and output curves of TFTs, the static characteristics can be obtained, depicted in Figure 1.3. Quantitative parameters such as mobility, on-off ratio current (I_{on}/I_{off}), V_T and turn-on voltage (V_{on}) can be extracted by the transfer characteristics (Figure 1.3a) [37, 62].

The mobility is the facility that carriers have to move through the material [5]; in the linear region the mobility is defined as μ_{FE} and is given by Equation 1.3:

$$\mu_{FE} = \frac{\frac{\partial \sqrt{I_D}}{\partial V_{GS}}}{\frac{W}{L} C_i V_{DS}} \tag{1.3}$$

For saturation regime mobility is defined as saturation mobility (μ_{sat}), given by Equation 1.4:

$$\mu_{sat} = \frac{\left(\frac{\partial \sqrt{I_D}}{\partial V_{GS}}\right)^2}{\frac{1}{2} C_i \frac{W}{L}} \tag{1.4}$$

The SS is the minimum V_{GS} to increase I_{DS} by one decade, and is obtained by Equation 1.5:

$$SS = \left(\left. \frac{d log I_{DS}}{d V_{GS}} \right|_{max} \right)^{-1} \tag{1.5}$$

The I_{on}/I_{off} is given by the ratio of the maximum and minimum I_{DS}; for typical electronic applications, it is usually required values above 10^6. V_T can be determined by different methodologies, such as linear extrapolation of $\sqrt{I_{DS}}$-V_{GS} plot for high V_{DS}; it gives the V_{GS} value at which the conductive channel is formed close to the semiconductor/dielectric interface. V_{on} corresponds to the V_{GS} value at which I_{DS} starts to increase. Output curves are plotted for different V_{GS} values, allowing to distinguish linear and saturation regimes, in function of V_{DS} for a fixed V_{GS} (Figure 1.3b) [37].

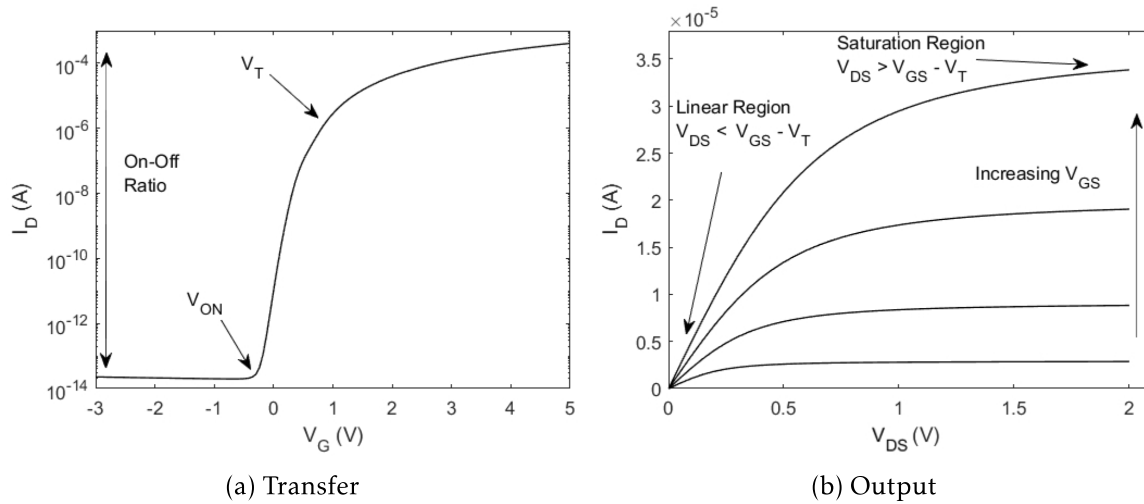

(a) Transfer (b) Output

Figure 1.3: Typical transfer and output characteristics of a TFT.

Chapter 2

Materials and Methods

This section summarises the main procedures and techniques used during this work, concerning the production of IGZO solutions, as well as their characterisation, and fabrication and electrical characterisation of IGZO TFTs.

IGZO TFTs were studied by varying the molar ratio of metallic cations and the number of active layers, to determine the best condition to apply as TFT channel. Finally, TFTs with the best performing conditions were produced and patterned.

2.1 Precursor solutions preparation and characterisation

The metallic oxide precursor solutions were prepared by dissolving individually indium (III) nitrate hydrate ($In(NO_3)_3 \cdot xH_2O$, Sigma, 99.9%), gallium (III) nitrate hydrate ($Ga(NO_3)_3 \cdot xH_2O$, Sigma, 99.9%) and zinc nitrate hexahydrate ($Zn(NO_3)_2 \cdot 6H_2O$, ACROS Organics, 98%) in 2-Methoxyethahol (2-ME) ($C_3H_8O_2$, ACROS Organics, >99.5%), to yield solutions with a concentration of 0.2 M. For the combustion reaction, urea ($CO(NH_2)_2$, Sigma, 98%) was added as fuel to each precursor solution, with molar ratios between urea and indium nitrate, gallium nitrate, and zinc nitrate of 2.5:1, 2.5:1 and 1.67:1 respectively, to guarantee the redox stoichiometry of the reaction (see Appendix A). All precursor solutions were magnetically stirred at 430 rpm for 1 h at room temperature in air environment.

The IGZO semiconductor precursor solutions were prepared by mixing indium nitrate, gallium nitrate and zinc nitrate precursor solutions to obtain In_2O_3:Ga_2O_3:ZnO molar ratios of of 1:1:1, 2:1:1, 2:1:2 and 3:1:1, all with a 0.2 M concentration. IGZO solutions were magnetically stirred at 430 rpm for at least 24 h at room temperature in air environment. All IGZO precursor solutions were filtrated through 0.2 µm hydrophilic filters.

Thermal and chemical characterisation of precursor solutions were performed by Differential Scanning Calorimetry (DSC) and Thermogravimetry (TG), Fourier Transform-Infrared Spectroscopy (FT-IR) and viscometer. DSC and TG analysis were performed under air atmosphere up to 500 °C with a 10 °C/min heating rate in an aluminium crucible with a punctured lid using a simultaneous thermal analyser, Netzsch (TG-DSC - STA 449 F3 Jupiter). FT-IR spectroscopy characterisation of IGZO solutions was performed using an Atenuated Total Reflectance (ATR) sampling accessory (Smart iTR) equipped with a single bounce diamond crystal on a Thermo Nicolet 6700 Spectrometer. The spectra were acquired with a 45° incident angle in the range of 4500-525 cm^{-1} and with a 3 cm^{-1} resolution. Viscosity measurements were performed by a BROOKFIELD Cap 2000+ with a rotation of 500 rpm, with the temperature increased up to 30 °C using a Cap01 spindle (see Appendix B).

2.2 Thin films deposition and characterisation

Prior to deposition all substrates (p^+Si with a 100 nm thermally grown SiO_2 layer, Si wafer and soda-lime glass, each one with an area of 2.5x2.5 cm^2) were cleaned in an ultrasonic bath at 60 °C in acetone for 15 min, then in Isopropyl Alcohol (IPA) for 15 min. Subsequently, the substrates were cleaned with Deionised Water (DIW) and dried under N_2, followed by a 15 min Ultraviolet (UV)/Ozone surface activation step for a distance lamp of 7 cm using a PSD-UV Novascan system.

To study the effect of the number of active layers, IGZO thin films were deposited onto SiO_2 substrates by sequentially spin coating 1 to 3 layers of IGZO precursor solution for 35 s at 3000 rpm (Laurell Technologies), followed by an immediate hot plate annealing at 300 °C for 30 min after each layer, in ambient conditions, to ensure the exothermic reaction. The structure of the films was assessed by Grazing Angle X-Ray Diffraction (GAXRD) , using a X'Pert PRO PANalytical diffractometer with Cu Kα line radiation (λ = 1.540598 Å) and an angle of incidence of the X-ray beam fixed at 0.75°, in the range of 20° to 50° (2θ). The films' surface morphology was studied by Scanning Electron Microscopy (SEM) Zeiss Auriga Crossbeam electron microscope and Atomic Force Microscopy (AFM) Asylum MFP3D. Electron Dispersive X-Ray Spectroscopy (EDS) was performed to study the chemical composition of the thin films. Spectroscopic ellipsometry was used to measure the thin films thickness deposited on Si substrates, with an energy range from 1.5 to 5.5 eV and an incident angle of 45° using a Jobin Yvon Uvisel system. The acquired data were modulated using the DELTAPSI software, and the fitting procedure was done pursuing the minimisation of the error function (χ^2). FT-IR spectroscopy characterisation of thin films deposited in Si substrates was performed the same way as used for IGZO precursor solutions. The optical properties were obtained by a Perkin Elmer lambda 950 UV/Visible (Vis)/Near Infrared (NIR) spectrophotometer. The transmittance (T) and reflectance (R) were obtained in a wavelength range from 200 to 2500 nm.

2.3 Electronic devices fabrication and characterisation

Non-patterned TFTs were produced in a staggered bottom-gate, top-contact structure by spin coating IGZO thin films (see section 2.2) onto 100-nm-thick SiO_2 thermally oxidised on p^+Si wafer ($C_i = 35 \times 10^{-9}$ F/m^2). Aluminium source and drain electrodes (80 nm thick) were deposited on IGZO films via a shadow mask by thermal evaporation. The channel length and width of the IGZO TFTs were 1400 µm and 100 µm, respectively (W/L=14). A post-annealing step was performed on a hot plate for 1 h at 120 °C in air environment.

Regarding the semiconductor patterning of TFTs, positive Photoresist (PR) AZ ECL 3012 was spin-coated onto the IGZO thin films (Headway Research PWM32), firstly at 3000 rpm for 10 s and then at 4000 rpm for 20 s. After that, substrates were soft-baked in a hot-plate at 115 °C for 1 min and 15 s. Lithography mask with semiconductor patterns was aligned with the substrate in a mask aligner (Karl-Suss MA6); then, UV exposure in soft-contact mode was proceeded for 2.5 s. Substrates were dipped in a developer solution (AZ 726 MIF) to

obtain the PR pattern, and immersed in etching solution ($HCl \cdot H_2O$ 20:1) for 20 s to etch IGZO with the desired pattern, then dipped sequentially in acetone and DIW to remove the remaining PR and water to clean the sample. The final step comprised the aluminium contacts patterning: first PR was spin-coated and soft-baked with the same conditions as for IGZO, followed by alignment of a negative mask containing source-drain electrodes patterns with the existing IGZO ones to UV exposure. Substrates were dipped in developer and aluminium was deposited via thermal evaporation. Finally, the aluminium in excess was removed by dipping the substrates in acetone to remove PR and all aluminium above PR (lift-off). A post-annealing step was performed on a hot plate for 1 h at 120 °C in air environment.

Electrical characterisation was performed by measurement of current-voltage characteristics of the devices using a semiconductor parameter analyser (Agilent 4155C) attached to a microprobe station (Cascade M150), inside a Faraday cage, in the dark and room temperature.

Chapter 3

Results and Discussion

This chapter discusses the results regarding the characterisation of solutions, thin films and the electrical characterisations of the produced TFTs.

3.1 Solutions characterisation

Analysis of elements through characteristic spectra of IGZO thin films using urea as fuel was performed by FT-IR, using ATR, and data presented in wavenumber range of 4000-525 cm^{-1}. Figure 3.1 depicts the FT-IR spectra of IGZO solutions for each molar ratio studied. Correction of the atmospheric contribution was performed for all spectra. Most of the peaks are related with organic compounds present in 2-ME, identified in Table 3.1. [63, 64].

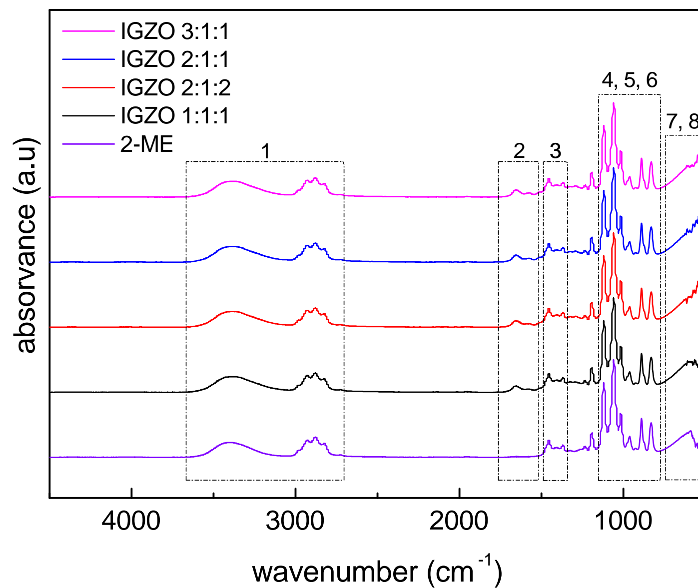

Figure 3.1: FT-IR spectra of IGZO solutions, with different molar ratios.

Table 3.1: Characteristic absorbance peaks and associated vibrational modes of the corresponding chemical bonds for analysed FT-IR spectra of IGZO solutions.

Number	Position (cm^{-1})	Mode type	Chemical bond
1	3500	Stretching vibration	M-OH
2, 5	1620, 1015	Bending vibration	M-OH
3	1388	Stretching vibration	$NO_3{}^-$
4	1107	Transversal optic stretching	Si-O
6	833	Bending vibration	$NO_3{}^-$
7, 8	620, 509	Stretching vibration	M-O

3.1.1 Thermal characterisation

Thermal characterisation was performed to evaluate the decomposition of metal oxides. IGZO 0.2 M solutions were analysed, with and without urea for further comparison. Figure 3.2 depicts the DSC-TG results for IGZO 3:1:1 with and without urea in 2-ME. DSC and TG results for IGZO 1:1:1, 2:1:2 and 2:1:2 are represented in Appendix C.

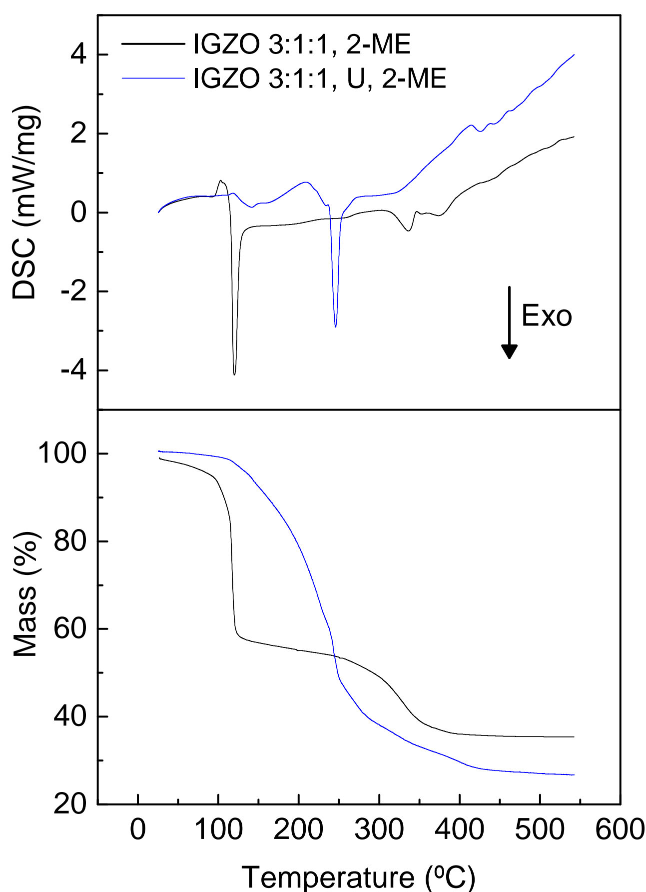

Figure 3.2: DSC-TG analysis of IGZO 3:1:1 precursor solutions with 2-ME as solvent and using urea as fuel or not.

Regarding IGZO solution with urea, two endothermic peaks are present (at 112 °C and 211 °C) accompanied by a mass loss, related with evaporation of solvent and water. Then there is an intense exothermic peak (at 245 °C) accompanied by a large mass loss, corresponding to the redox reaction of the formation of oxides. A smaller endothermic peak at 426 °C is related with degradation of residual organics.

Concerning IGZO solution without urea, it is visible a small endothermic peak around 100 °C, which is related with water and solvent evaporation events [59]. Then, there is an intense exothermic peak at 121 °C accompanied by an abrupt mass loss, corresponding to the formation of oxides. Comparing with the solution without urea, the exothermic peak at lower temperature can be justified by the solvent 2-ME acting as fuel itself to initiate the redox reaction. According to Salgueiro *et al.* the organic solvent possesses a reducing nature, then it can also act as fuel, leading to a combustion reaction [59]. The exothermic

peak of IGZO with urea is more intense, since the addition of urea increases the organic content in the solution, therefore additional energy is required to ensure the combustion. Also, the exothermic peak at 335 °C is associated with residual organics, meaning that the degradation of organics requires at least two phases without use of urea. Nevertheless, the exothermic peak of IGZO with urea occurs at a temperature below 300 °C, meaning that the annealing temperature used during the production of thin films is enough to promote the redox reaction.

It is important to mention that process parameters can strongly influence the DSC-TG measurements, namely the heating rate and the evaporation solvent step previous to DSC-TG analysis. In the case of solutions with urea, during the evaporation of solvent some urea could initiate combustion reaction prior to the DSC-TG analysis, leading to a non-stoichiometric condition during DSC-TG measurements, with the fuel/oxidiser ratio (φ) < 1 (see Appendix A). This leads to the formation of more organic compounds as products of the reaction.

3.2 Thin films characterisation

FT-IR spectra of 3-layer IGZO thin films spin coated on Si substrates after being annealed at 300 °C for 30 min were obtained, with correction of the atmospheric contribution performed for all spectra (Figure 3.3).

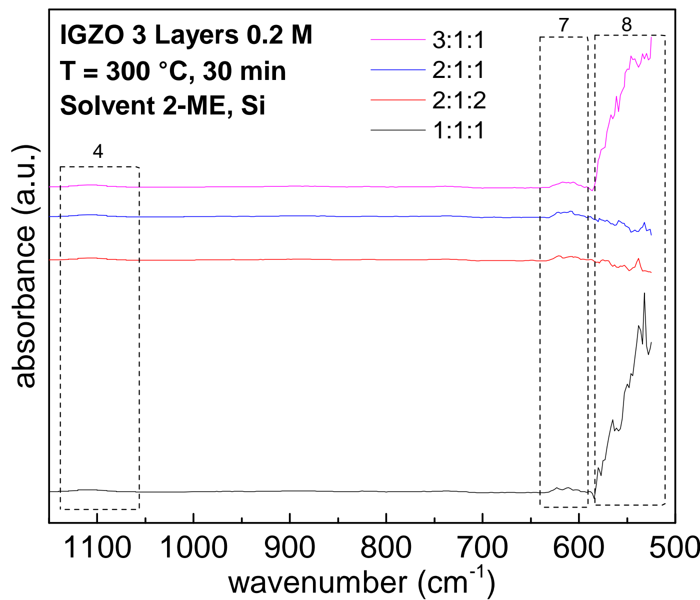

Figure 3.3: FT-IR spectra of 3-layer IGZO thin films on Si substrates, with different molar ratios, after annealing at 300 °C for 30 min.

Si-O peak is observed at 1107 cm^{-1}, which is related with Si substrate; two M-O stretching vibration peaks at 620 cm^{-1} and 509 cm^{-1}, are observed (although only the increase of the latter peak is observed due to the range measurement of the equipment), confirming

the presence of M-O bonds in thin films after annealing. Note that FT-IR spectra above $1150\,cm^{-1}$ is not shown in Figure 3.3 because no peaks were observed.

3.2.1 Optical characterisation

Spectroscopic ellipsometry was used to measure the thickness of all thin films. The measured thickness values are shown on table 3.2, for each number of IGZO layers and molar ratios.

Table 3.2: Thickness of measured films (nm) by spectroscopy ellipsometry, for all IGZO molar ratios, with films spin coated onto Si substrates and annealed at 300 °C.

Number of Layers	IGZO molar ratio			
	1:1:1	2:1:2	2:1:1	3:1:1
1	13.6 ± 0.1	14.2 ± 0.1	13.7 ± 0.1	14.2 ± 0.1
2	28.1 ± 0.2	27.4 ± 0.3	24.0 ± 0.6	26.6 ± 0.2
3	38.8 ± 0.1	38.2 ± 0.3	36.2 ± 0.3	35.9 ± 0.4

For a fixed number of spin coated layers, the values are similar, regardless the molar ratios.

Both transmittance and reflectance of IGZO thin films on soda-lima glass substrates were measured, in a wavelength range of 200-2500 nm with a step of 3 nm. Figure 3.4 depicts transmittance spectra for IGZO thin films. The values of transmittance are around 90% in almost entire wavelength range. The increasing number of deposited layers affects the transmittance in the visible region due to the increase of the thickness; despite this, values between 85-90% are obtained for all conditions [65]. Reflectance spectra of IGZO thin films are represented in Appendix D.

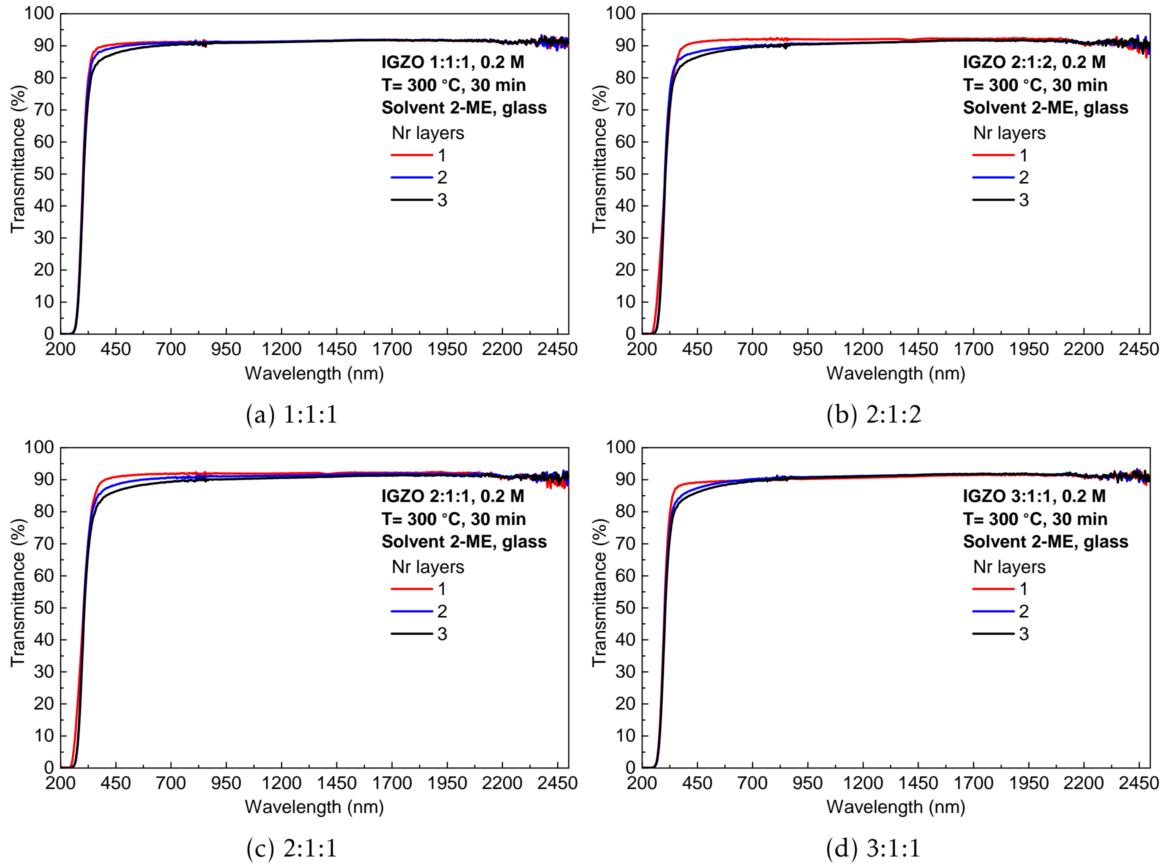

(a) 1:1:1

(b) 2:1:2

(c) 2:1:1

(d) 3:1:1

Figure 3.4: Transmittance spectra of IGZO thin films on glass substrates.

E_{opt} values were obtained by Tauc-bandgap plots; the values are represented in table 3.3, and the calculation steps are explained in Appendix E.

Table 3.3: E_{opt} of measured films (eV) determined by linear fit of Tauc-plots, for all IGZO molar ratios, with films spin coated onto Si substrates and annealed at 300 °C.

Number of Layers	IGZO molar ratio			
	1:1:1	2:1:2	2:1:1	3:1:1
1	3.73	3.75	3.71	3.72
2	3.74	3.73	3.74	3.73
3	3.72	3.74	3.68	3.72

In multicomponent oxides, E_{opt} is affected by atomic composition of each cation, and values are generally closer to the E_{opt} of the dominant cations. Therefore, In IGZO 2:1:1 and 3:1:1 (4:2:1 and 6:2:1 in atomic ratio, respectively), it is expected to obtain an E_{opt} similar to the obtained in literature by In_2O_3 (about 3.5-3.7 eV). In IGZO 1:1:1 (2:2:1 in atomic ratio), the Ga_2O_3 content leads to higher E_{opt} values because it has a E_{opt} around 4.16 eV; therefore obtained values were intermediate to E_{opt} of In_2O_3 and Ga_2O_3, as expected. Finally, IGZO 2:1:2 (4:2:2) ZnO should contribute to a decrease in E_{opt} due to its lower reported E_{opt} (3.24 eV). Despite this, all obtained values are in a range of 3.68-3.75 eV, regardless the composition. These small variations might be attributed to the introduction

of defects due to a high porous structure in all thin films, combined with small thickness values. Nevertheless, all values are above 3 eV, meaning that all films produced meet the required criteria for optical transparent applications [37].

3.2.2 Structural and morphological characterisation

To evaluate the amorphous character of the thin films structure, GAXRD measurements were performed on 3-layer IGZO thin films annealed at 300 °C. GAXRD diffractograms of thin films with IGZO molar ratios of 1:1:1, 2:1:1, 2:1:2 and 3:1:1 are shown in Figure 3.5.

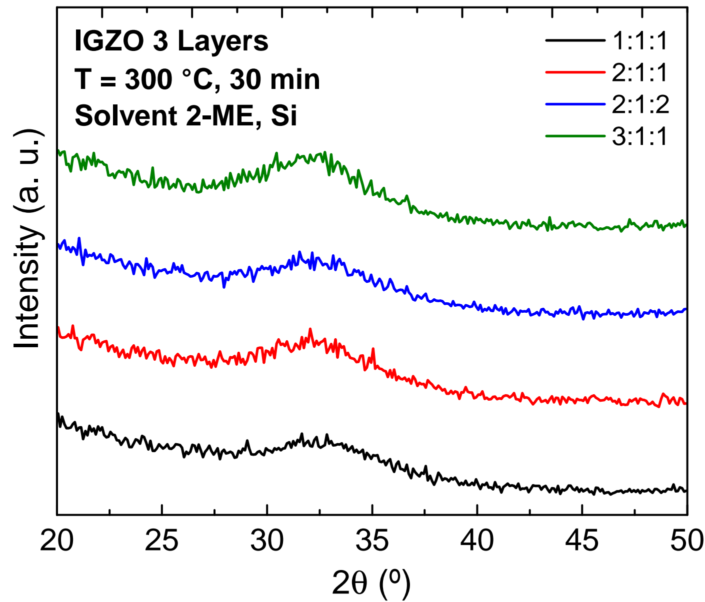

Figure 3.5: GAXRD diffractograms of 3-layer IGZO thin films on Si substrates, with different molar ratios.

GAXRD diffractograms have shown that thin films are amorphous independently the IGZO molar ratio, exhibiting only a broad peak centred at 2θ = 32-34° in all samples, typical of amorphous binary and multicomponent oxide films composed by indium, gallium and/or zinc [37, 66, 67]. Since IGZO is a quaternary multicomponent oxide composed by three different metallic cations, the degree of disorder of the structure is higher than binary/ternary oxides as aforementioned before in section 1.2, therefore IGZO it is harder to crystallise at this temperature.

The surface topography of IGZO thin films spin coated on Si substrates was measured using AFM. Surface roughness was obtained by measuring Root mean square (Rms) in alternate mode and the topographic images were analysed in data analysis software Gwyddion. Surface topographies of all thin films are presented in Figure 3.6. The surface roughness of the films was determined from the AFM height profile of a 2×2 μm^2 area scan. Acquired AFM images for films revealed a very smooth and homogeneous surface, with Rms close to 0.2 nm in all cases, typical for reported combustion-processed amorphous semiconductors [6, 25].

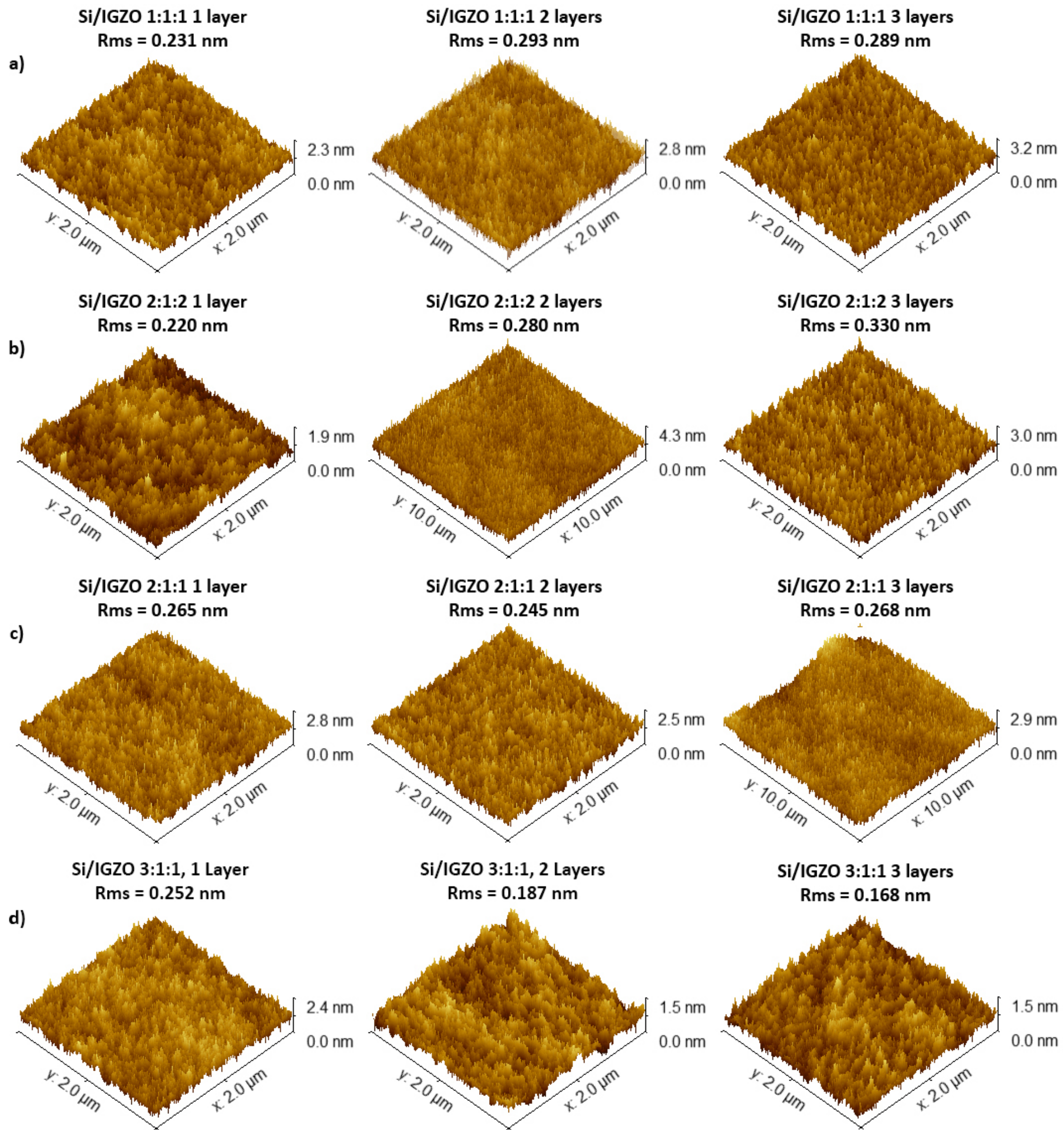

Figure 3.6: Morphological characterisation IGZO a) 1:1:1, b) 2:1:2, c) 2:1:1 and d) 3:1:1 thin films for a concentration of 0.2 M. AFM deflection images of 2×2 μm^2 to an annealing at 300 °C during 30 min, with different number of IGZO layers.

SEM images were acquired for all 3-layer IGZO thin films on Si substrates; EDS technique was used to determine chemical composition the thin films. Figure 3.7 depicts the surface of IGZO 3:1:1 3-layer deposited on Si.

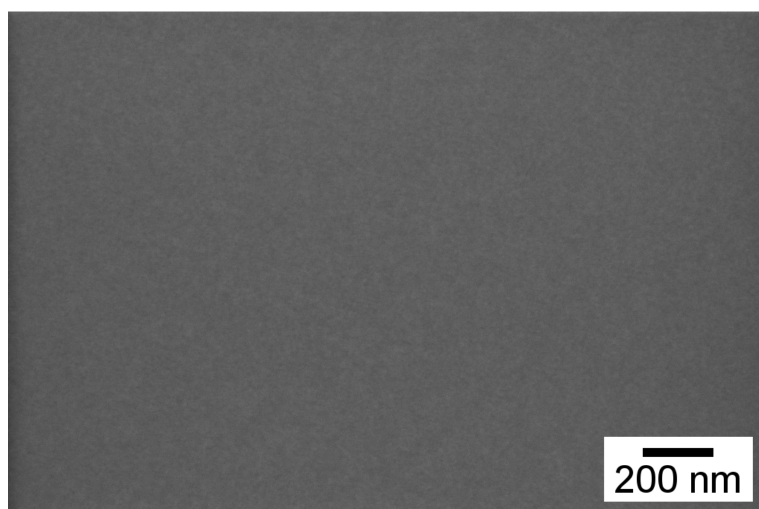

Figure 3.7: SEM surface of 3-layer IGZO 3:1:1 thin film on Si substrate, with annealing 300 °C for 30 min.

Despite the resolution of the image, crystalline structures are not visible, giving support to GAXRD results regarding the amorphous character of the thin films.

Figure 3.8 shows the obtained molecular concentration of each metallic oxide, for each studied IGZO molar ratio. EDS analysis results have shown that most of the molecular compositions are closer to the expected; some discrepancies, especially regarding In content in IGZO 1:1:1, can be related to non-uniformity of the scanned area during EDS analysis.

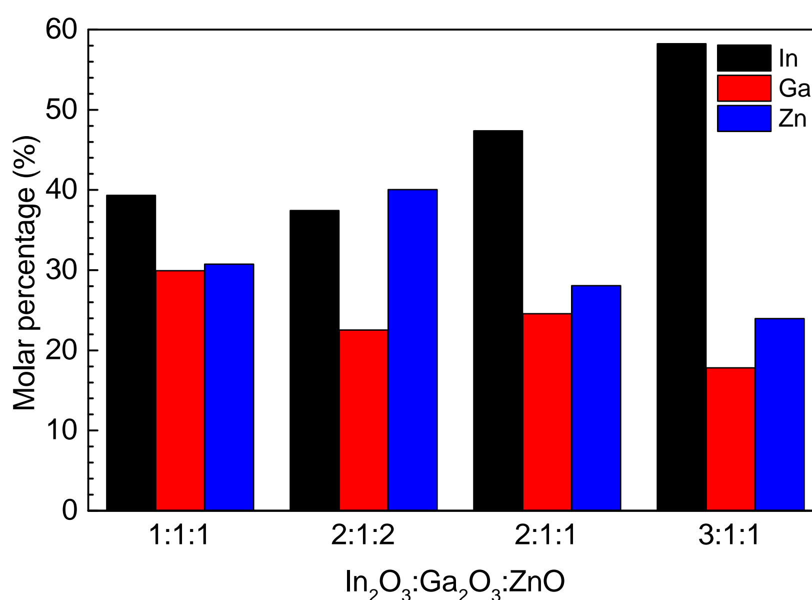

Figure 3.8: Molecular concentration (%) of each metallic oxide in IGZO thin films with 3 layers on Si substrates, annealed at 300 °C for 30 min.

3.3 Electrical characterisation of solution-based IGZO TFTs

The main focus of this work is the study of solution-processed IGZO applied as channel layer on TFTs, therefore electrical characterisation of these devices is crucial, by measuring the Current-Voltage (I-V) curves, which allow to determine their important electric parameters, as well evaluate the current behaviour in function of the voltage applied.

For all devices, four consecutive stabilisation characteristics were measured (one single and three appends), with V_{GS} ranging from -10 to 20 V and V_{DS} values being 20 and 10 V for non-patterned and patterned devices, respectively. Then, transfer curves were performed in double sweep mode and used to extract V_{on}, V_T,V_{Hyst}, SS, μ_{sat} and I_{on}/I_{off}, with the same values of V_{GS} range and V_{DS}. Output characteristics were measured with V_{DS} values described before and 8 steps of V_{GS}, from 0 to 20 V. The transconductance (g_m) variation with V_{GS}-V_T was obtained for each condition, being the plots depicted in Appendix F. Electrical parameters were extracted for the best three performing devices and their average and standard deviation were calculated.

All non-patterned devices studied have a W/L of 1400 μm/100μm, while patterned devices were studied with W/L values of 80/20, 160/20 and 320/20 μm/μm.

Ageing effects are also presented in this section, being depicted in the I-V curves measured when devices were fabricated and 8 weeks later.

In this work four different IGZO molar ratios were studied: 1:1:1, 2:1:2, 2:1:1 and 3:1:1. These proportions were chosen in order to evaluate the influence of each cation composition in TFT performance. IGZO 1:1:1 has the same percentage of each oxide molecules, while IGZO 2:1:2 has more indium and zinc than IGZO 1:1:1. IGZO 2:1:1 has indium as dominant cation, and as it will be seen later, this is a crucial condition to obtain TFTs with desired behaviour and electrical parameters; for this reason, IGZO 3:1:1 using urea was also studied.

Prior to the study of IGZO TFTs based on solution combustion synthesis route, TFTs without urea as fuel were fabricated for further comparison. Figure 3.9 depicts the stabilisation characteristics of TFTs with IGZO 1:1:1, 2:1:2 and 2:1:1 without urea.

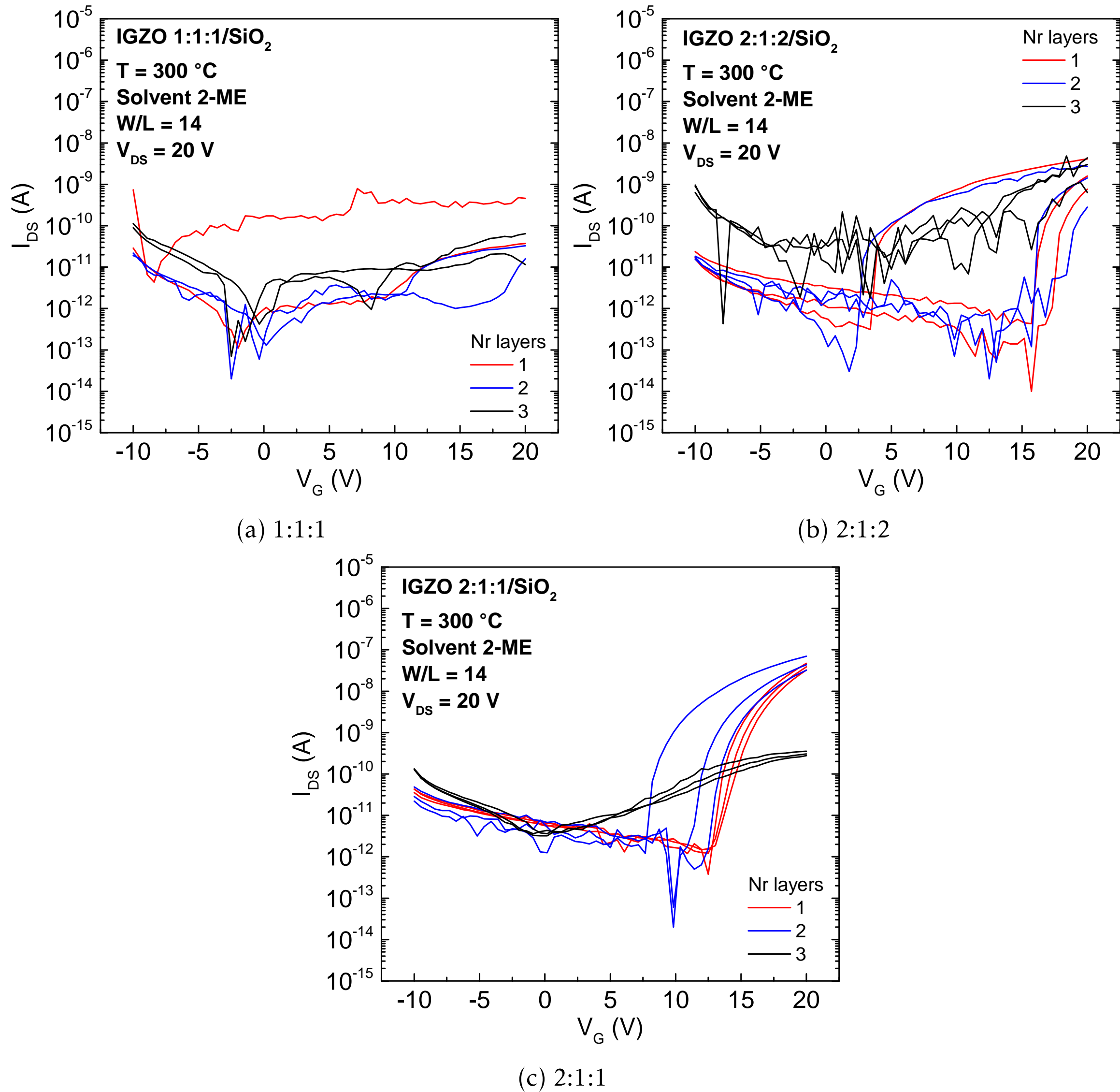

(a) 1:1:1

(b) 2:1:2

(c) 2:1:1

Figure 3.9: Stabilisation curves of IGZO 1:1:1, 2:1:2 and 2:1:1 0.2 M TFTs with 1, 2 and 3 active layers, without urea as fuel.

Most of the devices studied present high instability; TFTs with IGZO 2:1:1 1 layer have shown better stability and their electrical parameters were extracted from transfer curve present in Figure 3.10. The device has an I_{on}/I_{off} of 6.4×10^4, V_{on}, V_T and V_{hyst} of 14.29, 18.81 and 1.8, respectively, an SS of 0.92 V/dec and μ_{sat} of 0.01 $cm^2 V^{-1} s^{-1}$. In all cases, instability can be attributed to incomplete formation of M-O-M lattice during annealing. Using urea as fuel might ignite a more intense exothermic reaction, releasing more local energy to fully convert metal hydroxides into M-O-M lattice, with less residual organics, as it was observed in thermal characterisation of precursor solutions. Besides this, it can be observed an increasing degree of instability with higher number of layers. This can be related with increasing number of interfaces between deposited semiconducting layers, where electron traps can be incorporated, consequently degrading severely stabilisation and electric parameters.

Concerning the metallic cations composition, IGZO 2:1:1 has shown better stabilisation characteristics probably because, as it will be seen later in IGZO TFTs produced with urea as fuel, the presence of indium as dominant cation is crucial to obtain better stability and electrical parameters.

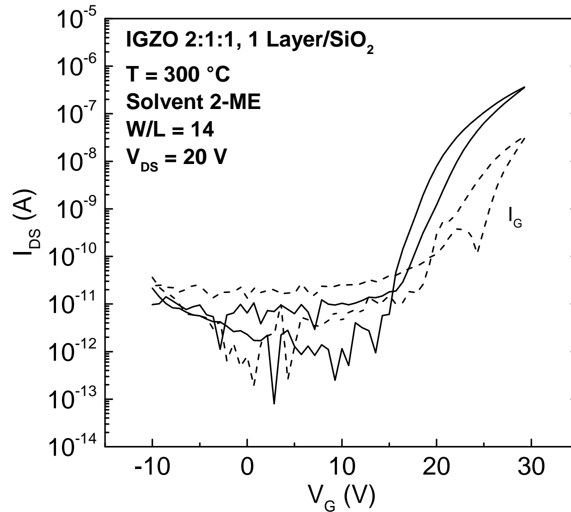

Figure 3.10: Transfer curve of IGZO 2:1:1 0.2 M TFTs with 1 active layer, without urea as fuel.

TFTs with IGZO 1:1:1 molar ratio using urea as fuel were studied. Figure 3.11 depicts the transfer curve of a TFT with 1 IGZO 1:1:1 active layer, and extracted electrical parameters of three devices are shown in Table 3.4. TFTs with 2 and 3 IGZO 1:1:1 active layers have shown high instability (see Appendix G).

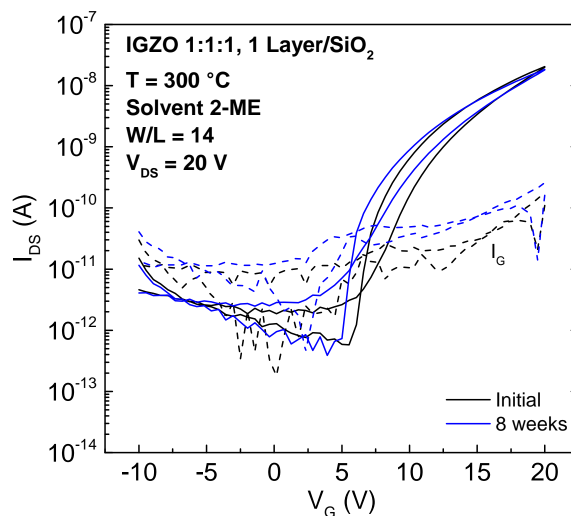

Figure 3.11: Transfer curve of IGZO 1:1:1 0.2 M TFT with 1 active layer, measured initially and 8 weeks later.

Table 3.4: Average and standard deviation of electrical parameters of three measured TFTs with IGZO 1:1:1 1 layer as channel layer, measured initially and 8 weeks later.

Layers	Age	I_{on}/I_{off}	V_{on} (V)	V_T (V)	V_{Hyst} (V)	SS (V/dec)	μ_{sat} ($cm^2 V^{-1} s^{-1}$)
1	Initial	$(4.26 \pm 1.52) \times 10^4$	4.46 ± 1.15	7.52 ± 0.37	1.68 ± 0.12	0.91 ± 0.38	$(9.00 \pm 0.82) \times 10^{-4}$
	8 weeks	$(2.43 \pm 0.44) \times 10^4$	3.93 ± 1.16	6.67 ± 0.61	1.52 ± 0.09	0.71 ± 0.07	$(7.30 \pm 1.20) \times 10^{-4}$

Figure 3.12 depicts the transfer curves of TFTs with 1 and 2 IGZO 2:1:2 active layers; IGZO 2:1:2 TFTs with 3 layers have shown high instability, as shown in Figure G.2 in Appendix G. Extracted electrical parameters of three devices are shown in Table 3.5.

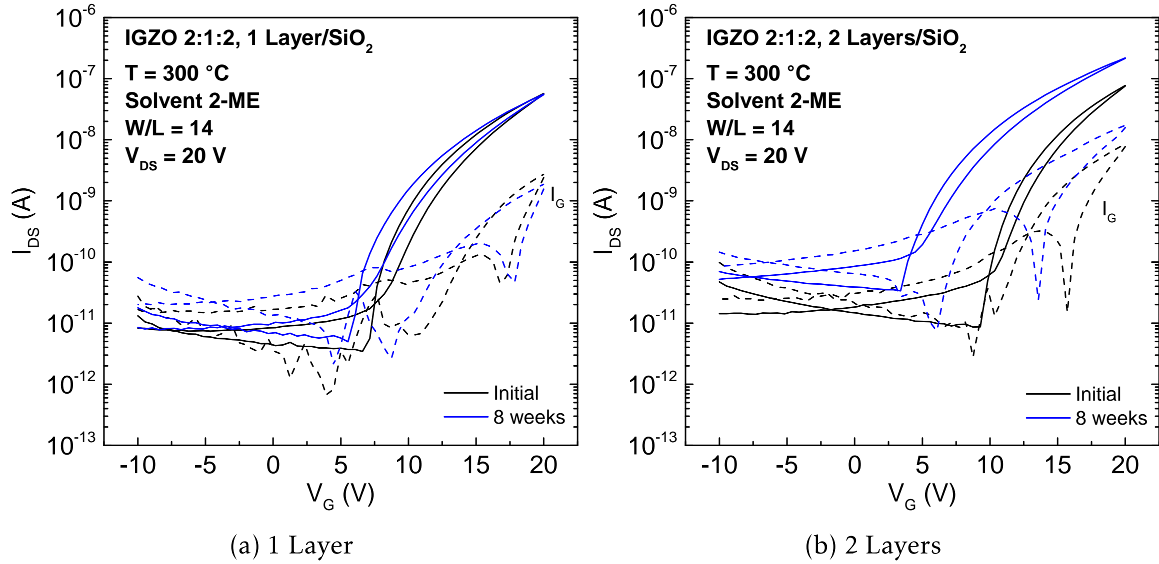

(a) 1 Layer (b) 2 Layers

Figure 3.12: Transfer curves of IGZO 2:1:2 0.2 M TFTs with 1 and 2 active layers, measured initially and 8 weeks later.

Table 3.5: Average and standard deviation of electrical parameters of three measured TFTs with IGZO 2:1:2 as channel layer, measured initially and 8 weeks later.

Layers	Age	I_{on}/I_{off}	V_{on} (V)	V_T (V)	V_{Hyst} (V)	SS (V/dec)	μ_{sat} ($cm^2 V^{-1} s^{-1}$)
1	Initial	$(1.35 \pm 0.72) \times 10^4$	6.07 ± 1.00	9.10 ± 0.81	1.09 ± 0.35	1.11 ± 0.31	$(3.00 \pm 0.70) \times 10^{-3}$
	8 weeks	$(7.82 \pm 3.49) \times 10^3$	6.25 ± 0.50	9.23 ± 0.43	1.33 ± 0.16	0.97 ± 0.19	$(2.33 \pm 0.47) \times 10^{-3}$
2	Initial	$(1.02 \pm 0.42) \times 10^4$	7.68 ± 2.21	9.63 ± 1.77	1.15 ± 0.23	0.88 ± 0.09	$(6.00 \pm 0.14) \times 10^{-3}$
	8 weeks	$(9.13 \pm 3.88) \times 10^3$	4.46 ± 1.52	7.46 ± 0.79	1.09 ± 0.16	1.17 ± 0.25	$(5.53 \pm 0.18) \times 10^{-3}$

Transfer curves of TFTs with 1, 2 and 3 IGZO 2:1:1 layers are shown in Figure 3.13. Statistic parameters of the three best devices are represented in Table 3.6.

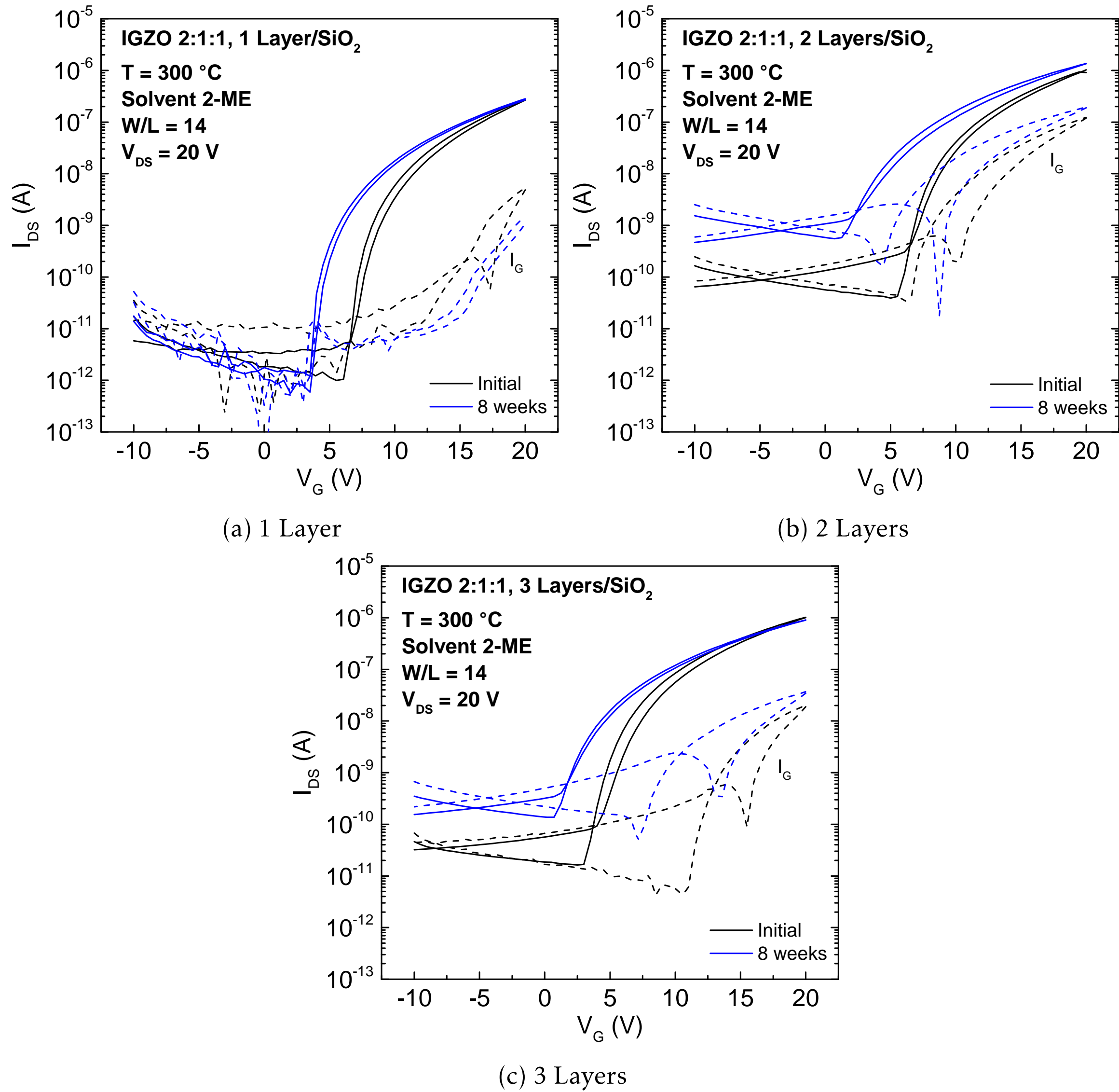

(a) 1 Layer

(b) 2 Layers

(c) 3 Layers

Figure 3.13: Transfer curves of IGZO 2:1:1 0.2 M TFTs with 1, 2 and 3 active layers, measured initially and 8 weeks later.

Table 3.6: Average and standard deviation of electrical parameters of three measured TFTs with IGZO 2:1:1 as channel layer, measured initially and 8 weeks later.

Layers	Age	I_{on}/I_{off}	V_{on} (V)	V_T (V)	V_{Hyst} (V)	SS (V/dec)	μ_{sat} ($cm^2 V^{-1} s^{-1}$)
1	Initial	$(1.48 \pm 0.75) \times 10^5$	6.07 ± 0.44	8.14 ± 0.51	0.75 ± 0.09	0.61 ± 0.05	$(1.00 \pm 0.03) \times 10^{-2}$
	8 weeks	$(4.18 \pm 0.47) \times 10^5$	3.61 ± 0.23	6.96 ± 0.16	0.74 ± 0.27	0.47 ± 0.05	$(7.33 \pm 0.1) \times 10^{-3}$
2	Initial	$(1.50 \pm 0.50) \times 10^4$	4.46 ± 0.75	6.33 ± 0.70	0.47 ± 0.06	0.86 ± 0.27	$(2.33 \pm 0.47) \times 10^{-2}$
	8 weeks	$(5.08 \pm 2.34) \times 10^3$	0.01 ± 0.67	4.42 ± 0.42	0.74 ± 0.07	2.01 ± 0.26	$(2.33 \pm 0.47) \times 10^{-2}$
3	Initial	$(4.54 \pm 2.86) \times 10^4$	4.00 ± 1.41	5.99 ± 1.40	0.80 ± 0.11	0.95 ± 0.20	$(2.30 \pm 0.47) \times 10^{-2}$
	8 weeks	$(1.02 \pm 0.41) \times 10^4$	0.71 ± 0.44	2.96 ± 0.38	0.45 ± 0.02	1.24 ± 0.13	$(2.00 \pm 0.03) \times 10^{-2}$

TFTs with IGZO 3:1:1 were studied, to evaluate the influence of indium content in electrical parameters. Transfer curves of TFTs with 1, 2 and 3 IGZO 3:1:1 layers are shown in Figure 3.14. Statistic parameters of the three best devices are represented in table 3.7.

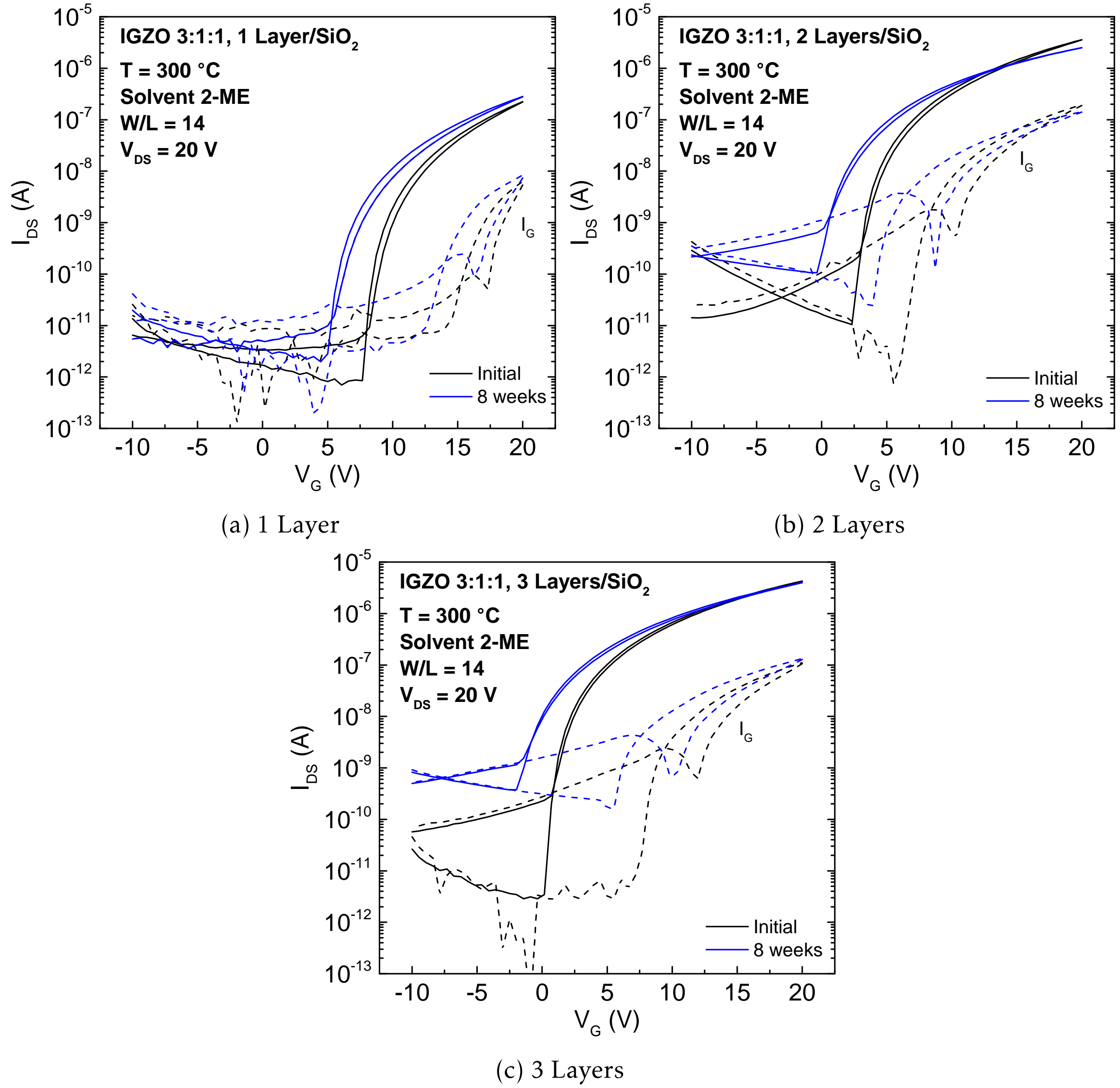

(a) 1 Layer

(b) 2 Layers

(c) 3 Layers

Figure 3.14: Transfer curves of IGZO 3:1:1 0.2 M TFTs with 1, 2 and 3 active layers, measured initially and 8 weeks later.

Table 3.7: Average and standard deviation of electrical parameters of three measured TFTs with IGZO 3:1:1 as channel layer, measured initially and 8 weeks later.

Layers	Age	I_{on}/I_{off}	V_{on} (V)	V_T (V)	V_{Hyst} (V)	SS (V/dec)	μ_{sat} ($cm^2\,V^{-1}\,s^{-1}$)
1	Initial	$(1.99 \pm 0.57) \times 10^5$	7.86 ± 0.25	9.57 ± 0.25	0.67 ± 0.14	0.49 ± 0.04	$(1.00 \pm 0.03) \times 10^{-2}$
	8 weeks	$(7.45 \pm 3.91) \times 10^4$	5.71 ± 1.01	8.67 ± 0.48	0.64 ± 0.03	0.69 ± 0.12	$(9.00 \pm 0.03) \times 10^{-3}$
2	Initial	$(5.31 \pm 2.54) \times 10^5$	1.96 ± 0.50	4.09 ± 0.39	0.59 ± 0.19	0.51 ± 0.01	$(6.67 \pm 0.94) \times 10^{-2}$
	8 weeks	$(7.89 \pm 7.35) \times 10^4$	0.18 ± 0.44	2.29 ± 0.61	0.49 ± 0.12	0.76 ± 0.17	$(3.00 \pm 0.03) \times 10^{-2}$
3	Initial	$(8.17 \pm 3.48) \times 10^5$	0.40 ± 0.44	1.72 ± 0.42	0.31 ± 0.04	0.43 ± 0.05	$(7.33 \pm 0.47) \times 10^{-2}$
	8 weeks	$(9.01 \pm 2.00) \times 10^3$	-1.96 ± 0.03	0.80 ± 0.18	0.35 ± 0.02	1.28 ± 0.11	$(5.00 \pm 0.03) \times 10^{-2}$

Regarding the effect of the number of semiconductor layers, it is noted that V_{on} and V_T decreased with the increasing number of layers, regardless the molar ratio composition. These effects are essentially due to higher number of free carriers in the bulk of a thicker

active layer, leading to an easier accumulation of charges in the semiconductor/dielectric interface. Thus, the formation of a highly conductive channel occurs at lower V_{GS} values. An increasing I_{off} with the number of layers is generally visible in transfer and stabilisation curves, associated with the decreasing resistance of the active layer with increasing thickness, leading to a higher flow of electrons passing through source and drain electrodes [39]. The effect of the number of layers on I_{on}/I_{off} and SS is easily noted with the ageing effect, as it will be explained further ahead.

Concerning composition effects, in IGZO TFTs 1:1:1 and 2:1:2 the performance of both conditions was poorer than 2:1:1 and 3:1:1. In amorphous films, mobility is expected to increase for higher N, which increases for lower gallium or zinc concentrations. The Conduction Band Minimum (CBM) is fundamentally composed by In^{3+}, where potential barriers from random distribution of zinc and gallium exist; an increasing N leads to decrease in potential barriers from structural randomness, because higher N is associated with lower gallium and/or zinc content; also, it causes the dislocation of the Fermi level (E_F) above these potential barriers, enhancing mobility. Moreover, less zinc content increases the possibility of direct overlap of s-orbital of neighbouring In^{3+} ions and hence enhances the mobility. Given this, the dominant-indium content is crucial for high-mobility IGZO TFTs, and gallium and zinc content should be in sufficient amount to prevent the crystallisation of the films and guarantee the amorphous character of the structure. This sustains the low-mobilities and I_{on}/I_{off} of IGZO 1:1:1 and 2:1:2 [2, 37].

TFTs with IGZO 1:1:1 2 and 3 layers, and IGZO 2:1:2 with 3 layers have shown high instability, which can be associated with their compositions combined with higher number of interfaces that are responsible for introducing more defects, leading to instability in the devices (see Appendix G).

TFTs with IGZO 1:1:1 1-layer possess low I_{on}/I_{off} and μ_{sat}, due to high gallium content, since it leads to suppression of free carriers, therefore for higher levels of gallium doping the electron transport is expected to degrade, decreasing both I_{on} and I_{off}, μ_{sat}; V_T and V_{on} have high values because these parameters are controlled by N. In TFTs with IGZO 2:1:2 the same principles are applied, combined with high content of zinc, leading to poorer electrical performance. [6, 26, 38].

For IGZO 2:1:1 and 3:1:1, the values of μ_{sat} are generally higher, because as mentioned before, a composition with indium as dominating cation is fundamental to enhance mobility, since In^{3+} spherical s-orbital has the largest radius of the three cations, thus the orbitals of neighbouring cations can easily overlap, allowing to create a good pathway for electron transport. Besides that, the higher N associated with higher indium content leads to higher I_{on}, resulting in higher I_{on}/I_{off} values. Also, it facilitates the channel formation at lower V_{GS}, leading to a negative shift, which justifies the lower V_{on} and V_T [7, 68, 69]. IGZO 2:1:1 and 3:1:1 TFTs have shown lower V_{hyst} and SS values than IGZO 1:1:1 and 2:1:2, meaning that a composition with indium as dominant cation has a major role in these parameters.

In all cases μ_{sat} has very low values compared to the obtained in literature; in this work several factors could led to such results. Using SiO_2 as dielectric compared to high-k oxide insulators leads to lower performance in the device; in contrast, in high-k oxides mobility is

enhanced due mainly to a strong accumulation of interfacial carriers from a high capacity density, compared to conventional SiO_2 [70]. Furthermore, the problems regarding solution-based processes can contribute to low μ_{sat} values, as it will be explained further ahead.

By analysing ageing effects, V_{on} and V_T generally decrease over time, regardless the composition. This negative shift might be caused by desorption phenomena of oxygen atoms in the M-O-M lattice, according to expression 3.1:

$$2\,O^-\,(s) \longrightarrow O_2\,(g) + e^- \tag{3.1}$$

Given this, the semiconductor layer become more conductive over time, decreasing V_{on} and V_T, and increasing I_{off}. However, the variation of I_{on} is very small and negligible, thus I_{on}/I_{off} decreases over time [39, 71].

SS values increase with higher density of surface traps at the interfaces, therefore is more severe in devices with more layers, due to higher number of interfaces; also, it is expected that SS increase over time due to incorporation of more surface traps from atmospheric molecules. [7, 68].

It was demonstrated TFTs IGZO 3:1:1 3 layers have generally better performance after their fabrication, and for this reason, it was the chosen condition to apply in patterned devices. However, this does not hold true when comparing the performance of TFTs with different molar ratios 8 weeks after their fabrication. In fact, TFTs with IGZO 3:1:1 2 layers have shown better I_{on}/I_{off} and lower SS 8 weeks later than IGZO 3:1:1 3 layers; also, IGZO 3:1:1 2 layers has a positive V_{on} after 8 weeks, while in IGZO 3:1:1 this value is negative. As aforementioned above, higher number of layers leads to degradation of some properties due to the number of interfaces. Moreover, for TFT applications it is desirable a V_{on} positive and closer to 0 V. Taking these considerations into account, a minimum number of layers for TFT combined with optimised V_{on} and V_T is preferred.

High leakage current (I_G) is visible in all transfer curves, associated to non-patterned semiconductor and gate electrode layers. Due to this, patterning techniques were implemented on the best-performing analysed semiconductor condition in this section (3-layer IGZO 3:1:1, at the time of fabrication of the devices) [25, 46].

The values obtained for the electrical parameters, specially mobility, are essentially associated with the main problems regarding solution-based routes. Although the electrical characteristics of TFTs fabricated by both solution-based processes or vacuum techniques are mainly influenced by the chemical composition, the formation mechanism of free carriers is slightly different in each one, being the reason of poorer performance in solution TFTs. In solution processes, N is more difficult to control due to solution chemistry and non-controlled atmosphere, while in vacuum processes it is possible to control the oxygen vapour pressure. Also, additional physical and chemical defects introduced during annealing, caused by residual organics and fixed charges contribute to inferior TFT performance, in addition of the porosity caused by solvent volatilisation and chemical reactions [5, 7, 49].

TFTs with semiconductor patterned were studied by varying two parameters: W/L values and TFT annealing temperature. TFTs annealed at 120 °C have shown generally better

performance, since at 180 °C aluminium could have been oxidised and/or migrated to the interior of semiconductor layer; for TFTs annealed 180 °C, the devices' stabilisation, transfer and output curves and their electrical parameters are shown in Appendix H.

Patterned devices were studied with W/L values of 80/20, 160/20 and 320/20 µm/µm, and their transfer characteristics are represented in Figure 3.15, as well as the variation of maximum I_{DS} in function of W. Average and standard deviation of electrical parameters of three devices are represented in Table 3.8. Stabilisation and output characteristics are shown in Appendix I.

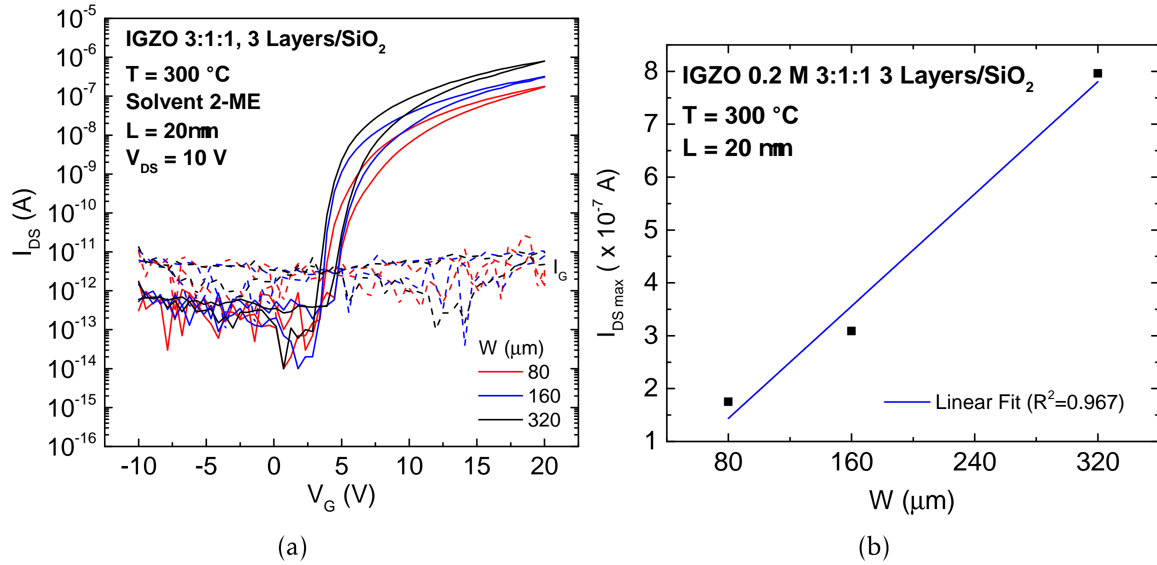

Figure 3.15: a) Transfer curves of patterned IGZO 3:1:1 3-layer IGZO; b) variation of maximum I_{DS} with W values studied.

Table 3.8: Average and standard deviation of electrical parameters of three measured TFTs annealed at 120 °C with patterned-IGZO 3:1:1 as channel layer, measured initially and 8 weeks later.

W/L	Age	I_{on}/I_{off}	V_{on} (V)	V_T (V)	V_{Hyst} (V)	SS (V/dec)	μ_{sat} ($cm^2 V^{-1} s^{-1}$)
80/20	Initial	$(7.80 \pm 5.39) \times 10^6$	3.04 ± 0.91	4.87 ± 1.76	1.73 ± 0.55	0.43 ± 0.10	$(1.93 \pm 0.90) \times 10^{-2}$
	8 weeks	$(1.07 \pm 0.48) \times 10^6$	2.68 ± 0.67	4.21 ± 1.02	1.68 ± 0.48	0.42 ± 0.03	$(9.00 \pm 1.41) \times 10^{-3}$
160/20	Initial	$(3.75 \pm 2.73) \times 10^7$	1.25 ± 0.44	3.74 ± 0.21	1.40 ± 0.25	0.44 ± 0.10	$(1.67 \pm 0.47) \times 10^{-2}$
	8 weeks	$(1.71 \pm 1.24) \times 10^7$	1.61 ± 0.25	4.28 ± 0.05	1.97 ± 0.20	0.40 ± 0.06	$(9.00 \pm 0.82) \times 10^{-2}$
320/20	Initial	$(4.19 \pm 6.42) \times 10^7$	0.58 ± 0.79	3.83 ± 0.87	2.71 ± 0.32	0.63 ± 0.11	$(1.75 \pm 0.83) \times 10^{-2}$
	8 weeks	$(1.43 \pm 0.66) \times 10^7$	2.46 ± 1.03	4.01 ± 1.12	1.89 ± 0.42	0.35 ± 0.02	$(1.13 \pm 0.52) \times 10^{-2}$

It is clearly noted that all I_G decreased, with values in the order of 10^{-11} A or less achieved, which was expected for patterned devices. Secondly, it is visible the increasing I_{DS} with higher W/L, since W is proportional to I_{DS}. This linear increase has also shown that contribution by fringing and parasitic effects was very small in fabricated patterned devices.

Concerning electrical parameters, I_{on}/I_{off} values obtained for patterned TFTs were higher than for non-patterned (even for small W/L), which is also associated with the patterning.

V_{hyst} is higher compared with non-patterned devices, possibly due to a degradation of back channel during the deposition of PR, which causes an increase in trap states that originate from chemical species or water molecules.

In non-patterned devices the measured I_{DS} has contribution by fringing effects, i.e. it is overestimated for the W/L values studied in this work, erroneously leading to a higher mobility measure. Therefore, in non-patterned devices it is expected that obtained values are higher than the real ones.

As a final note, by comparing the extracted electrical parameters from patterned IGZO 3:1:1 3-layer TFTs annealed at 120 °C with the values obtained from literature (see table J.1 in Appendix J), it is clearly evident that the better mobility values were obtained using solution-based methods, and therefore further investigation should be done to optimise this parameter.

Chapter 4

Conclusions and future perspectives

The main goal of this work was the study and optimisation of solution-processed a-IGZO using SCS, to implement as semiconductor channel layer in TFTs, and evaluate their performance. After optimisation, patterned TFTs were produced to reduce the I_G and obtain better electrical parameters.

First, IGZO TFTs with and without urea as fuel were produced and analysed, using different metallic oxides ratios (In_2O_3:Ga_2O_3:ZnO of 1:1:1, 2:1:2, 2:1:1, and 3:1:1), while the number of deposited IGZO layers was varied to obtain better V_{on} and V_T values. After a study, TFTs using urea have shown better results, in particular IGZO 3:1:1 and 2:1:1: higher stability, μ_{sat}, I_{on}/I_{off} ratio, and lower V_{hyst} and SS when compared with 1:1:1 and 2:1:2 conditions; 3-layer IGZO channel have shown the best V_{on} and V_T values, due to their proximity to 0 V. TFTs with 3 layers of IGZO 2:1:1 and 3:1:1 were compared; 3:1:1 have shown better electrical parameters at the time of fabrication of TFTs, namely higher μ_{sat} and I_{on}/I_{off} ratio, and lower V_T and V_{on} . Since all TFTs fabricated in this study have shown high I_G due to non-patterning, 3-layer IGZO 3:1:1 TFTs were patterned. A study of the TFTs performance over time was also done, and helped to conclude that non-patterned devices were more conductive over time due to oxygen desorption phenomena, while in patterned devices in most cases electrical parameters have shown very small variations. Optimised patterned IGZO 3:1:1 3-layer TFTs have show an average I_{on}/I_{off} ratio of $(4.19 \pm 6.42) \times 10^7$, μ_{sat} of $(1.75 \pm 0.83) \times 10^{-2}$ cm^2 V^{-1} s^{-1}, SS of 0.63 ± 0.11 V/dec, V_{on} of 0.58 ± 0.79 V and V_T of 3.83 ± 0.87 V. However, in both cases, very small mobilities (in the order of 10^{-2}cm^2 V^{-1} s^{-1}) were obtained, and future investigation should be made to optimise these values. FT-IR analysis was performed to guarantee that organic compounds were removed after annealing the thin films, while GAXRD, SEM and AFM characterisations confirmed that thin films were amorphous and very smooth, important characteristics to ensure high-performing devices. Optical characterisation confirmed that solution-processed IGZO had high transmittance, close to 90%, and E_{opt} values slightly close to 3.70 eV, important characteristics for applications in TAOSs. DSC-TG analysis were performed to confirm the exothermic nature of the redox reaction, associated with the use of urea as fuel and also to conclude that the ignition temperature of the reaction occurs below the annealing temperature of the thin films.

Future perspectives

After this research work, there are still parameters that should be improved to obtain better performing solution IGZO TFTs for displays applications, mainly the μ_{sat}; some suggestions for future work are:

- Increase the indium molar ratio content to increase μ_{sat}: the role of indium is undoubtedly crucial in electrical performance, and more indium content could be a viable way to increase μ_{sat}. However one should take into account that crystallisation is favoured with higher concentration of one cation relatively to the other ones; to solve this, a trade-off between higher indium content and slightly lower annealing temperatures should be studied;

- Use of passivation layers (such as PMMA), to prevent the absorption of atmospheric water and oxygen on the back surface that affects I_{off}, V_T and mobility.

- Increase the gallium content in the third spin coated layer of 3-layer semiconductor structures, to be more effective in suppression of the carriers, thus decreasing I_{off} and improving the I_{on}/I_{off} ratio.

- Fabricate all solution-processed TFTs, using high-k dielectric, to improve mobility.

Bibliography

[1] H. Hosono. “Ionic amorphous oxide semiconductors: Material design, carrier transport, and device application”. In: *Journal of Non-Crystalline Solids* 352.9-20 (2006), pp. 851–858.

[2] K. Nomura, H. Ohta, A. Takagi, T. Kamiya, M. Hirano, and H. Hosono. “Room-temperature fabrication of transparent flexible thin-film transistors using amorphous oxide semiconductors.” In: *Nature* 432.7016 (2004), pp. 488–492.

[3] T. Sameshima, S. Usui, and M. Sekiya. “XeCl Excimer laser annealing used in the fabrication of poly-Si TFT’s”. In: *IEEE Electron Device Letters* 7.5 (1986), pp. 276–278.

[4] M.-K. Kang, S. J. Kim, and H. J. Kim. “Fabrication of high performance thin-film transistors via pressure-induced nucleation”. In: *Scientific Reports* 4.1 (2015), p. 6858.

[5] R. M. Pasquarelli, D. S. Ginley, and R. O’Hayre. “Solution processing of transparent conductors: from flask to film”. In: *Chemical Society Reviews* 40.11 (2011), p. 5406.

[6] J. W. Hennek, J. Smith, A. Yan, M.-G. Kim, W. Zhao, V. P. Dravid, A. Facchetti, and T. J. Marks. “Oxygen "getter" effects on microstructure and carrier transport in low temperature combustion-processed a-InXZnO (X = Ga, Sc, Y, La) transistors.” In: *Journal of the American Chemical Society* 135.29 (2013), pp. 10729–41.

[7] S. J. Kim, S. Yoon, and H. J. Kim. “Review of solution-processed oxide thin-film transistors”. In: *Japanese Journal of Applied Physics* 53.2S (2014), 02BA02.

[8] M.-G. Kim, M. G. Kanatzidis, A. Facchetti, and T. J. Marks. “Low-temperature fabrication of high-performance metal oxide thin-film electronics via combustion processing”. In: *Nature Materials* 10.5 (2011), pp. 382–388.

[9] Y.-H. Kim, J.-S. Heo, T.-H. Kim, S. Park, M.-H. Yoon, J. Kim, M. S. Oh, G.-R. Yi, Y.-Y. Noh, and S. K. Park. “Flexible metal-oxide devices made by room-temperature photochemical activation of sol–gel films”. In: *Nature* 489.7414 (2012), pp. 128–132.

[10] S. Yoon, S. J. Kim, Y. J. Tak, and H. J. Kim. “A solution-processed quaternary oxide system obtained at low-temperature using a vertical diffusion technique”. In: *Scientific Reports* 7.February (2017), p. 43216.

[11] A. Facchetti and T. Marks. *Transparent Electronics*. Ed. by A. Facchetti and T. J. Marks. Chichester, UK: John Wiley & Sons, Ltd, 2010.

[12] K. Nomura. “Thin-Film Transistor Fabricated in Single-Crystalline Transparent Oxide Semiconductor”. In: *Science* 300.5623 (2003), pp. 1269–1272.

[13] J. Socratous, K. K. Banger, Y. Vaynzof, A. Sadhanala, A. D. Brown, A. Sepe, U. Steiner, and H. Sirringhaus. “Electronic Structure of Low-Temperature Solution-Processed Amorphous Metal Oxide Semiconductors for Thin-Film Transistor Applications”. In: *Advanced Functional Materials* 25.12 (2015), pp. 1873–1885.

[14] P. Barquinha, R. Martins, L. Pereira, and E. Fortunato. *Transparent Oxide Electronics: From Materials to Devices*. Chichester, UK: John Wiley & Sons, Ltd, 2012, pp. 1–295.

[15] E. Fortunato, P. Barquinha, and R. Martins. “Oxide Semiconductor Thin-Film Transistors: A Review of Recent Advances”. In: *Advanced Materials* 24.22 (2012), pp. 2945–2986.

[16] B. D. Ahn, H.-j. Jeon, J. Sheng, J. Park, and J.-S. Park. “A review on the recent developments of solution processes for oxide thin film transistors”. In: *Semiconductor Science and Technology* 30.6 (2015), p. 064001.

[17] T. Kamiya and H. Hosono. “Material characteristics and applications of transparent amorphous oxide semiconductors”. In: *NPG Asia Materials* 2.1 (2010), pp. 15–22.

[18] M. Grundmann, H. Frenzel, A. Lajn, M. Lorenz, F. Schein, and H. Von Wenckstern. “Transparent semiconducting oxides: Materials and devices”. In: *Physica Status Solidi (A) Applications and Materials Science* 207.6 (2010), pp. 1437–1449.

[19] S. Aikawa, P. Darmawan, K. Yanagisawa, T. Nabatame, Y. Abe, and K. Tsukagoshi. “Thin-film transistors fabricated by low-temperature process based on Ga- and Zn-free amorphous oxide semiconductor”. In: *Applied Physics Letters* 102.10 (2013), p. 102101.

[20] D. P. Norton, Y. W. Heo, M. P. Ivill, K. Ip, S. J. Pearton, M. F. Chisholm, and T. Steiner. “ZnO: Growth, doping & processing”. In: *Materials Today* 7.6 (2004), pp. 34–40.

[21] R. L. Hoffman, B. J. Norris, and J. F. Wager. “ZnO-based transparent thin-film transistors”. In: *Applied Physics Letters* 82.5 (2003), pp. 733–735.

[22] J. W. Hennek, M.-G. Kim, M. G. Kanatzidis, A. Facchetti, and T. J. Marks. “Exploratory Combustion Synthesis: Amorphous Indium Yttrium Oxide for Thin-Film Transistors”. In: *Journal of the American Chemical Society* 134.23 (2012), pp. 9593–9596.

[23] M. Estrada, Y. Hernandez-Barrios, A. Cerdeira, F. Ávila-Herrera, J. Tinoco, O. Moldovan, F. Lime, and B. Iñiguez. “Crystalline-like temperature dependence of the electrical characteristics in amorphous Indium-Gallium-Zinc-Oxide thin film transistors”. In: *Solid-State Electronics* 135 (2017), pp. 43–48.

[24] G. H. Kim, W. H. Jeong, and H. J. Kim. “Electrical characteristics of solution-processed InGaZnO thin film transistors depending on Ga concentration”. In: *physica status solidi (a)* 207.7 (2010), pp. 1677–1679.

[25] J. Leppäniemi, K. Ojanperä, T. Kololuoma, O.-H. Huttunen, J. Dahl, M. Tuominen, P. Laukkanen, H. Majumdar, and A Alastalo. “Rapid low-temperature processing of metal-oxide thin film transistors with combined far ultraviolet and thermal annealing”. In: *Applied Physics Letters* 105.11 (2014), p. 113514.

[26] S. Jeong, Y. G. Ha, J. Moon, A. Facchetti, and T. J. Marks. “Role of gallium doping in dramatically lowering amorphous-oxide processing temperatures for solution-derived indium zinc oxide thin-film transistors”. In: *Advanced Materials* 22.12 (2010), pp. 1346–1350.

[27] N. Oka, T. Aoi, R. Hayashi, H. Kumomi, and Y. Shigesato. “Electronic State of Amorphous Indium Gallium Zinc Oxide Films Deposited by DC Magnetron Sputtering with Water Vapor Introduction”. In: *Applied Physics Express* 5.7 (2012), p. 075802.

[28] P. Barquinha, A. M. Vila, G. Gonçalves, L. Pereira, R. Martins, J. R. Morante, and E. Fortunato. "Gallium-indium-zinc-oxide-based thin-film transistors: Influence of the source/drain material". In: *IEEE Transactions on Electron Devices* 55.4 (2008), pp. 954–960.

[29] G. H. Kim, H. S. Shin, B. D. Ahn, K. H. Kim, W. J. Park, and H. J. Kim. "Formation Mechanism of Solution-Processed Nanocrystalline InGaZnO Thin Film as Active Channel Layer in Thin-Film Transistor". In: *Journal of The Electrochemical Society* 156.1 (2009), H7.

[30] C.-G. Lee and A. Dodabalapur. "Solution-processed zinc–tin oxide thin-film transistors with low interfacial trap density and improved performance". In: *Applied Physics Letters* 96.24 (2010), p. 243501.

[31] R. Martins, P. Barquinha, I. Ferreira, L. Pereira, G. Gonçalves, and E. Fortunato. "Role of order and disorder on the electronic performances of oxide semiconductor thin film transistors". In: *Journal of Applied Physics* 101.4 (2007), p. 044505.

[32] B.-Y. Su, S.-Y. Chu, Y.-D. Juang, and H.-C. Chen. "High-performance low-temperature solution-processed InGaZnO thin-film transistors via ultraviolet-ozone photo-annealing". In: *Applied Physics Letters* 102.19 (2013), p. 192101.

[33] H. Cheong, S. Ogura, H. Ushijima, M. Yoshida, N. Fukuda, and S. Uemura. "Rapid preparation of solution-processed InGaZnO thin films by microwave annealing and photoirradiation". In: *AIP Advances* 5.6 (2015), p. 067127.

[34] P. K. Nayak, T. Busani, E. Elamurugu, P. Barquinha, R. Martins, Y. Hong, and E. Fortunato. "Zinc concentration dependence study of solution processed amorphous indium gallium zinc oxide thin film transistors using high-k dielectric". In: *Applied Physics Letters* 97.18 (2010), p. 183504.

[35] J. Xu, Q. Wu, L. Xu, H. Xie, G. Liu, L. Zhang, and C. Dong. "Ambient effect on thermal stability of amorphous InGaZnO thin film transistors". In: *Solid-State Electronics* 126 (2016), pp. 170–174.

[36] H.-y. Jeong, B.-y. Lee, Y.-j. Lee, J.-i. Lee, M.-s. Yang, I.-b. Kang, M. Mativenga, and J. Jang. "Coplanar amorphous-indium-gallium-zinc-oxide thin film transistor with He plasma treated heavily doped layer". In: *Applied Physics Letters* 104.2 (2014), p. 022115.

[37] P. Barquinha. "Transparent Oxide Thin-Film Transistors: Production, characterization and integration". PhD thesis. Faculdade de Ciências e Tecnologias da Universidade Nova de Lisboa, Portugal, 2010.

[38] D. Kim, C. Y. Koo, K. Song, Y. Jeong, and J. Moon. "Compositional influence on sol-gel-derived amorphous oxide semiconductor thin film transistors". In: *Applied Physics Letters* 95.10 (2009), p. 103501.

[39] P. Barquinha, A. Pimentel, A. Marques, L. Pereira, R. Martins, and E. Fortunato. "Influence of the semiconductor thickness on the electrical properties of transparent TFTs based on indium zinc oxide". In: *Journal of Non-Crystalline Solids* 352.9-20 SPEC. ISS. (2006), pp. 1749–1752.

[40] H. Q. Chiang, J. F. Wager, R. L. Hoffman, J. Jeong, and D. A. Keszler. "High mobility transparent thin-film transistors with amorphous zinc tin oxide channel layer". In: *Applied Physics Letters* 86.1 (2005), p. 013503.

[41] P. F. Carcia, R. S. McLean, M. H. Reilly, and G. Nunes. "Transparent ZnO thin-film transistor fabricated by rf magnetron sputtering". In: *Applied Physics Letters* 82.7 (2003), pp. 1117–1119.

[42] K Ellmer. "Resistivity of polycrystalline zinc oxide films: current status and physical limit". In: *Journal of Physics D: Applied Physics* 34.21 (2001), pp. 3097–3108.

[43] E. M. C. Fortunato, P. M. C. Barquinha, A. C.M.B. G. Pimentel, A. M. F. Gonçalves, A. J. S. Marques, R. F. P. Martins, and L. M. Pereira. "Wide-bandgap high-mobility ZnO thin-film transistors produced at room temperature". In: *Applied Physics Letters* 85.13 (2004), pp. 2541–2543.

[44] J. Park, K.-t. Oh, D.-H. Kim, H.-J. Jeong, Y. C. Park, H.-s. Kim, and J.-s. Park. "High-Performance Zinc Tin Oxide Semiconductor Grown by Atmospheric-Pressure Mist-CVD and the Associated Thin-Film Transistor Properties". In: *ACS Applied Materials & Interfaces* 9.24 (2017), pp. 20656–20663.

[45] S. J. Kim, G. H. Kim, D. L. Kim, D. N. Kim, and H. J. Kim. "InGaZnO thin-film transistors with YHfZnO gate insulator by solution process". In: *physica status solidi (a)* 207.7 (2010), pp. 1668–1671.

[46] Y. S. Rim, H. S. Lim, and H. J. Kim. "Low-Temperature Metal-Oxide Thin-Film Transistors Formed by Directly Photopatternable and Combustible Solution Synthesis". In: *ACS Applied Materials & Interfaces* 5.9 (2013), pp. 3565–3571.

[47] R. Branquinho, D. Salgueiro, L. Santos, P. Barquinha, L. Pereira, R. Martins, and E. Fortunato. "Aqueous Combustion Synthesis of Aluminum Oxide Thin Films and Application as Gate Dielectric in GZTO Solution-Based TFTs". In: *ACS Applied Materials & Interfaces* 6.22 (2014), pp. 19592–19599.

[48] R. Branquinho, A. Santa, E. Carlos, D. Salgueiro, P. Barquinha, R. Martins, and E. Fortunato. "Solution Combustion Synthesis: Applications in Oxide Electronics". In: *Developments in Combustion Technology*. October. InTech, 2016, pp. 397–417.

[49] G. H. Kim, B. Du Ahn, H. S. Shin, W. H. Jeong, H. J. Kim, and H. J. Kim. "Effect of indium composition ratio on solution-processed nanocrystalline InGaZnO thin film transistors". In: *Applied Physics Letters* 94.23 (2009), p. 233501.

[50] S. Parthiban, K. Ramamurthi, E. Elangovan, R. Martins, and E. Fortunato. "Spray deposited molybdenum doped indium oxide thin films with high near infrared transparency and carrier mobility". In: *Applied Physics Letters* 94.21 (2009), pp. 65–68.

[51] H. Lee, S. M. Dellatore, W. M. Miller, and P. B. Messersmith. "Mussel-Inspired Surface Chemistry for Multifunctional Coatings". In: *Science* 318.5849 (2007), pp. 426–430.

[52] J. W. Hennek, Y. Xia, K. Everaerts, M. C. Hersam, A. Facchetti, and T. J. Marks. "Reduced Contact Resistance in Inkjet Printed High-Performance Amorphous Indium Gallium Zinc Oxide Transistors". In: *ACS Applied Materials & Interfaces* 4.3 (2012), pp. 1614–1619.

[53] H.-C. Cheng, C.-F. Chen, and C.-C. Lee. "Thin-film transistors with active layers of zinc oxide (ZnO) fabricated by low-temperature chemical bath method". In: *Thin Solid Films* 498.1-2 (2006), pp. 142–145.

[54] Y. Sun and J. A. Rogers. "Inorganic Semiconductors for Flexible Electronics". In: *Advanced Materials* 19.15 (2007), pp. 1897–1916.

[55] W. A. MacDonald. "Engineered films for display technologies". In: *Journal of Materials Chemistry* 14.1 (2004), p. 4.

[56] E. J. Bae, Y. H. Kang, M. Han, C. Lee, and S. Y. Cho. "Soluble oxide gate dielectrics prepared using the self-combustion reaction for high-performance thin-film transistors". In: *J. Mater. Chem. C* 2.28 (2014), pp. 5695–5703.

[57] S. J. Kim, A. R. Song, S. S. Lee, S. Nahm, Y. Choi, K.-B. Chung, and S. Jeong. "Independent chemical/physical role of combustive exothermic heat in solution-processed metal oxide semiconductors for thin-film transistors". In: *J. Mater. Chem. C* 3.7 (2015), pp. 1457–1462.

[58] S. L. González-Cortés and F. E. Imbert. "Fundamentals, properties and applications of solid catalysts prepared by solution combustion synthesis (SCS)". In: *Applied Catalysis A: General* 452 (2013), pp. 117–131.

[59] D. Salgueiro, A. Kiazadeh, R. Branquinho, L. Santos, P. Barquinha, R. Martins, and E. Fortunato. "Solution based zinc tin oxide TFTs: the dual role of the organic solvent". In: *Journal of Physics D: Applied Physics* 50.6 (2017), p. 065106.

[60] R. Branquinho, D. Salgueiro, A. Santa, A. Kiazadeh, P. Barquinha, L. Pereira, R. Martins, and E. Fortunato. "Towards environmental friendly solution-based ZTO/AlO x TFTs". In: *Semiconductor Science and Technology* 30.2 (2015), p. 024007.

[61] L. Pereira. "Produção e caracterização de silício policristalino e sua aplicação a TFTs". PhD thesis. Faculdade de Ciências e Tecnologias da Universidade Nova de Lisboa, Portugal, 2008.

[62] C. R. Kagan and P. Andry and S. Brody. *Thin-Film Transistors*. New York: Marcel Dekker, Inc, 2003.

[63] M. Xie, S. Wu, Z. Chen, Q. Khan, X. Wu, S. Shao, and Z. Cui. "Performance improvement for printed indium gallium zinc oxide thin-film transistors with a preheating process". In: *RSC Adv.* 6.47 (2016), pp. 41439–41446.

[64] K. Nomura, T. Kamiya, and H. Hosono. “Effects of Diffusion of Hydrogen and Oxygen on Electrical Properties of Amorphous Oxide Semiconductor, In-Ga-Zn-O”. In: *ECS Journal of Solid State Science and Technology* 2.1 (2012), P5–P8.

[65] S. K. Park, Y.-H. Kim, and J.-I. Han. “All solution-processed high-resolution bottom-contact transparent metal-oxide thin film transistors”. In: *Journal of Physics D: Applied Physics* 42.12 (2009), p. 125102.

[66] N Ito, Y Sato, P. Song, A Kaijio, K Inoue, and Y Shigesato. “Electrical and optical properties of amorphous indium zinc oxide films”. In: *Thin Solid Films* 496.1 (2006), pp. 99–103.

[67] K. Tominaga, T. Takao, A. Fukushima, T. Moriga, and I. Nakabayashi. “Amorphous ZnO–In2O3 transparent conductive films by simultaneous sputtering method of ZnO and In2O3 targets”. In: *Vacuum* 66.3-4 (2002), pp. 505–509.

[68] J.-S. Ahn, J.-J. Lee, G. W. Hyung, Y. K. Kim, and H. Yang. “Colloidal ZnO quantum dot-based, solution-processed transparent field-effect transistors”. In: *Journal of Physics D: Applied Physics* 43.27 (2010), p. 275102.

[69] Y.-H. Kim, M.-K. Han, J.-I. Han, and S. K. Park. “Effect of Metallic Composition on Electrical Properties of Solution-Processed Indium-Gallium-Zinc-Oxide Thin-Film Transistors”. In: *IEEE Transactions on Electron Devices* 57.5 (2010), pp. 1009–1014.

[70] H. Wang, W. Xu, S. Zhou, F. Xie, Y. Xiao, L. Ye, J. Chen, and J. Xu. “Oxygen plasma assisted high performance solution-processed Al 2 O x gate insulator for combustion-processed InGaZnO x thin film transistors”. In: *Journal of Applied Physics* 117.3 (2015), p. 035703.

[71] J. K. Jeong, H. Won Yang, J. H. Jeong, Y.-G. Mo, and H. D. Kim. “Origin of threshold voltage instability in indium-gallium-zinc oxide thin film transistors”. In: *Applied Physics Letters* 93.12 (2008), p. 123508.

[72] S. Jain, K. Adiga, and V. Pai Verneker. “A new approach to thermochemical calculations of condensed fuel-oxidizer mixtures”. In: *Combustion and Flame* 40.C (1981), pp. 71–79.

[73] H. J. Cheong, N. Fukuda, S. Ogura, H. Sakai, M. Yoshida, T. Kodzasa, H. Tokuhisa, K. Tokoro, K. Takeuchi, R. Nagahata, T. Nakamura, and S. Uemura. “Effect of Microwave Annealing on Oxide-Semiconductor-Precursor Ink”. In: *Journal of Photopolymer Science and Technology* 27.3 (2014), pp. 339–342.

[74] X. Liu, T.-J. Tarn, F. Huang, and J. Fan. “Recent advances in inkjet printing synthesis of functional metal oxides”. In: *Particuology* 19 (2015), pp. 1–13.

[75] Y. S. Rim, W. H. Jeong, D. L. Kim, H. S. Lim, K. M. Kim, and H. J. Kim. “Simultaneous modification of pyrolysis and densification for low-temperature solution-processed flexible oxide thin-film transistors”. In: *Journal of Materials Chemistry* 22.25 (2012), p. 12491.

Appendix A

Redox reactions

The SCS involves the reduction of metallic nitrates reactions, which are converted into metal oxides, and the oxidation reactions of fuel by the nitrate ions (Table A.1). Note that the metallic salts precursor solutions are balanced with urea used as fuel for the reaction.

Table A.1: Reduction and oxidation reactions.

Reduction Reaction	
Indium nitrate hydrate	$2\,In(NO_3)_3 \cdot H_2O \longrightarrow In_2O_3 + 2\,H_2O + 3\,N_2 + \frac{15}{2}\,O_2$
Gallium nitrate hydrate	$2\,Ga(NO_3)_3 \cdot H_2O \longrightarrow Ga_2O_3 + 2\,H_2O + 3\,N_2 + \frac{15}{2}\,O_2$
Zinc nitrate hexahydrate	$Zn(NO_3)_2 \cdot 6\,H_2O \longrightarrow ZnO + 6\,H_2O + N_2 + \frac{5}{2}\,O_2$
Oxidation Reaction	
Urea	$CO(NH_2)_2 + \frac{3}{2}\,O_2 \longrightarrow 2\,H_2O + CO_2 + N_2$
2-Methoxyethanol	$C_3H_8O_2 + 4\,O_2 \longrightarrow 4\,H_2O + 3\,CO_2$

The overall combustion reaction involves the combination of reduction and oxidation reaction; gaseous products are formed and released, including H_2O, N_2, CO_2 and O_2 [48]. 2-ME can act as fuel, however in this work it is used as solvent, being urea used as fuel [59]. These reactions are represented in Table A.2.

Table A.2: Combination of metal nitrate reduction and fuel oxidation reactions.

Precursor	Fuel	Overall reaction
Indium nitrate hydrate		$2\,In(NO_3)_3 \cdot H_2O + CO(NH_2)_2 \longrightarrow In_2O_3 + 4\,H_2O + CO_2 + 4\,N_2 + 6\,O_2$
Gallium nitrate hydrate	Urea	$2\,Ga(NO_3)_3 \cdot H_2O + CO(NH_2)_2 \longrightarrow Ga_2O_3 + 4\,H_2O + CO_2 + 4\,N_2 + 6\,O_2$
Zinc nitrate hexahydrate		$Zn(NO_3)_2 \cdot 6\,H_2O + CO(NH_2)_2 \longrightarrow ZnO + 8\,H_2O + CO_2 + 2\,N_2 + O_2$

By using the Jain method, the stoichiometric proportion of oxidiser and fuel can be calculated in order to obtain the molar ratio of reactants and ensure the redox stoichiometry of the reaction, given by Equation A.1 [72].

$$\varphi = \frac{RV}{OV} n \tag{A.1}$$

Where φ is the fuel/oxidiser ratio, RV and RO are reducing valence and oxidising valence respectively, and n is the number of moles of fuel per mole of oxidant.

If $\varphi = 1$, the ideal stoichiometric composition of redox mixture is obtained, because no additional oxygen is required to complete the reaction. However, if $\varphi < 1$, the redox mixture is in absence of enough fuel to complete the reaction, resulting in the production of molecular oxygen. In contrast, if $\varphi > 1$, the redox mixture has fuel in excess, meaning that more

molecular oxygen is required to convert completely the fuel. The values of oxidising/reducing valences of a redox mixture can be determined to obtain a condition where φ =1 for the reaction [58].

Indium and gallium, zinc, carbon and hydrogen count all as reducing agents with corresponding valences of +3, +2, +4 and +1, respectively. Oxygen and nitrogen are considered oxidiser agents with valence of -2 and 0, respectively. Calculations of oxidising and reducing valences values are represented in Table A.3 . Note that for metal nitrates hydrates, water molecules do not affect the overall valence [48].

Table A.3: Valence of the reagents.

Reagent		Calculation	Total
Oxidiser reagent (OV)	$In(NO_3)_3$	$3+(3\times 0)+[3\times 3\times(-2)]$	-15
	$Ga(NO_3)_3$	$3+(3\times 0)+[3\times 3\times(-2)]$	-15
	$Zn(NO_3)_2$	$2+(2\times 0)+[2\times 3\times(-2)]$	-10
Reducing reagent (RV)	$CO(NH_2)_2$	$4+(-2)+(2\times 0)+(2\times 2\times 1)$	+6

Therefore the number of moles needed to ensure stoichiometry of the redox reaction can be determined, with the values being shown in table A.4.

Table A.4: Number of moles of fuel per mole of oxidiser to ensure stoichiometry of the redox reaction.

Precursor	Fuel	φ	n
Indium nitrate hydrate			5/2
Gallium nitrate hydrate	Urea	1	5/2
Zinc nitrate hexahydrate			5/3

Finally, the global reactions are represented in Table A.5 considering the number of moles to ensure the stoichiometry of the redox reaction.

Table A.5: Overall reactions with correct stoichiometry.

Precursor	Fuel	Overall reaction
Indium nitrate hydrate		$2\,In(NO_3)_3\cdot 2\,H_2O + 5\,CO(NH_2)_2 \longrightarrow In_2O_3 + 14\,H_2O + 5\,CO_2 + 8\,N_2$
Gallium nitrate hydrate	Urea	$2\,Ga(NO_3)_3\cdot 2\,H_2O + 5\,CO(NH_2)_2 \longrightarrow Ga_2O_3 + 14\,H_2O + 5\,CO_2 + 8\,N_2$
Zinc nitrate hexahydrate		$3\,Zn(NO_3)_2\cdot 6\,H_2O + 5\,CO(NH_2)_2 \longrightarrow 3\,ZnO + 28\,H_2O + 5\,CO_2 + 8\,N_2$

Appendix B

IGZO solutions viscosity

Viscosities of IGZO solutions with different cation molar ratios, with and without urea, and 2-ME were measured, depicted in Table B.1. All measurements were performed at a speed of 500 rpm. The obtained values have shown that urea increases viscosity values, and metallic cations ratio does not influence significantly the values. Still, values in the range 1-10 cP were obtained, being an important requirement to apply solution-processed IGZO in spin-coating and inkjet printing methods [73, 74].

Table B.1: Viscosities of IGZO solutions with and without urea, and 2-ME.

Solution	Fuel	Viscosity (cP)	FSR (%)
IGZO 1:1:1	Urea	2.34 ± 0.08	14.22
IGZO 2:1:2		2.30 ± 0.08	14.67
IGZO 2:1:1		2.26 ± 0.06	14.03
IGZO 3:1:1		2.28 ± 0.06	14.15
IGZO 1:1:1	(No fuel)	1.89 ± 0.06	11.79
IGZO 2:1:2		2.10 ± 0.22	13.04
IGZO 2:1:1		1.89 ± 0.07	11.80
IGZO 3:1:1		1.95 ± 0.09	12.08
2-ME		1.45 ± 0.07	12.71

Appendix C

DSC-TG analysis of IGZO solutions

DSC-TG analysis of IGZO 0.2 M solutions with molar ratios of 1:1:1, 2:1:2 and 2:1:1 are depicted in Figures C.1 and C.2.

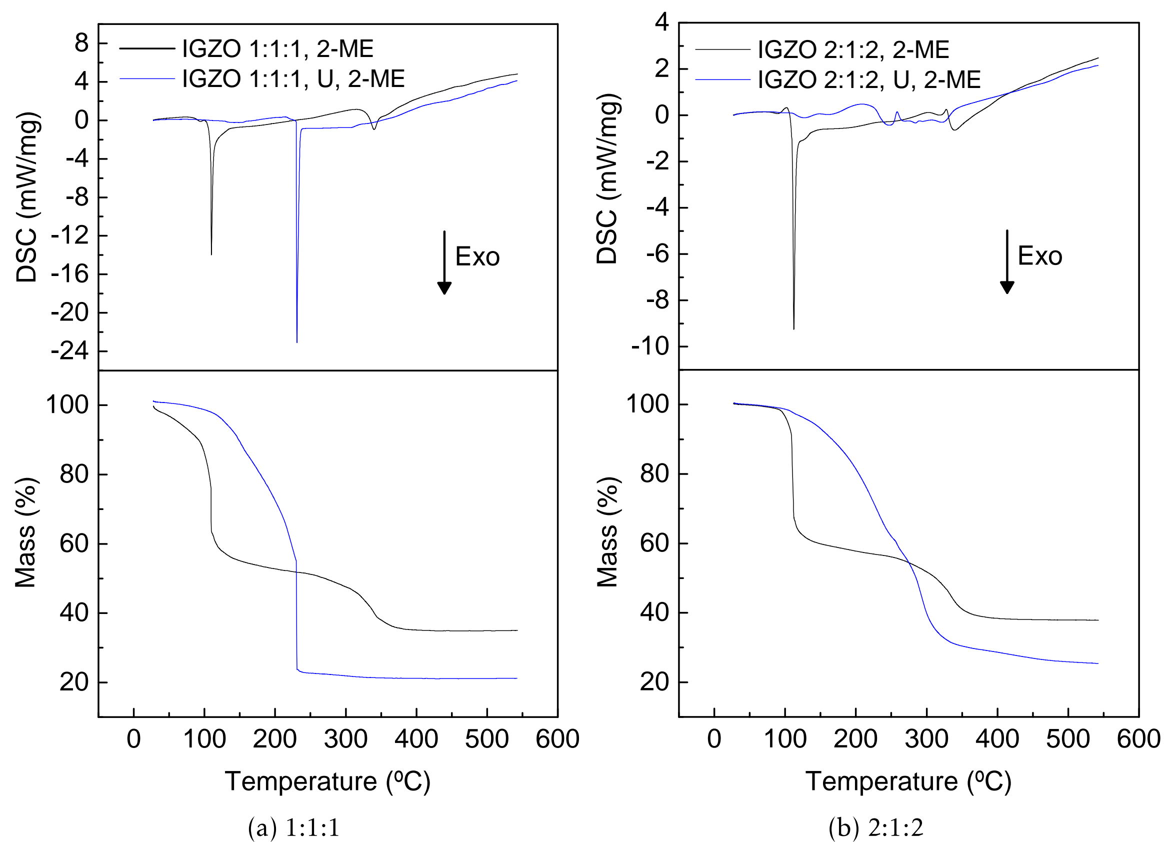

Figure C.1: DSC-TG analysis of IGZO 1:1:1 and 2:1:2 precursor solutions with 2-ME as solvent and using urea as fuel or not.

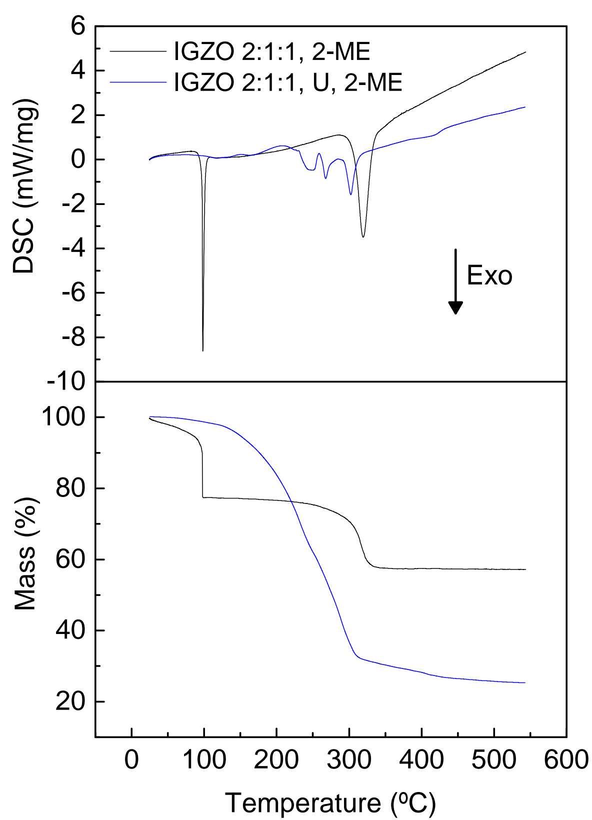

Figure C.2: DSC-TG analysis of IGZO 2:1:1 precursor solutions with 2-ME as solvent and using urea as fuel or not.

Appendix D

Reflectance of thin films

Reflectance spectra are represented in Figure D.1, and their results complement the obtained transmittance data, with reflectance values increasing with the number of spin coated layers, from 10 to about 15%. These values demonstrate that IGZO thin films have small reflectance, an important property for thin films applied in transparent devices.

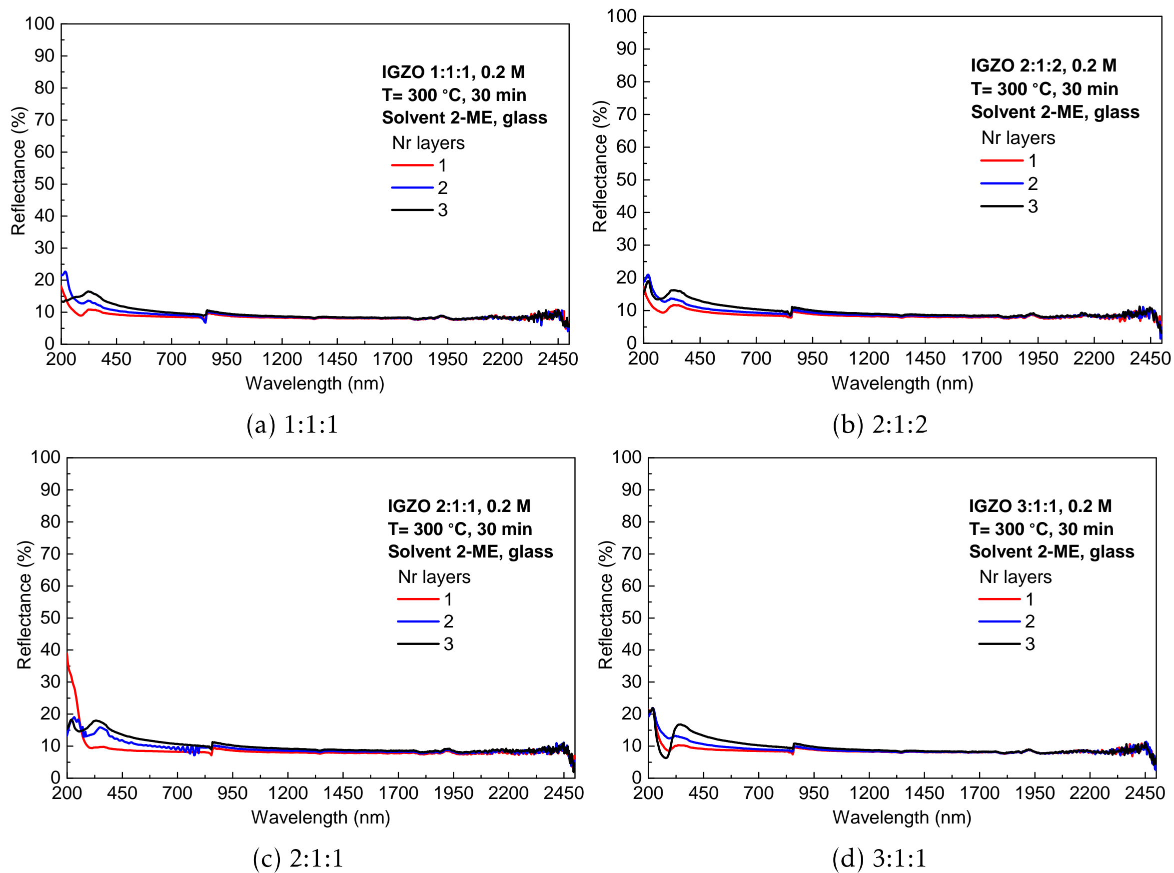

(a) 1:1:1

(b) 2:1:2

(c) 2:1:1

(d) 3:1:1

Figure D.1: Reflectance spectra of IGZO thin films on glass substrates.

Appendix E

Calculation of E_{opt} of IGZO thin films

The E_{opt} of IGZO thin films can be determined if the absorption coefficient (α) is known, which can be obtained by Equation E.1:

$$\alpha = \frac{1}{d_s} ln\left(\frac{1}{1-A}\right) \tag{E.1}$$

where d_s is the thin film' thickness and A is the optical absorption of the thin film. By substituting A with 1-T-R (where R is the reflectance) and neglecting R, approximate values of α are obtained and E_{opt} can be calculated. Assuming parabolic bands, the determination of E_{opt} is based on a linear fit at the onset of a α^x abrupt rise, given by Tauc's relation:

$$\alpha^x \propto h\nu - E_{opt} \tag{E.2}$$

Where x is a value related with the transition type, h is the Planck constant and ν is the photon frequency. In most of amorphous semiconductors, non-direct optical transitions are allowed, and in this case x assumes the value of 0.5 [37].

Figure E.1 depicts the Tauc plots used to determine E_{opt} for each IGZO molar ratio and number of layers studied. Table E.1 represents the values of coefficient of determination (R^2) of each linear fit.

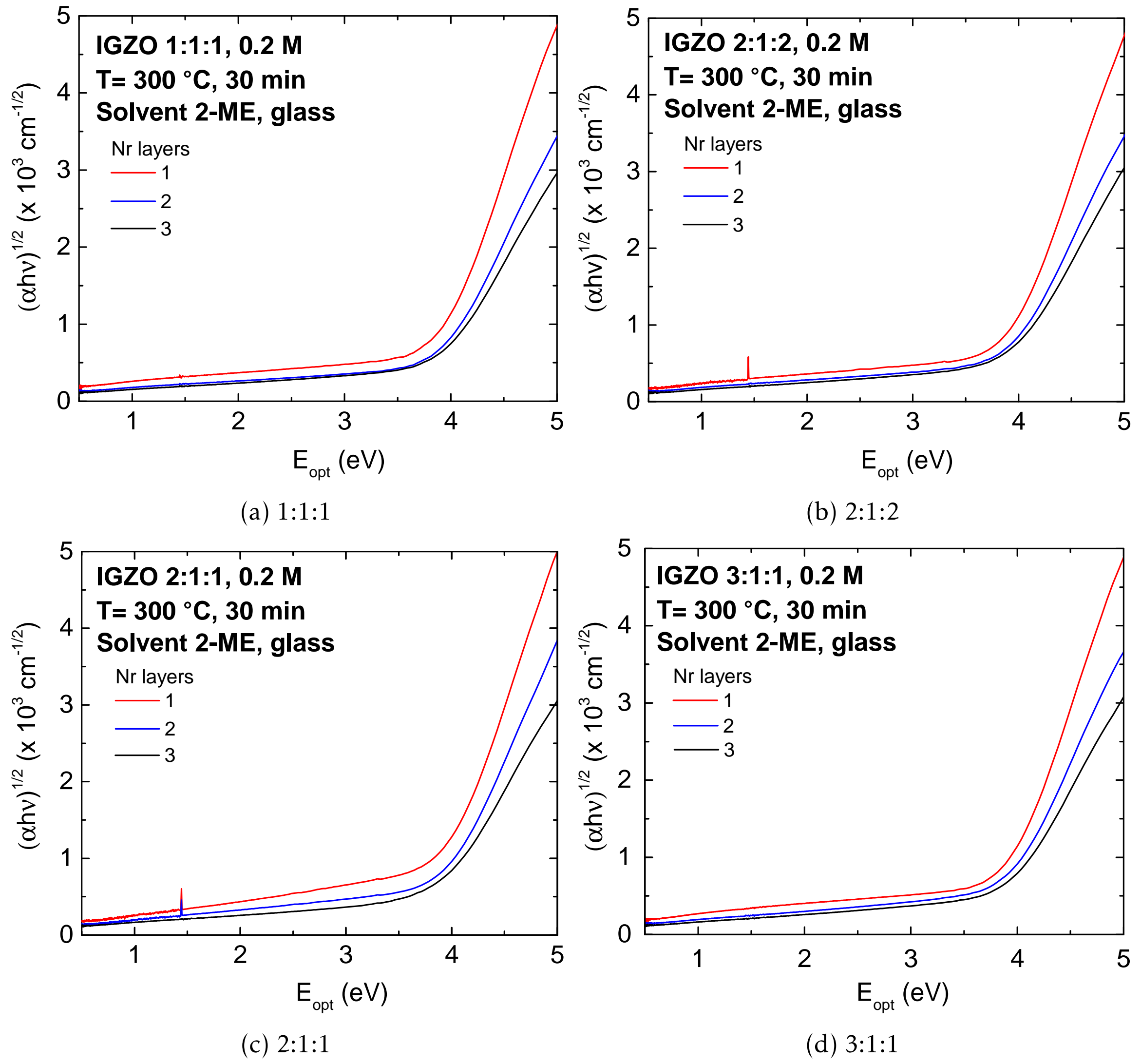

(a) 1:1:1 (b) 2:1:2

(c) 2:1:1 (d) 3:1:1

Figure E.1: Tauc-bandgap plots for the calculation of E_{opt}.

Table E.1: R^2 of each linear fit for determination of E_{opt}.

Number of Layers	IGZO molar ratio			
	1:1:1	2:1:2	2:1:1	3:1:1
1	0.99653	0.99877	0.99578	0.99081
2	0.99804	0.99859	0.99793	0.99705
3	0.99858	0.99891	0.99768	0.99859

Appendix F

Variation of transconductance with voltage

This section comprises the plots of g_m for each condition studied.

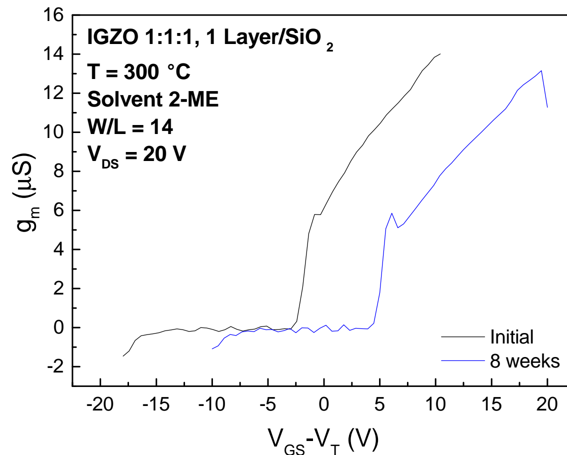

Figure F.1: Transconductance curve of IGZO 1:1:1 0.2 M TFT with 1 active layer, measured initially and 8 weeks later.

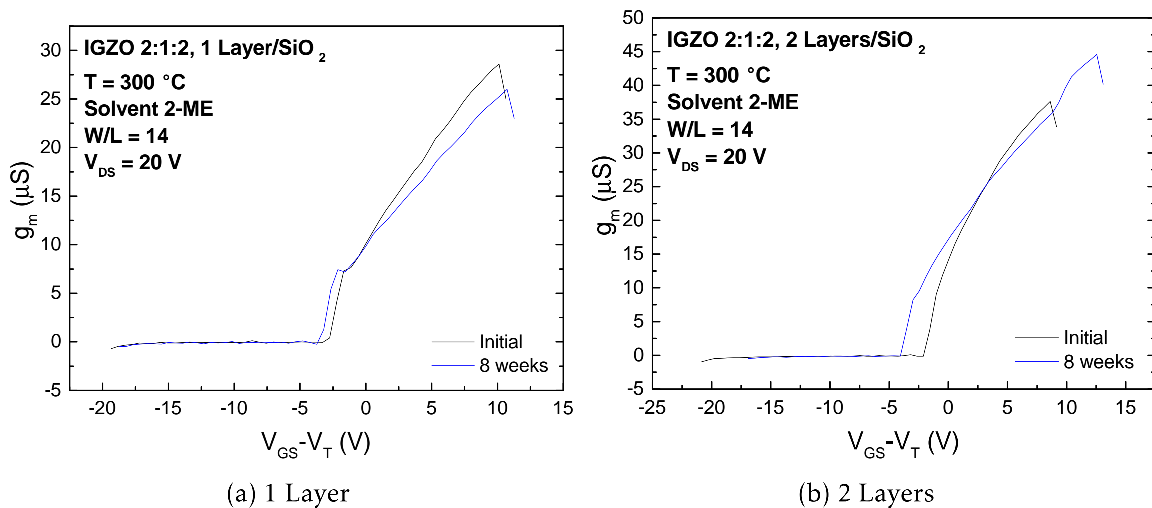

(a) 1 Layer

(b) 2 Layers

Figure F.2: Transconductance curves of IGZO 2:1:2 0.2 M TFT with 1 and 2 active layers, measured initially and 8 weeks later.

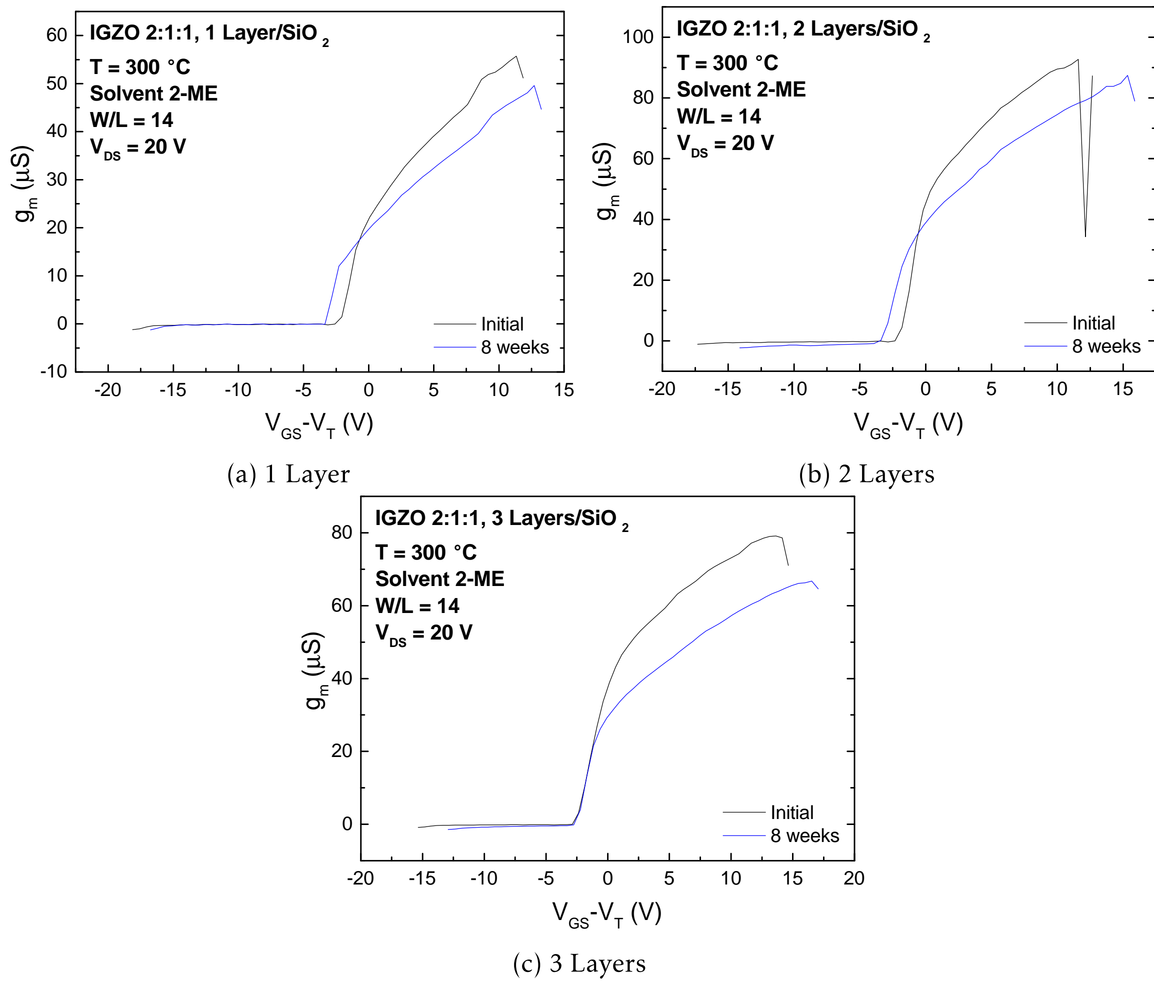

(a) 1 Layer

(b) 2 Layers

(c) 3 Layers

Figure F.3: Transconductance curves of IGZO 2:1:1 0.2 M TFT with 1, 2 and 3 active layers, measured initially and 8 weeks later.

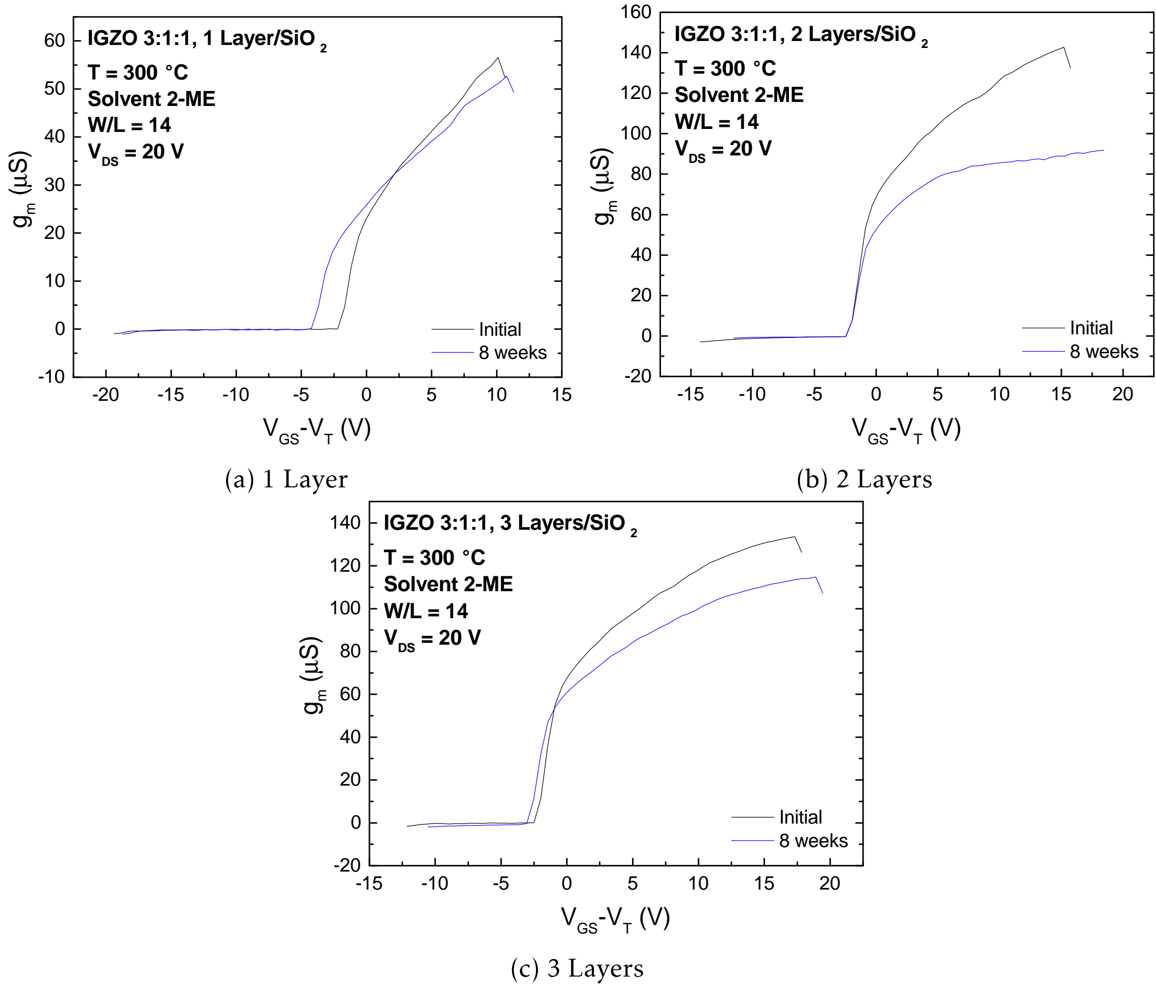

(a) 1 Layer

(b) 2 Layers

(c) 3 Layers

Figure F.4: Transconductance curves of IGZO 2:1:1 0.2 M TFT with 1, 2 and 3 active layers, measured initially and 8 weeks later.

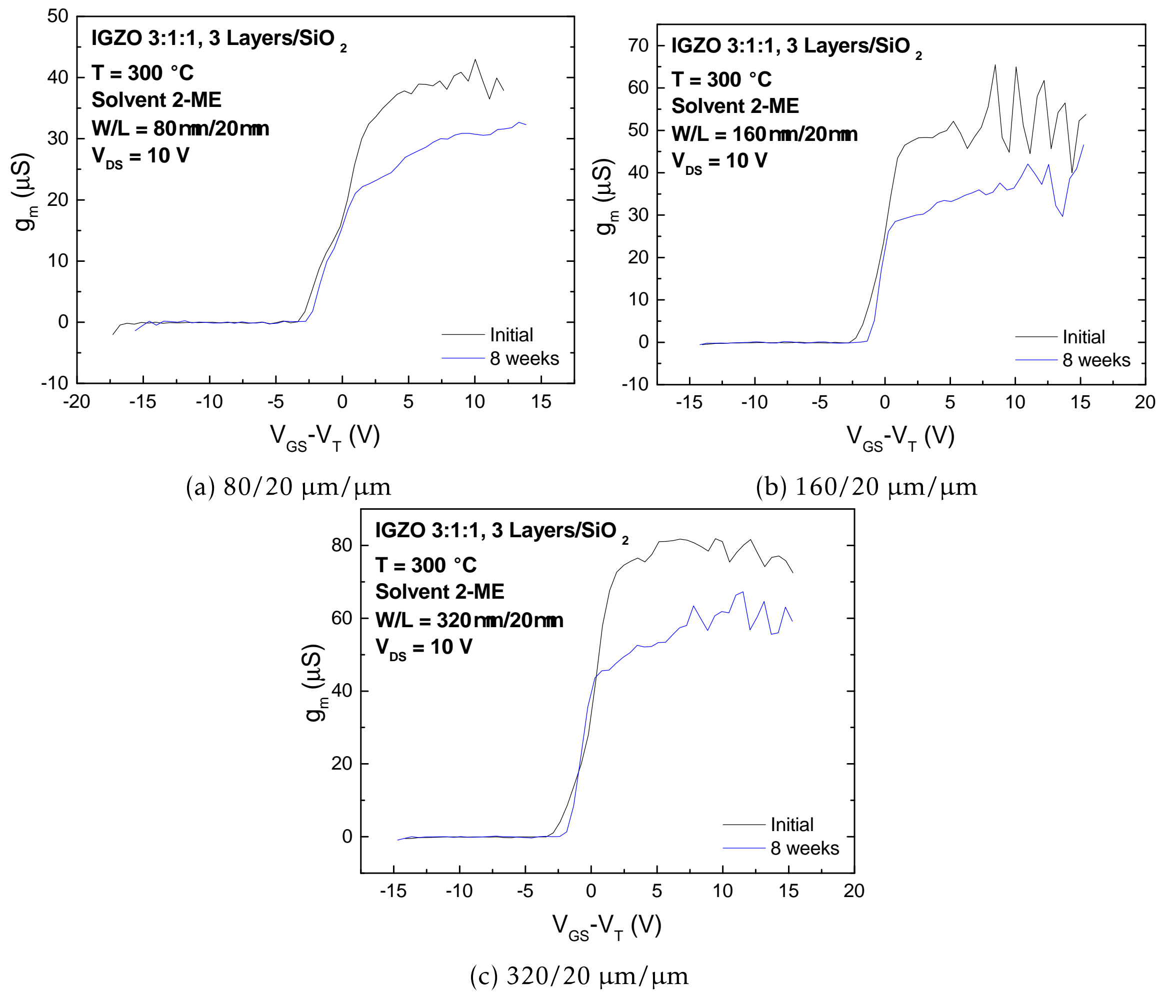

(a) 80/20 μm/μm

(b) 160/20 μm/μm

(c) 320/20 μm/μm

Figure F.5: Transconductance curves of TFTs annealed at 120 °C with patterned IGZO 3:1:1 3 layers, measured initially and 8 weeks later.

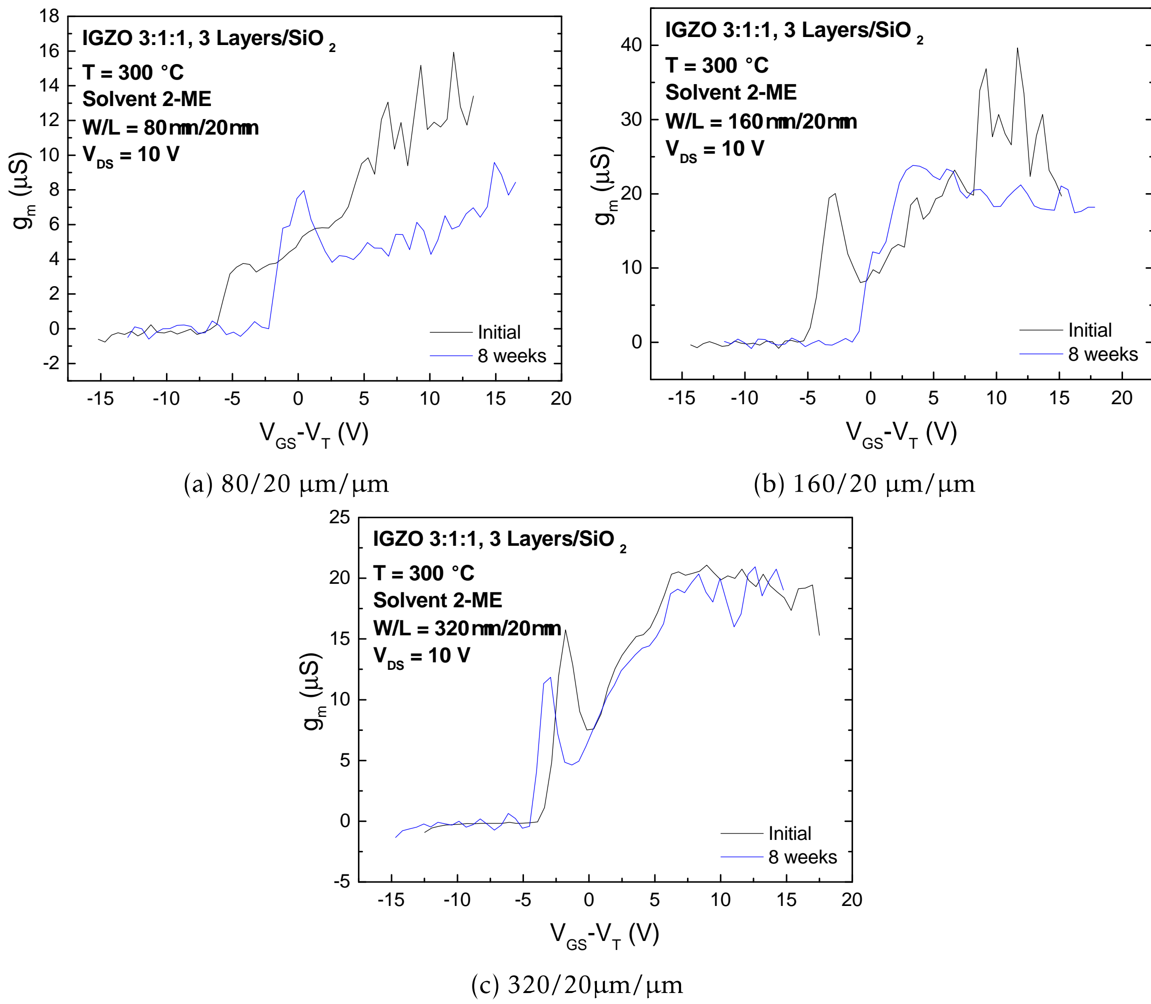

(a) 80/20 µm/µm

(b) 160/20 µm/µm

(c) 320/20µm/µm

Figure F.6: Transconductance curves of TFTs annealed at 180 °C with patterned IGZO 3:1:1 3 layers, measured initially and 8 weeks later.

Appendix G

Stabilisation and output curves non-patterned TFTs

Stabilisation characteristics of IGZO 1:1:1, 2:1:2, 2:1:1 and 3:1:1 are depicted in Figures G.1 G.2, G.3 and G.4, respectively:

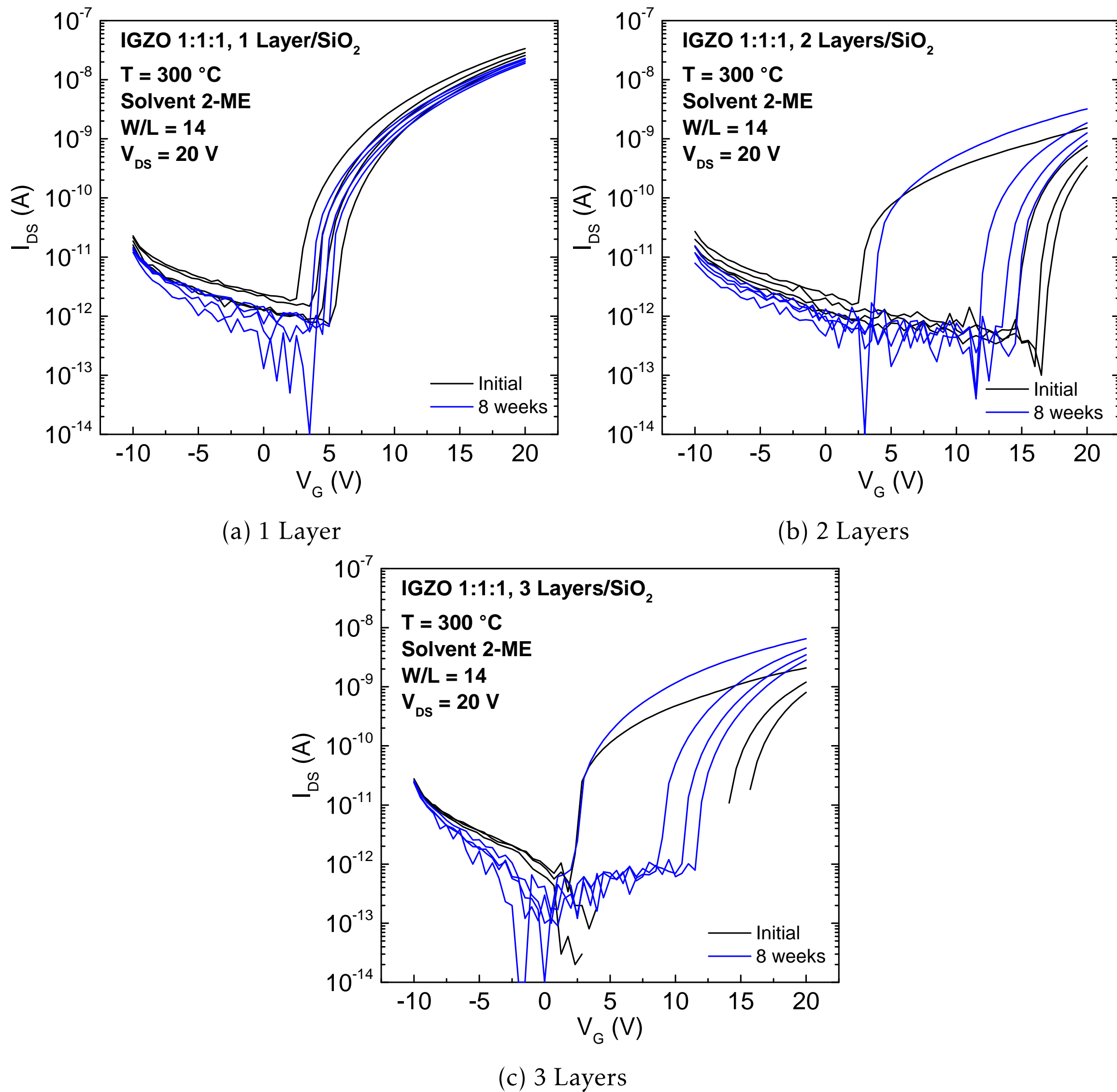

(a) 1 Layer

(b) 2 Layers

(c) 3 Layers

Figure G.1: Stabilisation curves of IGZO 1:1:1 0.2 M with 1, 2 and 3 active layers.

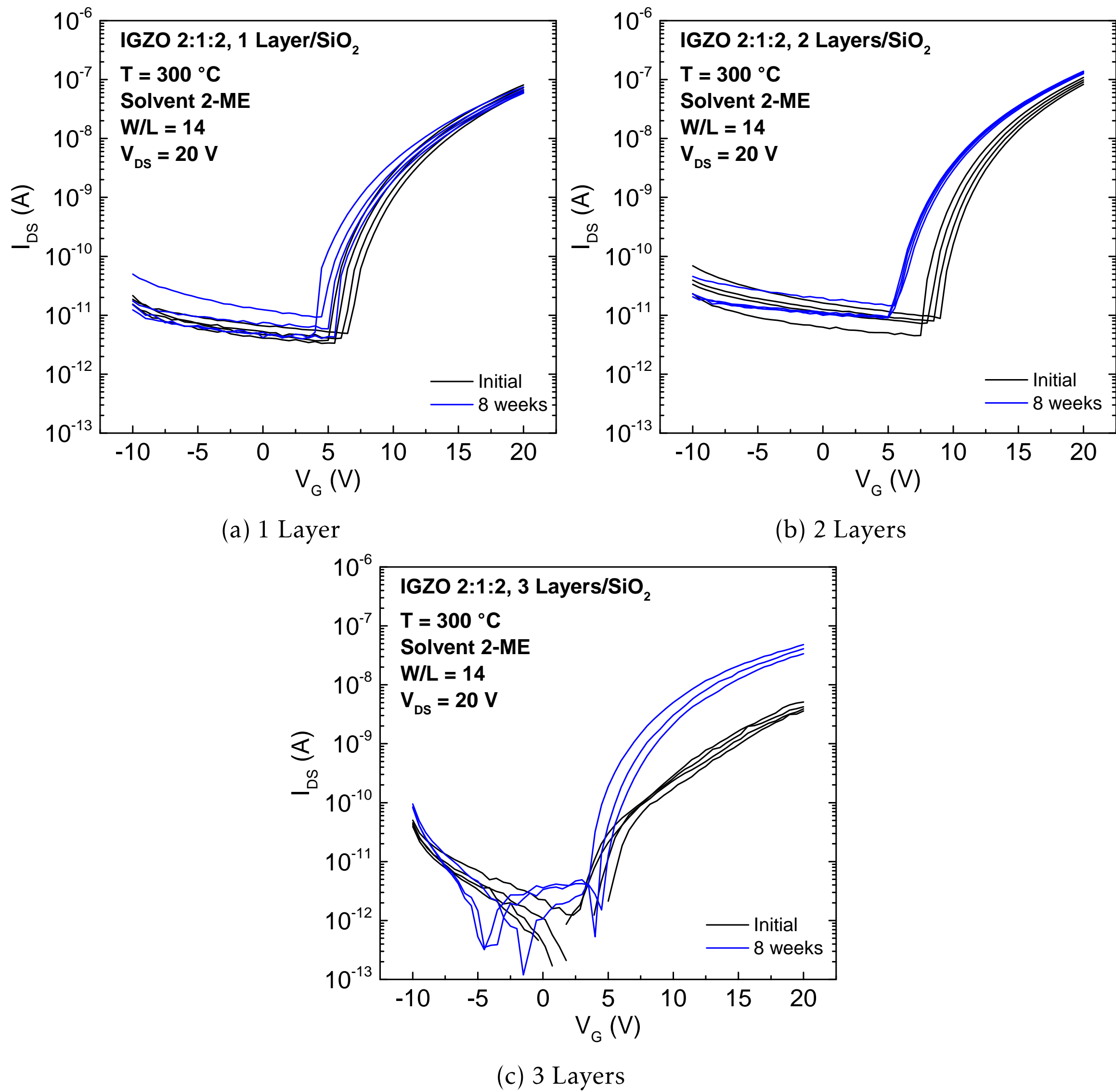

(a) 1 Layer

(b) 2 Layers

(c) 3 Layers

Figure G.2: Stabilisation curves of IGZO 2:1:2 0.2 M with 1, 2 and 3 active layers.

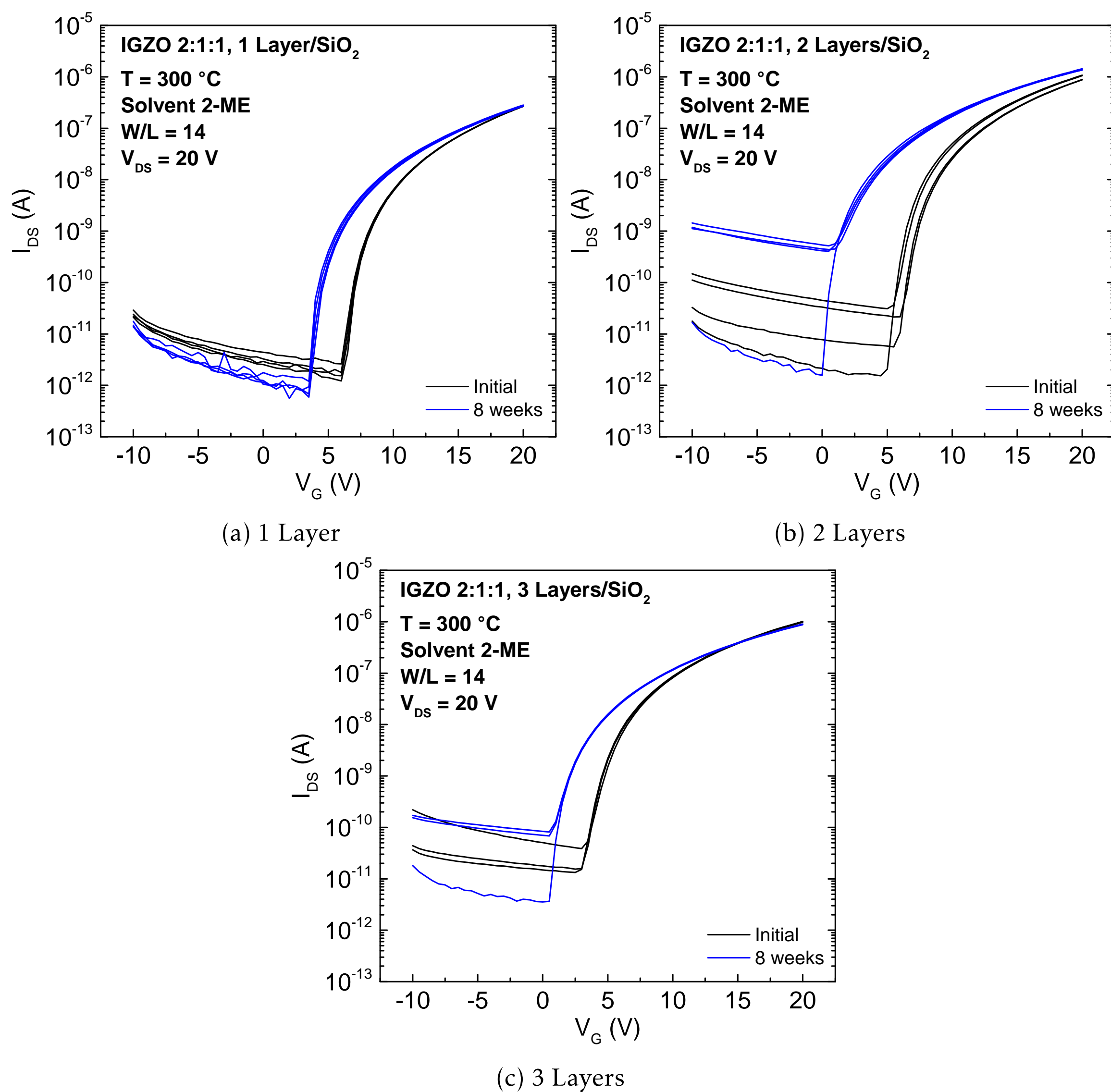

(a) 1 Layer

(b) 2 Layers

(c) 3 Layers

Figure G.3: Stabilisation curves of IGZO 2:1:1 0.2 M with 1, 2 and 3 active layers.

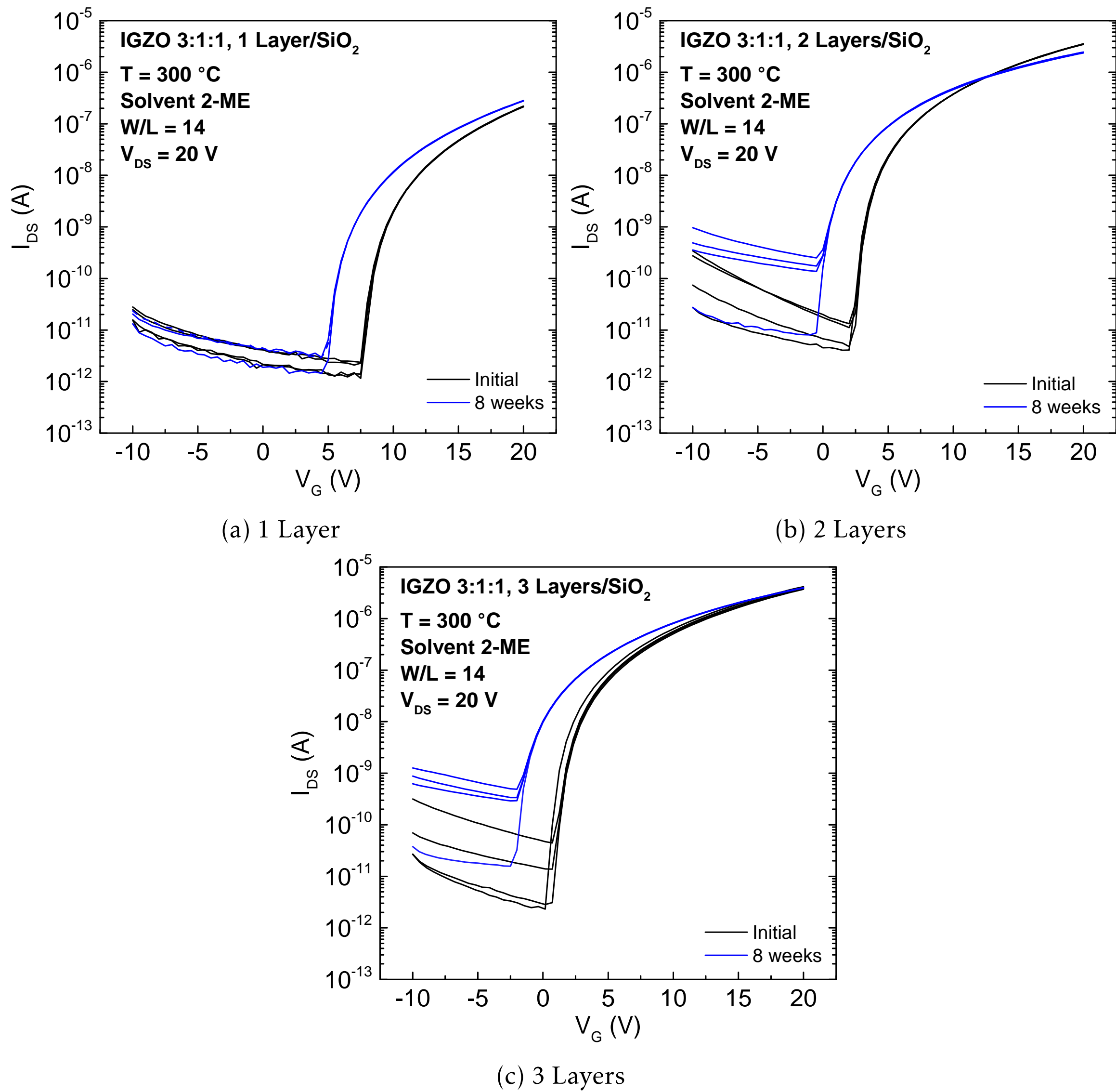

(a) 1 Layer

(b) 2 Layers

(c) 3 Layers

Figure G.4: Stabilisation curves of IGZO 3:1:1 0.2 M with 1, 2 and 3 active layers.

The output characteristics of IGZO 1:1:1 (1 layer), 2:1:2 (1 and 2 layers) 2:1:1 and 3:1:1 (both with 1, 2 and 3 layers) TFTs are depicted in Figures G.5, G.6, G.7 and G.8, respectively.

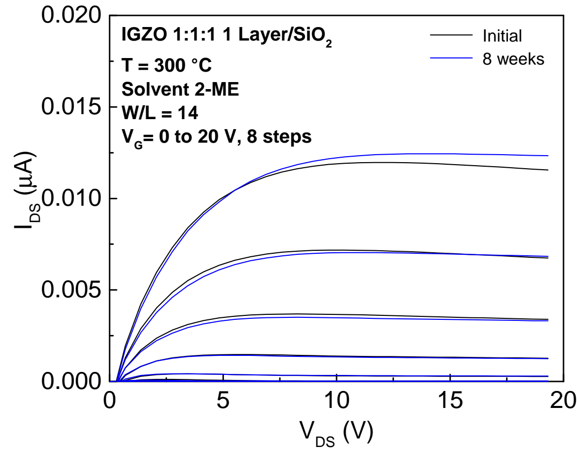

Figure G.5: Output curve of IGZO 1:1:1 0.2 M with 1 active layer.

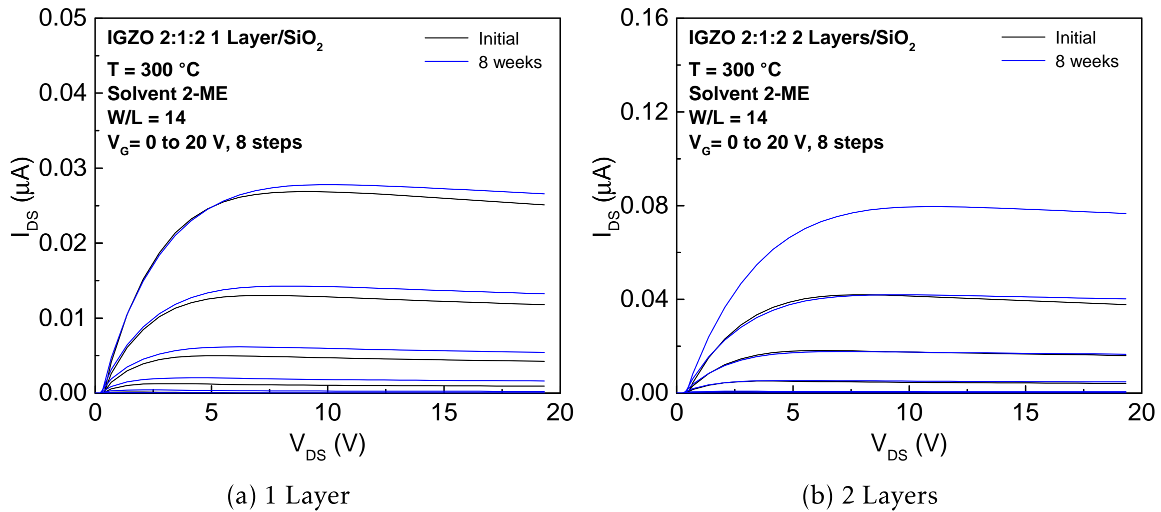

(a) 1 Layer

(b) 2 Layers

Figure G.6: Output curves of IGZO 2:1:2 0.2 M with 1 and 2 active layers.

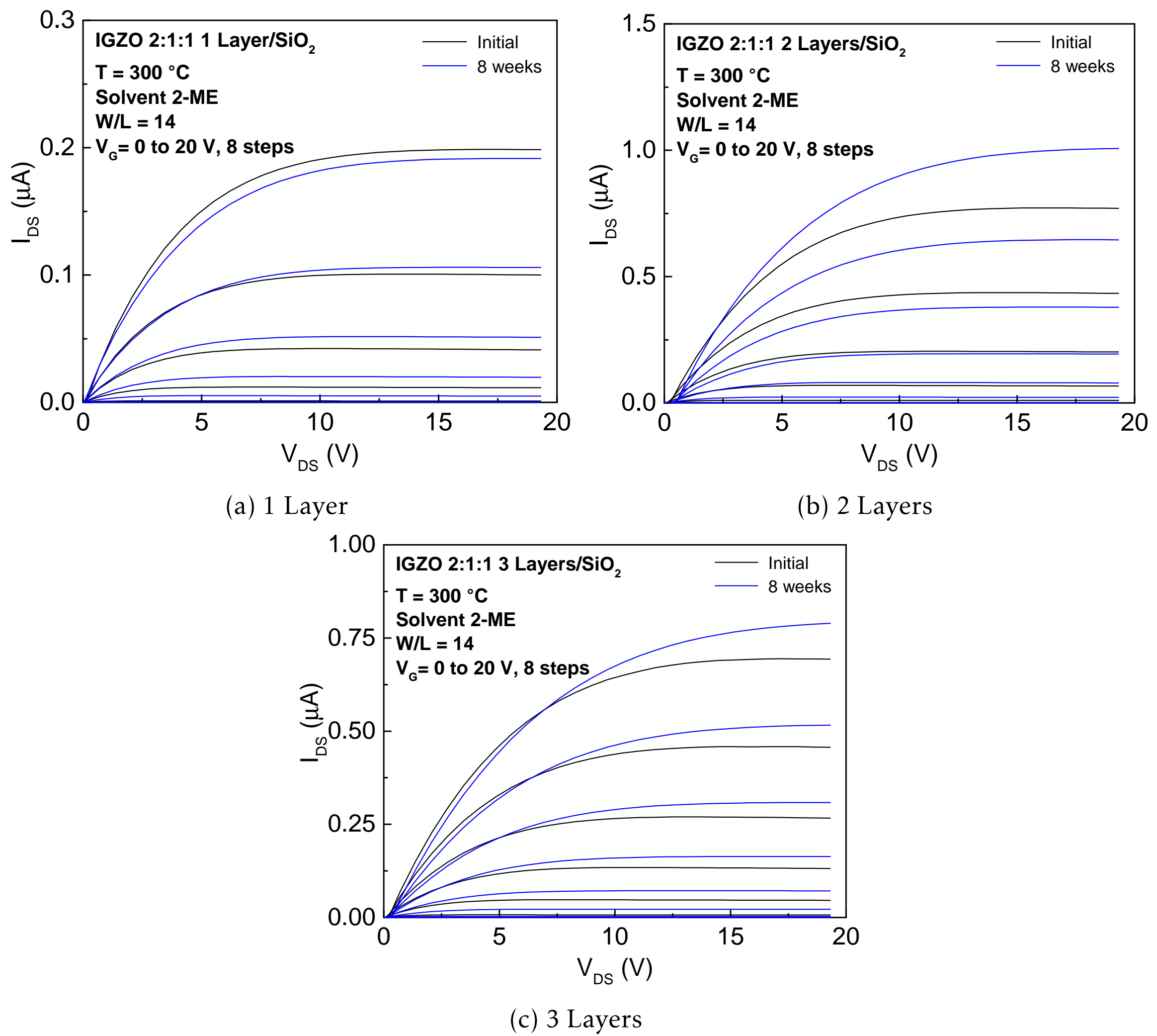

(a) 1 Layer

(b) 2 Layers

(c) 3 Layers

Figure G.7: Output curves of IGZO 2:1:1 0.2 M with 1, 2 and 3 active layers.

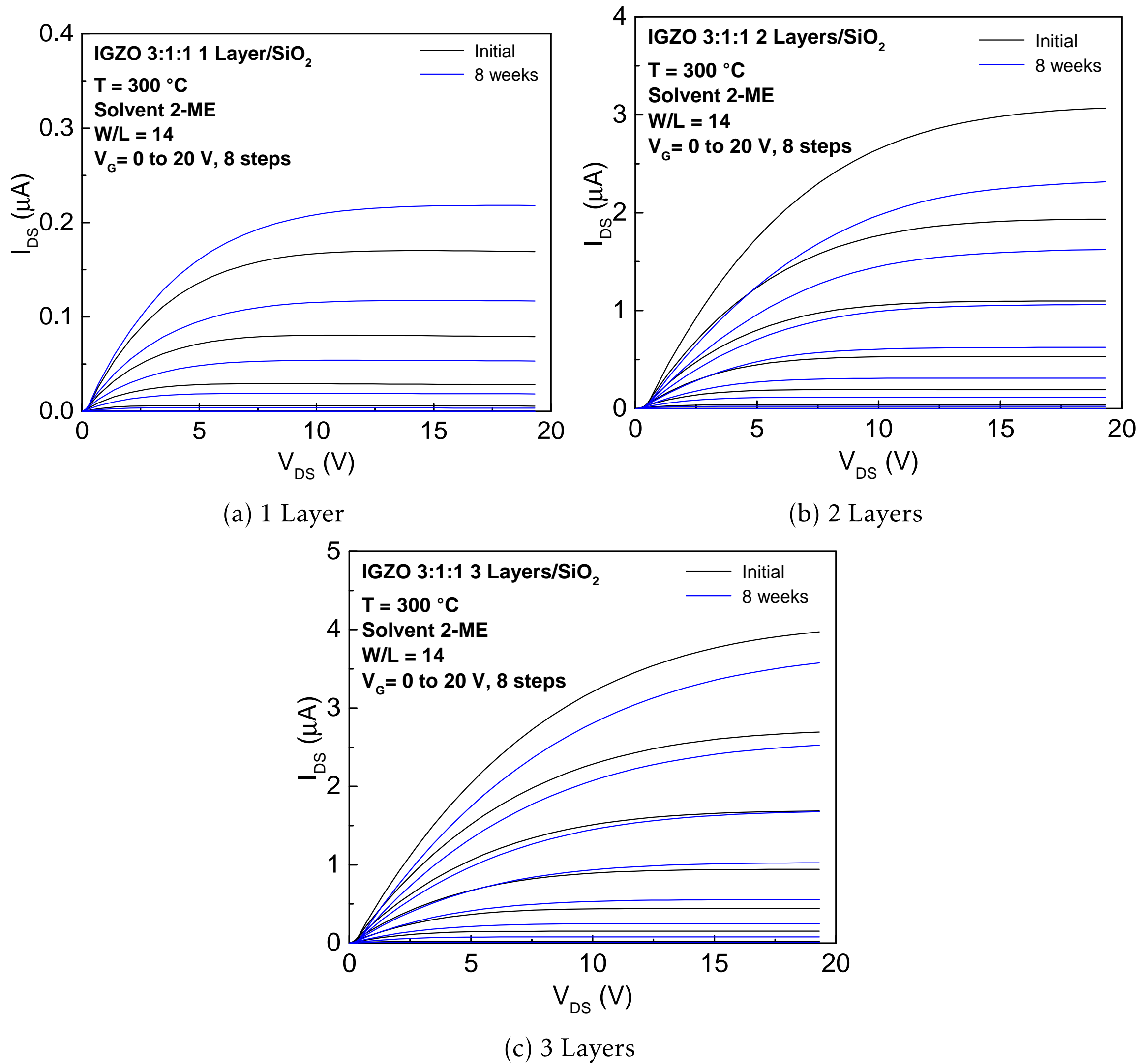

(a) 1 Layer

(b) 2 Layers

(c) 3 Layers

Figure G.8: Output curves of IGZO 3:1:1 0.2 M with 1, 2 and 3 active layers.

Appendix H

Patterned 3-layer TFTs annealed at 180 °C

This section comprises the stabilisation, transfer and output characteristics of TFTs with patterned IGZO 3:1:1 3 layers, annealed at 180 °C, depicted in Figures H.1, H.2 and H.3.

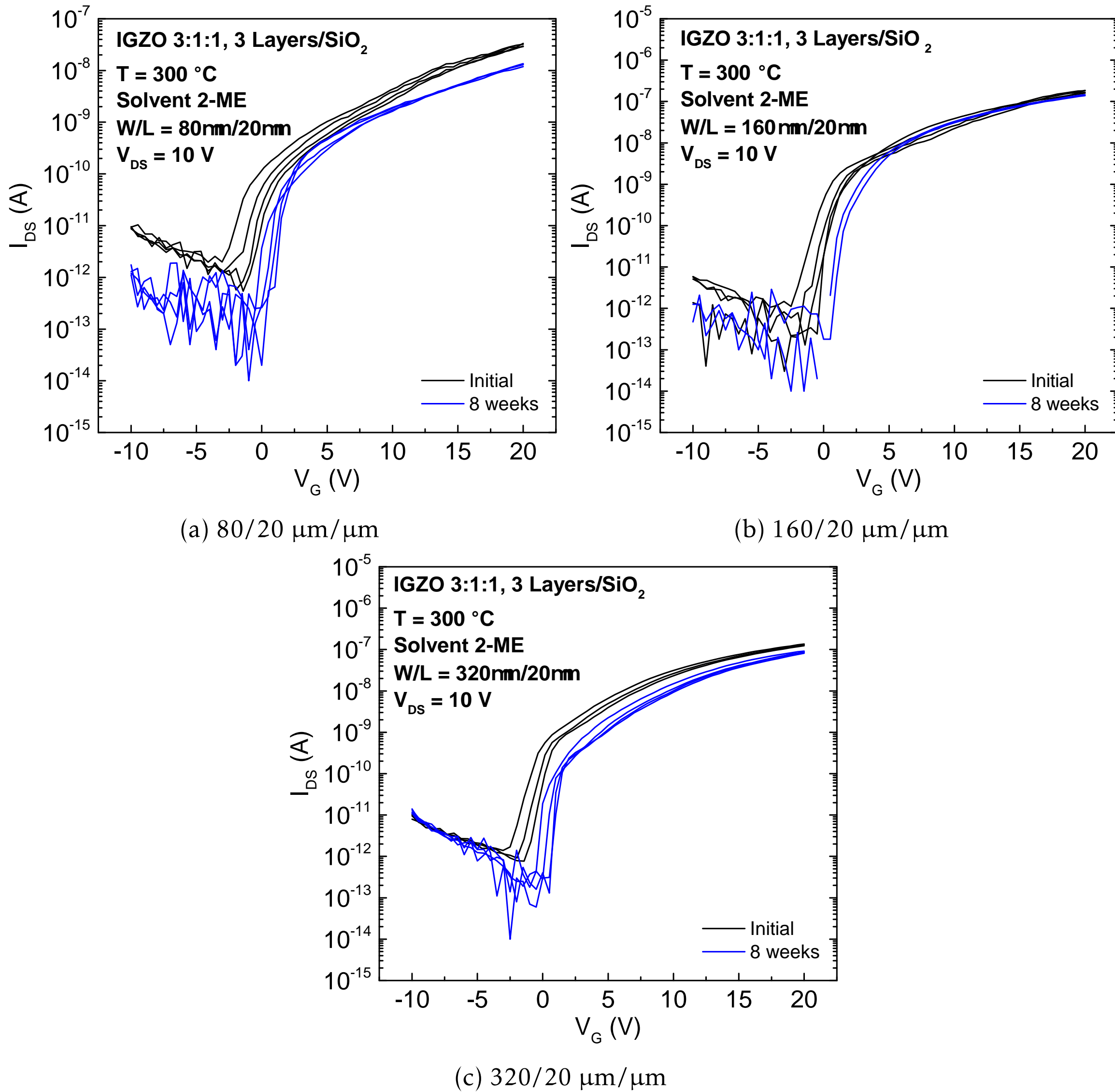

(a) 80/20 µm/µm

(b) 160/20 µm/µm

(c) 320/20 µm/µm

Figure H.1: Stabilisation curves of TFTs annealed at 180 °C with patterned IGZO 3:1:1 3 layers, measured initially and 8 weeks later

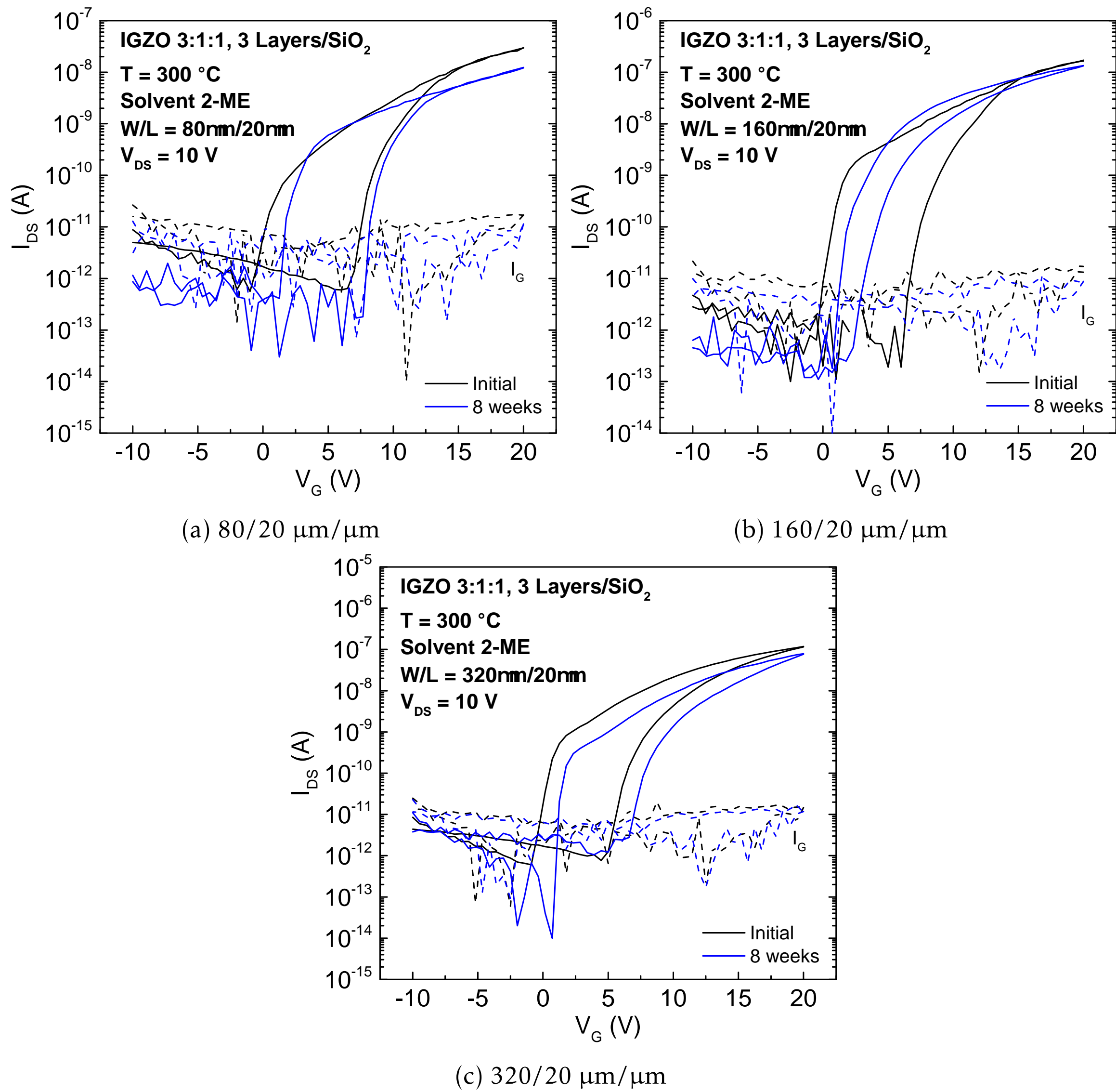

(a) 80/20 µm/µm

(b) 160/20 µm/µm

(c) 320/20 µm/µm

Figure H.2: Saturation curves of TFTs annealed at 180 °C with patterned IGZO 3:1:1 3 layers, measured initially and 8 weeks later

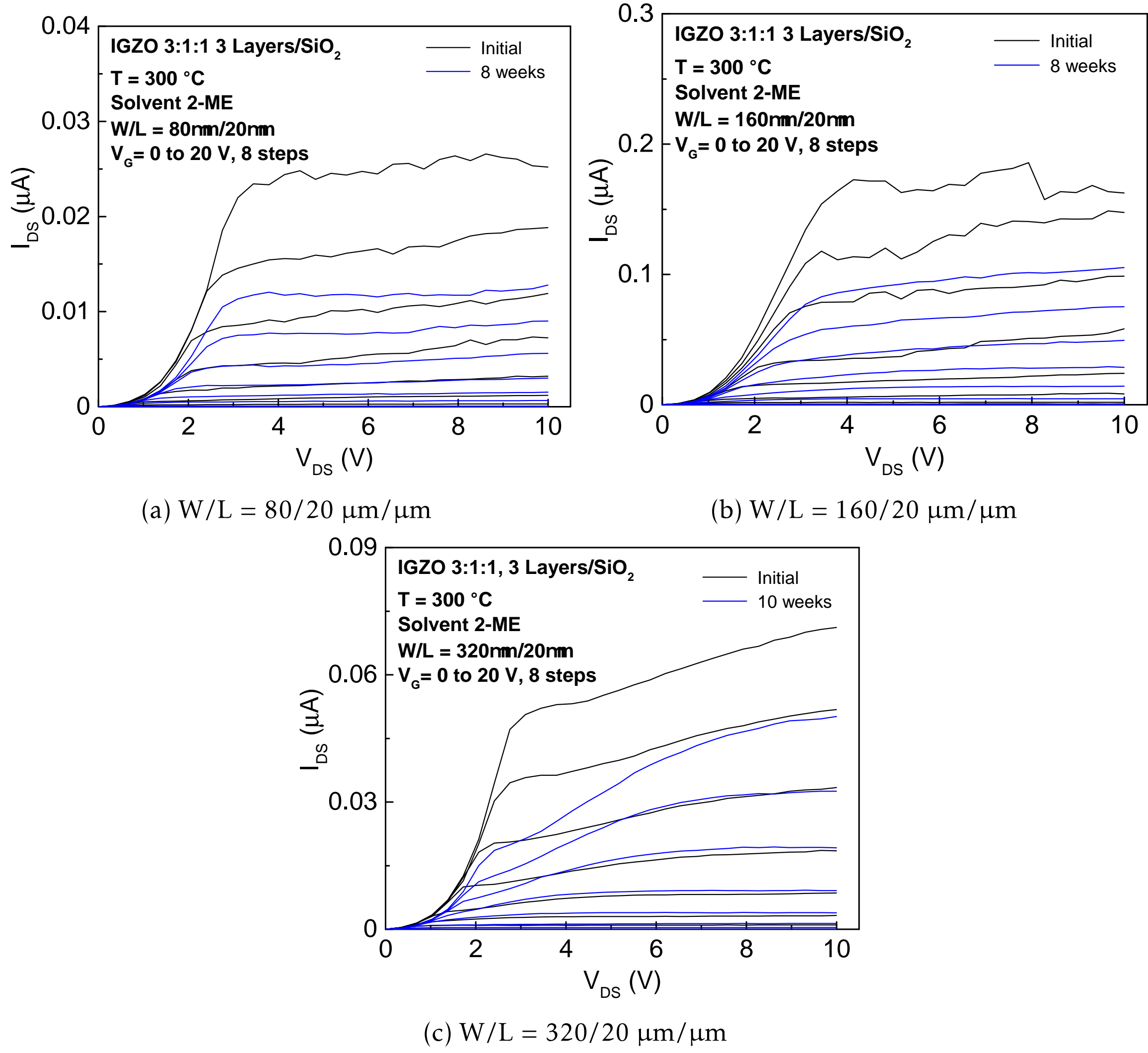

(a) W/L = 80/20 μm/μm

(b) W/L = 160/20 μm/μm

(c) W/L = 320/20 μm/μm

Figure H.3: Ouput curves of TFTs annealed at 180 °C with patterned IGZO 3:1:1 3 layers, measured initially and 8 weeks later

Table H.1: Average and standard deviation of electrical parameters of three measured TFTs annealed at 180 °C with patterned-IGZO 3-layer 3:1:1 as channel layer, measured initially and 8 weeks later.

W/L	Age	I_{on}/I_{off}	V_{on} (V)	V_T (V)	V_{Hyst} (V)	SS (V/dec)	μ_{sat} $(cm^2 V^{-1} s^{-1})$
80/20	Initial	$(1.76 \pm 1.23) \times 10^5$	-0.75 ± 0.25	2.79 ± 2.40	7.06 ± 0.82	0.69 ± 0.24	$(3.00 \pm 0) \times 10^{-3}$
	8 weeks	$(5.79 \pm 2.79) \times 10^4$	1.25 ± 0	2.85 ± 0.10	6.68 ± 0.52	0.47 ± 0.055	$(8.00 \pm 0) \times 10^{-4}$
160/20	Initial	$(1.60 \pm 0.97) \times 10^5$	-1.00 ± 0.50	$4.28 \pm 0.0.36$	7.14 ± 0.46	0.67 ± 0.14	$(3.50 \pm 1.50) \times 10^{-3}$
	8 weeks	$(6.03 \pm 1.41) \times 10^5$	0.45 ± 0.27	2.03 ± 0.39	3.18 ± 0.98	0.47 ± 0.065	$(2.00 \pm 1.00) \times 10^{-3}$
320/20	Initial	$(2.95 \pm 3.44) \times 10^6$	-1.07 ± 0.25	1.83 ± 1.28	5.06 ± 1.15	0.47 ± 0.12	$1.00 \pm 0) \times 10^{-3}$
	8 weeks	$(4.32 \pm 2.56) \times 10^6$	0.35 ± 0.50	2.77 ± 1.39	4.94 ± 0.80	0.32 ± 0.059	$(1.00 \pm 0) \times 10^{-3}$

Stabilisation and output curves of TFTs annealed at 120 °C

The stabilisation and output curves of patterned 3-layer IGZO 3:1:1 TFTs with W/L of 80/20, 160/20 and 320/20 µm/µm are depicted in Figures I.1 and I.2, respectively.

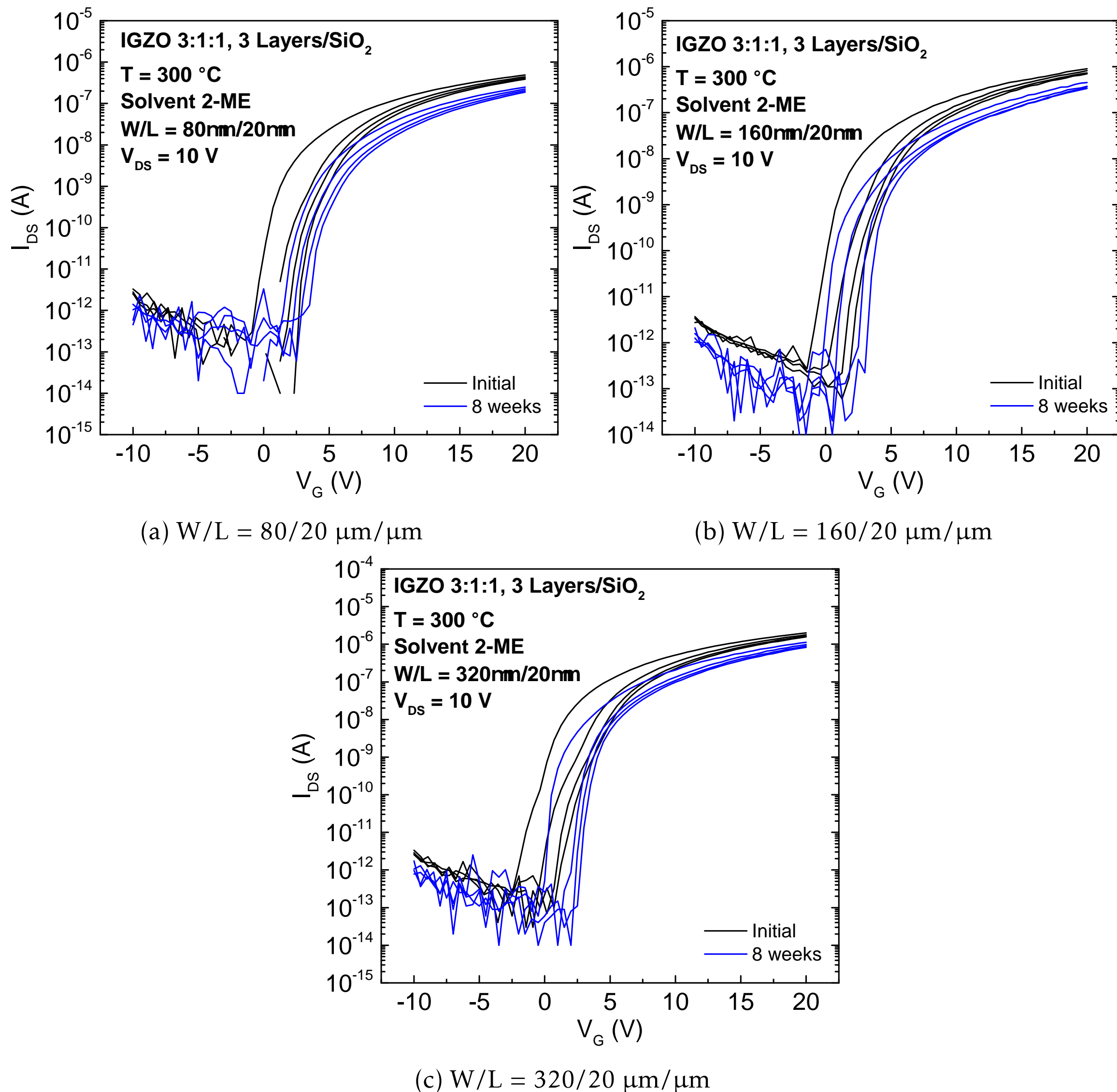

(a) W/L = 80/20 µm/µm

(b) W/L = 160/20 µm/µm

(c) W/L = 320/20 µm/µm

Figure I.1: Stabilisation curves of IGZO 3:1:1 0.2 M with W/L of 80/20, 160/20, 320/20 µm/µm, annealed at 120 °C

.

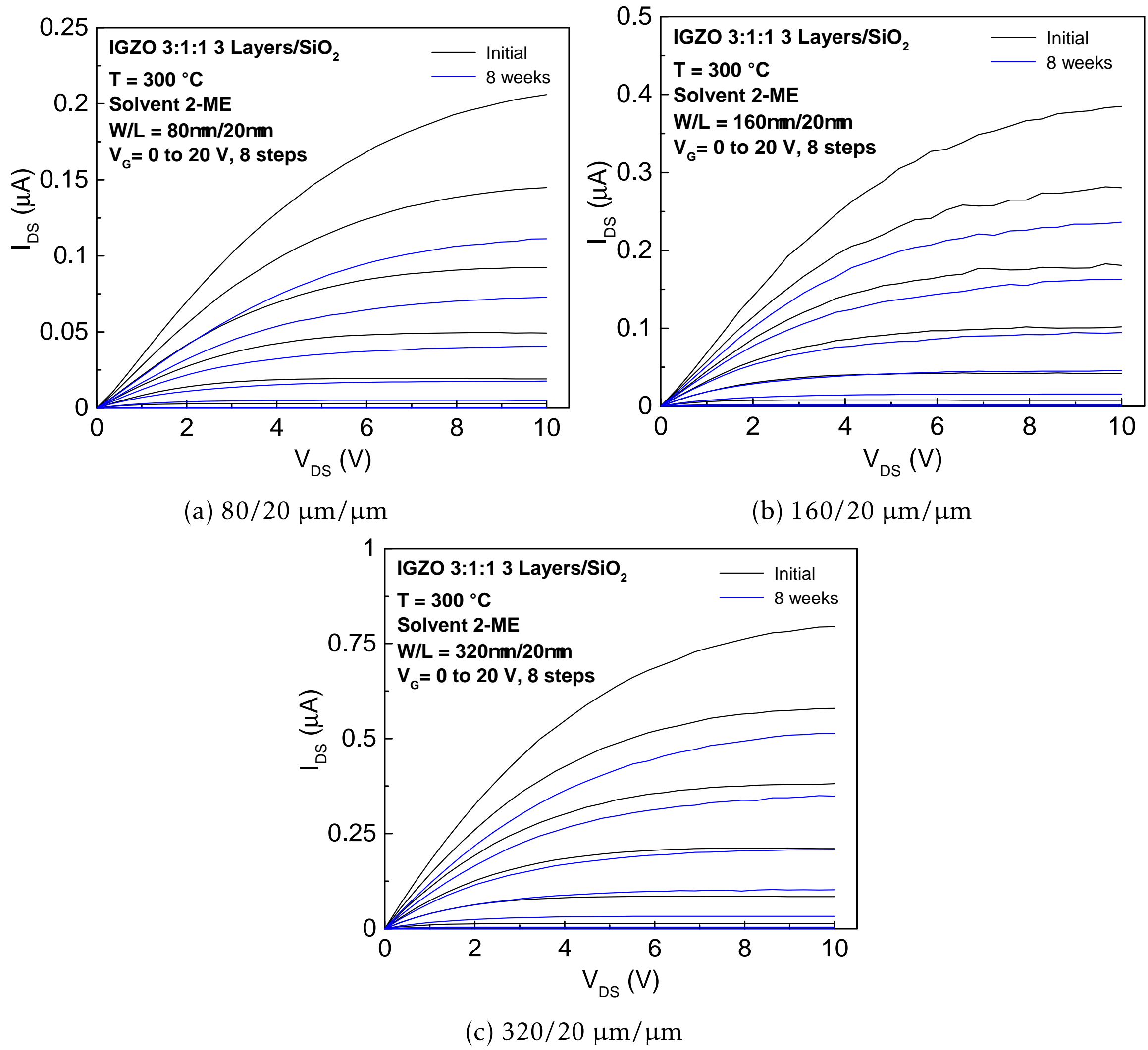

(a) 80/20 µm/µm

(b) 160/20 µm/µm

(c) 320/20 µm/µm

Figure I.2: Output characteristics of patterned IGZO 3:1:1 3 Layers, annealed at 120 °C
.

Appendix J

Comparison of TFTs in this work with literature

Table J.1: Selected processing details for several reported solution based TFTs deposited by solution processes ("n. a." means that the related data is not mentioned in the literature).

Ref.	TFT	T (°C)	Annealing time	SS V/dec	Mobility ($cm^2 V^{-1} s^{-1}$)	I_{on}/I_{off}	V_T (V)	V_G range (V)	SCS
[10]	IGZO/SiO_2	280	4 h	0.86	0.41	5×10^5	13.31	-30-30	Yes
[70]	IGZO/Al_2Ox	300	1 h	0.16	7.3	1×10^5	-0.3	-3-5	Yes
[75]	IGZO/TEOS	220	n. a.	0.79	0.05	7×10^6	4.26	-40-40	No
[6]	IGZO/SiO_2	300	n. a.	n. a.	5.43	1×10^8	17	n. a.	Yes
[29]	IGZO/SiNx	450	1 h	1.39	0.96	1×10^6	7.8	-15-55	No
[24]	IGZO/SiNx	450	3 h	0.63	0.86	1×10^6	6.89	-30-30	No
[34]	IGZO/ATO	400	10 min	0.47	5.8	6×10^7	8.1	-10-30	No
[32]	IGZO/SiO_2	400	n. a.	1.12	0.60	1×10^5	11.5	-10-40	No
[52]	IGZO/SiO_2	300	n. a.	n. a.	0.43	2×10^6	38.8	-20-100	No
This study	IGZO/SiO_2	300	30 min	0.63	0.018	4×10^7	3.83	-10-20	Yes